



Master's thesis

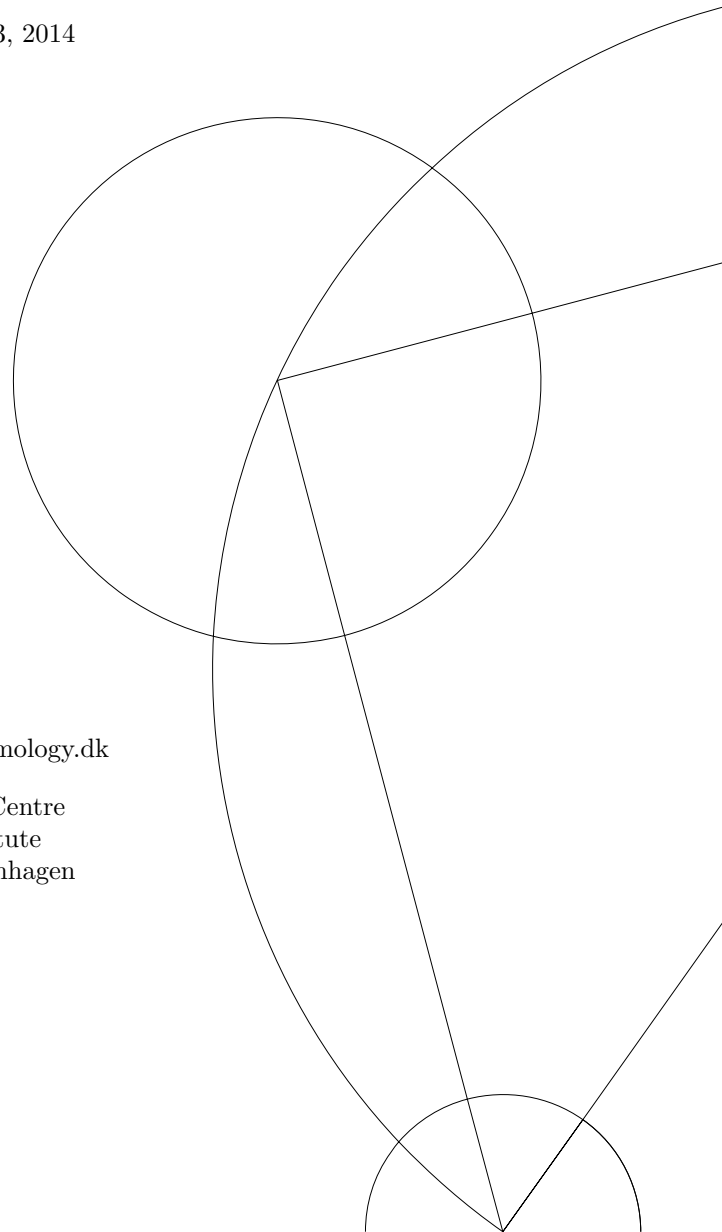
Extinction curves and the total-to-selective extinction
ratio for dust formed in the type II_n SN 2005ip

Ann-Sofie Bak Nielsen
Email: asbn@dark-cosmology.dk

Submitted: June 13, 2014

Supervisor
Jens Hjorth
Email: jens@dark-cosmology.dk

Dark Cosmology Centre
Niels Bohr Institute
University of Copenhagen



Contents

1	Abstract	3
2	Introduction	4
3	Stellar evolution	5
4	Supernovae	6
4.1	SN type I	7
4.1.1	Type Ia SN	7
4.1.2	Type Ib and Ic SN	8
4.2	SN type II	8
4.2.1	Type II-P supernova	9
4.2.2	Type II-L supernova	11
4.2.3	Type IIn supernova	11
5	Possible progenitor stars	13
5.1	Red Super Giant	14
5.2	Luminous Blue Variables	15
5.3	Wolf-Rayet stars	17
6	Dust	17
6.1	Dust formation	18
6.1.1	Sign of dust formation	19
6.1.2	Where and when is dust formed?	20
6.1.3	Shock physics and CDS	21
6.2	Interstellar extinction	21
7	SN 2005ip	22
7.1	Light curves	23
8	Extinction curve calculation for SN 2005ip	24
8.1	Linear fit	25
8.1.1	Monte Carlo simulation	26
8.1.2	Extinction curves	27
8.1.3	Galactic reddening	28
8.1.4	R_V calculation	30
8.2	Different B values	33
8.2.1	Range of B values	34
8.3	Polynomial fitted model	37
8.3.1	Other polynomial degrees	40

8.4	Logarithmic fit	41
8.4.1	The light curves	41
8.4.2	Extinction and R_V	42
8.4.3	Polynomial fit	43
8.5	No r -band	45
9	Results	46
9.1	MW, SMC and LMC	46
10	Discussion	49
10.1	Future prospects	51
11	Conclusion	52
12	Appendix	56
12.1	Poster for Nordic Physics Days 2013	56
12.2	Comparative light curves	57
12.3	Light curves over all time	58
12.4	Non converging fits	59
12.5	Plots for the B value model	60
12.5.1	Plots for $B=1$	60
12.5.2	Histograms $B=1$	61
12.5.3	Plots for $B=0.9$	62
12.5.4	Plots for $B=0.8$	64
12.5.5	Plots for $B=0.7$	66
12.5.6	Plots for $B=0.6$	68
12.5.7	Plots for $B=0.5$	70
12.5.8	Plots for $B=0.2$	72
12.6	Plots for Polynomial fits to B models	74
12.6.1	Polynomial model plots for $B=1$ and $B = 0.5$	74
12.6.2	Polynomial model plots for $B=0.9$	75
12.6.3	Polynomial model plots for $B=0.8$	76
12.6.4	Polynomial model plots for $B=0.7$	77
12.6.5	Polynomial model plots for $B=0.6$	78
12.6.6	Polynomial model plots for $B=0.2$	79
12.6.7	Polynomial model - Entire range og B values	80
12.7	Logarithmic fit	81
12.7.1	Logarithmic model with polynomial fit	82
12.8	The removed point	83

1 Abstract

Abstract

This project focus on calculating the extinction curves of the type IIn supernova SN 2005ip and from the extinction calculating the total-to-selective extinction ratio. The extinction is calculated by fitting different models to the light curves, in the optical and NIR photometric bands, for SN 2005ip. It is assumed that the drop off at approximately 50 days after discovery which is seen on the light curves for SN 2005ip is due to dust formation in a cold dense shell, in the supernova. There is then created different models for a possible evolution of the supernova light curves if there were no dust formation in the cold dense shell. From these models the extinction is calculated and extinction curves are found. The total-to-selective extinction ratio, which is a description of the slope of the extinction curves, and thus indirectly of the dust size, is then calculated. The total-to-selective extinction ration is then compared to the total-to-selective extinction ratio for the Milky Way, Small Magellanic and Large Magellanic clouds. Furthermore the total-to-selective extinction is also compared to the corresponding ratio for type Ia supernovae and for another type IIn supernova, SN 2010jl.

Resumé

Projektet

2 Introduction

Stars are formed from cosmic dust in the interstellar medium (ISM) in galaxies. The stars go through a lifetime of different nuclear burning and stars below $8M_{\odot}$ end their lives as planetary nebulae with a white dwarf (WD). Stars above $8-10M_{\odot}$ will end their lives in a huge cosmic explosion, as a supernova (SN), and typically with a remnant, either a Black hole (BH) or a neutron star (NS). In both low and high mass stars dust is thought to be produced. This means that stars will come from dust and at the end of their lives they will produce dust, all in a cosmic recycling system.

There are, however, some discussion about how much dust is produced by supernovae. Supernovae are divided into different sub-types, and research finds that there is a big difference in how much dust the different types of supernovae produce. The supernova dust production ranges from the almost dust free type Ia SN to type IIn which appear to produce a relatively large amount of dust. Type IIn SN appears to produce dust directly behind the forward shock. Dust needs a cold and dense area in order to form. This might occur between the forward and reverse shock in type IIn SN, in a cold dense shell (CDS).

There are several ways to confirm and examine the existence of dust in supernovae. One could e.g look at the $H\alpha$ lines in the spectrum, the IR emission or examine the evolution of the light curves. In this thesis light curves from a type IIn SN have been examined. This is the type IIn SN 2005ip. In the light curves of SN 2005ip there is an early time drop off in all the optical and NIR bands seen. This drop off is assumed to be due to dust formation in the CDS.

The dust formed is then examined by creating different models that assume how the light curves would evolve without dust formation. The extinction from the dust in the SN is then found, using these models, and from the extinction, the total-to-selective extinction ratio, R_V , is found. From the total-to-selective extinction it is then possible to compare the dust in SN 2005ip, the $R_{V_{SN2005ip}}$ to R_V for the Milky Way (MW), Large Magellanic cloud (LMC) and the Small Magellanic cloud (LMC). It is further possible to compare to R_V for type Ia SN and to R_V for another type IIn SN, SN 2010jl.

3 Stellar evolution

Stars have very different evolutionary tracks depending on their masses. Low mass stars ($M_{\star} < 8M_{\odot}$) (Woosley & Janka, 2005) spend most of their time on the main sequence where they burn hydrogen to helium (Christensen-Dalsgaard, 2008). When there is no more hydrogen to burn then stars move off the main sequence and go through a process of burning helium to carbon/oxygen. The end of a low mass star is at the asymptotic giant branch, AGB star, phase (Christensen-Dalsgaard, 2008). Here they pulsate and throw off mass into a cloud of dust, a planetary nebulae, and the only remnant is a relatively small dense clump of degenerate matter, a White Dwarf (WD) (Christensen-Dalsgaard, 2008). High mass stars ($8M_{\odot} < M_{\star}$) (Woosley & Janka, 2005) have different evolutionary tracks. The evolution of high mass stars is fast, and the stars quickly end their lives in a massive explosion, a supernova (SN), which destroys the star leaving only a remnant, which is either the very dense and very small neutron star or a black hole (Christensen-Dalsgaard, 2008). A sketch of the evolution of both high and low mass stars can be seen on Fig. 1.

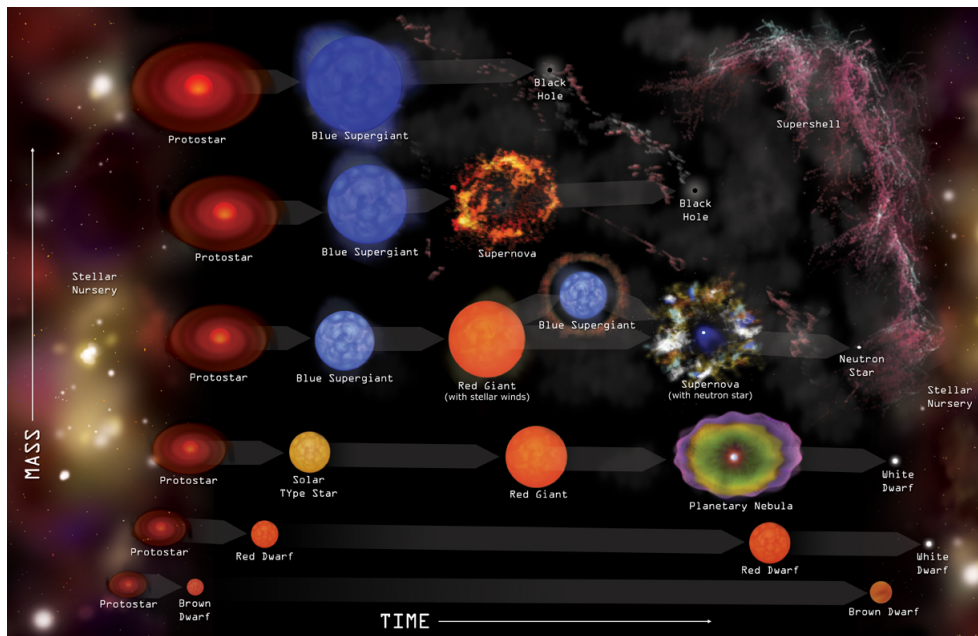


Figure 1: This figure shows an overview of the evolution of both high and low mass stars. Low mass stellar evolution is shown as the bottom three and high mass stars are the top three evolutionary steps. Figure source: Chandra X-ray Observatory (2012).

High mass stars burn their interiors until they reach iron. As long as the mean binding energy of a nucleon is increasing with increasing mass, then energy is released (Christensen-Dalsgaard, 2008). Iron is the most tightly bound element, and it would take more energy to burn iron to heavier elements than it took to reach iron, which is why the nuclear burning stops at iron (Christensen-Dalsgaard, 2008). On Fig. 2 it is seen how tightly bound elements are compared to each other.

Fig. 2 shows the binding energy on the y-axis and the atomic number on the z-axis. The burning phase until ${}^{56}\text{Fe}$ is $H \rightarrow He \rightarrow C \rightarrow O \rightarrow C, Ne, O, Si \rightarrow Fe$

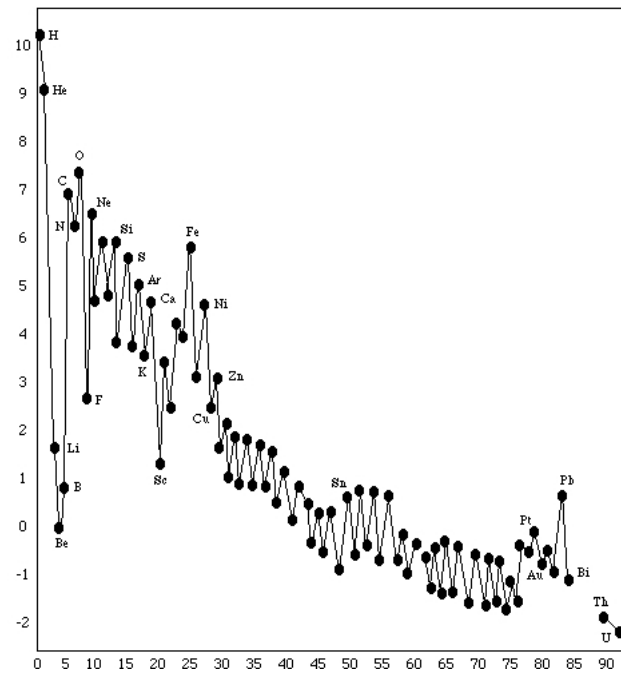


Figure 2: This Figure shows the binding energy of an atom/nucleus as a function of atomic number. Number 56 is iron, and this is the most tightly bound nucleus (Rosswog & Brüggem, 2007). It is the relative abundance on a logarithmic scale on the y-axis and atomic number on the x-axis. The figure have been changed a little from the original. Figure source: Siriwardane (2010).

and then the core collapses in a supernova (CCSN) (Heger et al., 2003) (Christensen-Dalsgaard, 2008). The burning happens first in the core and then in a shell (Heger et al., 2003). The mass of the core is dominated by nucleons and the pressure is dominated by electrons (Christensen-Dalsgaard, 2008). The electron pressure is only held up for as long as the core stays below a certain mass, the Chandrasekhar mass limit (Christensen-Dalsgaard, 2008). When the mass of the core exceeds the Chandrasekhar mass, the core can no longer uphold it self and it collapse in a CCSN (Heger et al., 2003) (Boles, 2005) (Anderson & James, 2008).

4 Supernovae

SNe are the result of violent explosions of stars (Rosswog & Brüggem, 2007) and are the most energetic explosions in the universe. They can be divided into two groups according to their explosion mechanism or according to their observational properties as seen on Fig. 3 (Boles, 2005) (Kozasa et al., 2009). The classification according to explosion mechanism is with a group of explosive thermonuclear burning, SN Ia, and a group of CCSN (Kozasa et al., 2009) (Anderson & James, 2008). SNe are observationally characterized by either having no-hydrogen lines in their spectra, or containing hydrogen, when the SN is at maximum brightness (Boles, 2005) (Woosley & Janka, 2005) (Arcavi et al., 2010).

Both type I and II are further divided into subclasses, as seen on Fig. 3. Furthermore the different SN types are also divided according to the shape of their light curves, which is the case for type II SNe (Anderson & James, 2008). The

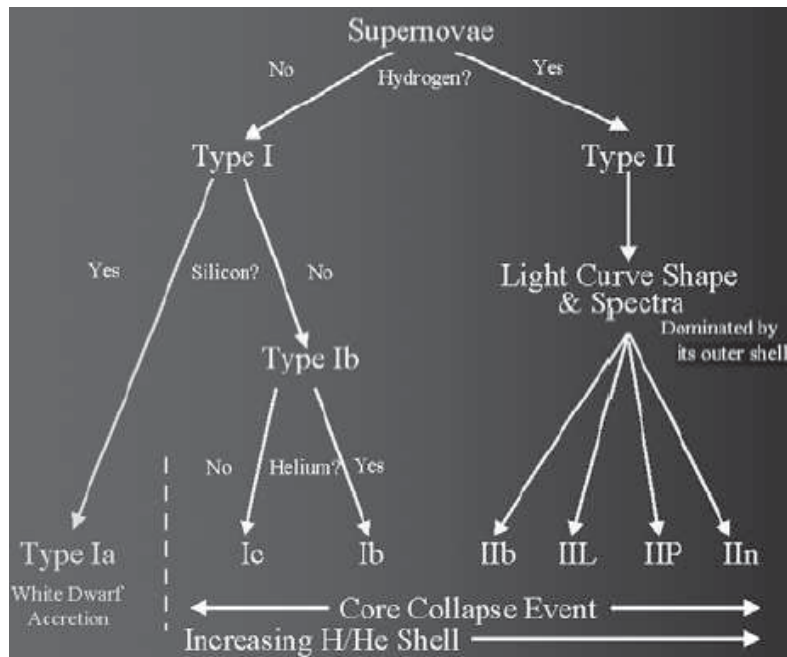


Figure 3: This figure shows the observational division of the supernovae types. Figure source: Boles (2005).

difference in the light curves of the different sub-types of the type II SN or I SN groups could be due to the differences in the progenitor stars where e.g. masses between $17 - 25M_{\odot}$ are sensitive to magnetic fields, metallicity or rotation, and therefore more likely to produce II_n, II_b, Ib or Ic SN than the more common type II-P (Gall, Hjorth & Andersen, 2011).

4.1 SN type I

The defining characteristic of type I SN is the absence of hydrogen lines in their spectra. Instead there is a large variety of intermediate elements, such as Silicon (Si) and Nickel (Ni) (Rosswog & Brüggen, 2007). The elements present give information on their progenitor stars, the SN must have undergone some nuclear processes before explosion. There are three sub-types of type I SN; Ia, Ib and Ic (Rosswog & Brüggen, 2007). Type Ia is a special type of SN and it has a very different evolution from the rest of the SN types. Type Ib and Ic are both CCSNe and have similar evolutions as the type II SNe. Type Ia, Ib and Ic are, however, not the main SN types examined in this thesis and are therefore only briefly described.

4.1.1 Type Ia SN

Type Ia SN is a fairly uniform explosion, where 85% of them show an almost identical light curve (Rosswog & Brüggen, 2007). The homogeneity implies that this SN type only occur under very specific circumstances. Type Ia occur in both spiral arms of galaxies, among young stars, but also in old elliptical galaxies (Rosswog & Brüggen, 2007). That they are found in elliptical galaxies imply that type Ia is not a product of massive stars since they are no longer present in these galaxies. This

gives rise to the theory that they originate from thermonuclear explosions of WD's (Rosswog & Brüggen, 2007). WD's are the leftovers of low-mass stars, that become AGB stars, which then throw off their outer layers, and what is left is the WD. Before becoming a SN, the WD is believed to have accreted mass from a companion star in a binary system. The WD reaches the Chandrasekhar limit, it subsequently ignites a thermonuclear explosion (Rosswog & Brüggen, 2007) (Boles, 2005) (Gall, Hjorth & Andersen, 2011). A WD is made up of degenerate material and this material is not sensitive to temperature and pressure changes right away, which means that the hydrogen that is transferred from the companion does not immediately effect the WD (Boles, 2005). The hydrogen on the surface fuse to helium and the star only reacts slowly, letting the fusion happen over the entire surface, resulting in total destruction of the star as it explodes, leaving no remnant (Boles, 2005).

4.1.2 Type Ib and Ic SN

The two other type I SN are type Ib and Ic. Both of these SNe originates from massive Wolf-Rayet stars (WR), and both are CCSN. WR stars are massive and are quickly losing mass due to a strong stellar wind. It is because of this wind, that the hydrogen layers have more or less disappeared before SN explosion, and there will not appear any hydrogen lines in the spectrum of the SN (Smartt, 2009) (Langer, 2012). Type Ib/c can also occur when a binary system exchange mass, and one of the stars explode in a SN (Rosswog & Brüggen, 2007). Further it is suggested that the Ib/c SNe origins from stars that are considerably more massive than the progenitors for type II SN (Anderson & James, 2008). The progenitor for type IIb SN have lost most of its hydrogen envelope before explosion. If the star suffers from further mass loss it could appear as a Ib or Ic SN (Arcavi et al., 2010). The Ib SN would have strong He lines, but no H lines, and the Ic SN would be lacking both H and He (Arcavi et al., 2010).

4.2 SN type II

Type II SNe are all CCSN and origin from massive stars with masses of $M_{\star} < 8M_{\odot}$ (Anderson & James, 2008) (Woosley & Janka, 2005). The type II SNe are very diverse, and almost none of their light curves are similar. The light curves depend on the initial radius of the star, ejecta mass and explosion energy of the SN (van Marle et al., 2010).

The type II SNe are characterized by the presence of hydrogen lines in their spectra (Boles, 2005)(Woosley & Janka, 2005), and all type II SN are core collapse (Woosley & Janka, 2005) (Boles, 2005). In most cases, when more fuel is added the burning continues, but the opposite happens when dealing with nuclear fuel. When more hydrogen is added, the gravitational pressure increase and the thermal temperature increase in the core of the star (Boles, 2005). The increased temperature speeds up the burning of hydrogen to helium and the massive stars then have a shortened life on the main sequence (Boles, 2005). When the hydrogen disappears the stars collapse under the gravitational pressure, and this happens so fast, that the outer parts of the star is not affected by the collapse at first. When the core cannot compress any more the core will bounce back throughout the outer

layers of the star (Boles, 2005). The energy of this bounce back is enough to blow apart the outer layers. The rebound is help by neutrino flow from the iron core. The expanding ejecta collides with the slower material outside of the star, and this is what creates the elements that are heavier than iron (Boles, 2005). The CCSN goes through burning hydrogen to helium and then to carbon, neon, oxygen and silicon. The different burning phases take less and less time, which is seen on Fig. 4 (Heger, Woosley & Baraffe, 2005) (Woosley & Janka, 2005). It can even be seen, that the time decrease rapidly with an increase in the stellar mass.

Burning stages		20 M_{\odot} star		200 M_{\odot} star	
Main Fuel	Main Product	T (10^9 K)	Duration (yr)	T (10^9 K)	Duration (yr)
H	He	0.037	8.1×10^6	0.14	2.2×10^6
He	O, C	0.19	1.2×10^6	0.24	2.5×10^5
C	Ne, Mg	0.87	9.8×10^2	1.1 [†]	4.5
Ne	O, Mg	1.6	0.60	2.4 [†]	1.1×10^{-6}
O	Si, S	2.0	1.3	3.5 [†]	3.5×10^{-8}
Si, S	Fe	3.3	0.031	4.3 [‡]	2.7×10^{-7}

[†]central radiative implosive burning

[‡]incomplete silicon burning at bounce

Figure 4: This figure shows how long the different phases of nuclear burning lasts, in years, for a $20M_{\odot}$ star and $200M_{\odot}$ star. Figure source: Heger, Woosley & Baraffe (2005).

The progenitor stars of core-collapse supernovae may be a variety of different stellar types. It is possibly either a WR star, a Luminous blue variable (LBV), or a Red Super Giant (RSG). It is thought, that the CCSN types is sorted after the increasing mass of the progenitor stars, which means that they would be ordered beginning with II-P, II-L, II-n, Ib, Ic (Gall, Hjorth & Andersen, 2011). There is an ongoing discussion about which stellar type is the progenitor star for the different SNe, and in particular for the type II-n SNe. This discussion is very much present when examining SN 2005ip, where there have been some dispute over whether it is a RSG or a LBV star that is the progenitor (Gall, Hjorth & Andersen, 2011) (Stritzinger et al., 2012). In the next sections different type II SNe are presented, and in section 5 possible progenitor stars will be presented.

4.2.1 Type II-P supernova

The type II-P SN is a CCSN, which is usually defined by having P-Cygni hydrogen lines and a long plateau in the light curves (Smartt, 2009). The plateau arise when the shock wave from the SN explosion hits the thick hydrogen envelope around the progenitor star. The shocked envelope expands and cools, and it recombines hydrogen, which releases energy at a constant rate. This is what creates the plateau (Arcavi et al., 2012) (Smartt, 2009) (Sanders et al., 2014). It has an expanding photosphere phase which is powered by the recombination of hydrogen (Smartt, 2009).

Type II-P are the most common and frequent CCSN, up to 50 – 70% of all massive star that become SNe are II-P SN (Langer, 2012) (Gall, Hjorth & Andersen, 2011). Most of the calculated type II-P spectra show good agreement of having a

RSG as a progenitor star (Langer, 2012) (Arcavi et al., 2010), which are stars of masses between $8 - 17M_{\odot}$ (Langer, 2012), since around $8M_{\odot}$ is the minimum mass of a CCSN and $17M_{\odot}$ is the maximum mass a star can have before evolving into e.g. a WR-star and creating a Ib or Ic SN instead (Smartt, 2009) (Langer, 2012) (Gall, Hjorth & Andersen, 2011). In an area with solar metallicity the upper mass limit may be up to $25M_{\odot}$ (Gall, Hjorth & Andersen, 2011).

The plateau phase that characterize type II-P SN can be seen on Fig. 5, where also light curve examples from Type Ia, Ib and II-L are shown. An additional figure of sample light curves is seen on Fig. 39 in Appendix 12.2. It is not actual light curves, but theoretical or rather calculated synthetic light curves. This is because not all SNe have specific and similar light curves, most type Ia light curves look alike, as well as II-P light curves look alike, but type II_n can be very different (Rosswog & Brüggen, 2007). Fig. 5 is only a possible way to interpret the light curves. Type II_n light curve is fainter than type Ia on Fig. 39 whereas in reality II_n SN can be some of the most luminous SN, even brighter than type Ia, and there is a whole range of superluminous SN that are much brighter than the bright type Ia. Fig. 5 and Fig. 39 only give an idea of the shape of the light curves, but not necessarily the brightness of the SN.

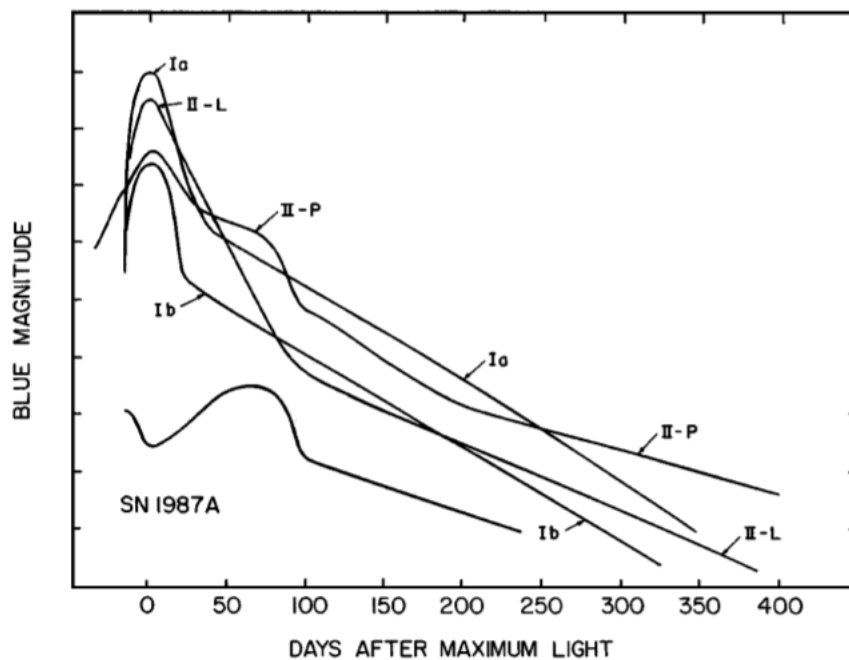


Figure 5: Sample light curves of 7 supernovae types are shown here. The type II-L and II_n have a late time peak and are often of a wide range of luminosities, and can be very luminous. II_b are instead of intermediate luminosity between II-P and II_n/II-L (Chevalier, 2003). Figure source: Filippenko (1997).

4.2.2 Type II-L supernova

If the mass of the hydrogen rich envelope around a RSG decreased then the light curve could transform from the type II-P plateau light curve to a linear declining light curve, which is the type II-L light curve (Langer, 2012) (Sanders et al., 2014). The spectrum of the II-L or II-P SN can be almost constant because the SNe expands at a rate, where the increase in radius compensates for the decreasing surface temperature, and the emission of light then becomes constant (Rosswog & Brüggen, 2007). The type II-L light curve is seen on Fig. 39 in Appendix 12.2 as the light blue curve, where the linear decline is clearly seen.

Type II-L accounts for around 6% of all SN that origin from massive stars (Langer, 2012). This type has about the same peak magnitude at every explosion (Rosswog & Brüggen, 2007). Type II-L and IIn are not distinct designations, they may change during the observation time of the SN. A SN may initially be described as type II-L, but then show narrow lines and then be designated the type IIn, as was the case for 1998S (Chevalier, 2003).

4.2.3 Type IIn supernova

The type IIn SNe was suggested as a sub-class of the type II SN in 1990 (Schlegel, 1990). Type IIn SN have hydrogen lines in their spectra as every other type II SN has (Boles, 2005) and they show a mixture of broad, intermediate and narrow lines (Fransson et al., 2013). For more detail see section 6.1.2 and in Fig. 9. The IIn SN are named after their narrow hydrogen emission lines which have a width around $< 700\text{kms}^{-1}$, and arise in a dense circumstellar medium (CSM), that is excited by x-ray and UV emission from the forward shock from the SN (Fox et al., 2011) (Mauerhan & Smith, 2012). Because the narrow lines arise from a dense CSM, the progenitor star of type IIn SN must have suffered from severe mass loss shortly before the SN exploded (Mauerhan & Smith, 2012).

Type IIn arise from the core-collapse of stars at $8 - 10M_{\odot}$ or from stars of masses above $20M_{\odot}$ (Gall, Hjorth & Andersen, 2011) (Stritzinger et al., 2012). There are only about 79 known type IIn events within a distance of 250Mpc (Fox et al., 2011) and this type only make up around 8 – 9% of CCSN (Smith, Mauerhan & Prieto, 2014) which may be all stars in the mass range $42 - 60M_{\odot}$ (Langer, 2012). The type IIn events have a variety of different spectral properties but they all have narrow Balmer emission lines (Stritzinger et al., 2012), where P-Cygni lines are seen (Kiewe et al., 2012). The Balmer lines may have three different components, a narrow ($v_{FWHM} < 700\text{kms}^{-1}$), intermediate ($v_{FWHM} = 2000 - 5000\text{kms}^{-1}$) and a broad component ($v_{FWHM} = 10^4\text{kms}^{-1}$) (Stritzinger et al., 2012) (Fox et al., 2011). The type IIn SN can be observed in almost all wavelengths from x-ray to radio depending on the nature of their CSM and the SN explosion (Stritzinger et al., 2012).

There has to be a diverse set of possible progenitor stars to explain the different spectral properties that type IIn SN may show (Stritzinger et al., 2012). The

progenitor star could be either a RSG or a LBV or even a WR stars (Gall, Hjorth & Andersen, 2011) (Van Dyk, 2013), and the only real restriction is that the progenitor should undergo mass loss before the SN explosion, and have formed a CSM (Gall, Hjorth & Andersen, 2011). The narrow emission could point to a wind velocity in the shell around the star of about 100kms^{-1} which would point towards blue supergiants as progenitors (Langer, 2012). The observational characteristics of SNe, and here type IIIn SN, are due to the progenitor star and the interaction between the forward shock and the CSM (Stritzinger et al., 2012). The light curves are thus affected by the morphology of the CSM and therefore of the characteristics of the progenitor star, which is not well known (van Marle et al., 2010). Type IIIn are often very luminous in comparison to other CCSN and can have magnitudes up to $M_V = -18.4\text{mag}$ (Kiewe et al., 2012), and they often have fast pre-SN stellar winds of $600 - 1400\text{kms}^{-1}$ and mass loss rates of $0.026 - 0.12M_{\odot}\text{yr}^{-1}$ (Kiewe et al., 2012). The need for a massive and dense CSM can favour LBVs as progenitor stars (van Marle et al., 2010).

The type IIIn SN have three main types, they can be very luminous, intermediate bright objects or objects of moderate peak brightness (Stritzinger et al., 2012). The intermediate and moderate peak brightness types have magnitudes of $M_V \approx -17$ to -19mag and are respectively 1988Z- or 1994W-like objects (Stritzinger et al., 2012). The 1988Z-like objects are believed to be powered by x-ray emission from the interaction between the SN shock wave and the CSM (Stritzinger et al., 2012). SN 2005ip appeared to be similar to a 1988Z-like object (Stritzinger et al., 2012). The 1994W-like objects show a light curve with a plateau phase around 100 days which is followed by a sudden drop in luminosity (Stritzinger et al., 2012). The very luminous IIIn SN have magnitudes of $M_V \approx -22\text{mag}$ and they are generally thought to need one or maybe two very dense shells of CSM arising from eruptions shedding the progenitor star of excessive amounts of mass, and it often points to an LBV as progenitor (Stritzinger et al., 2012). It is, however, not all type IIIn SN that needs LBV stars as progenitors, both RSG and dusty type Ia explosions have been considered as progenitors (Smith, Hinkle & Ryde, 2009) (Smith, Mauerhan & Prieto, 2014). The type IIIn event might originate from Ia explosions that have a dense CSM around it or it may be due to electron capture SN¹ of stars that have masses in the range $8 - 10M_{\odot}$ and which comes from RSG with dense winds (Smith, Mauerhan & Prieto, 2014).

Two implications from assuming that IIIn origins from stars of higher masses than what is needed for type II-P is, that first the stars would not shed all of their hydrogen envelope before explosion as was otherwise previously suggested (Langer, 2012). The second implication is, that it is not all massive stars that contract silently into a black hole as was previously suggested, but instead explode as very luminous SNe (Langer, 2012). It may be unknown what leads to these luminous explosions and whether it is still the neutrino driven winds that are the essential part, or if

¹Electron Capture SN (ECSN) arise when a star with a core of ONeMg reach the Chandrasekhar limit ($1.4M_{\odot}$). The Mg and Ne the have electron capture, which triggers a collapse before O and Ne are ignited (Smartt, 2009)

rotation and magnetic fields play a more important role in these explosions (Langer, 2012).

Often dust formation occur at around ≈ 600 days after SN explosion, because the dust forming material needs to be cold enough for dust to form. There have, however, been some evidence that dust formation occur much earlier in type II_n supernova, e.g. in 2005ip or 1998S (Gall, Hjorth & Andersen, 2011). This dust formation take place in a post-shock shell (Gall, Hjorth & Andersen, 2011). More on dust formation in section 6.1.

Type II_n SN often shows warm dust signs, which comes from the possibility for dust formation in the cold dense shell (CDS) and from the dense CSM which is being illuminated by the interaction with the SN forward shock (Fox et al., 2011). Type II_n also show infrared dust emission, IR-emission. The IR emission could come from the CSM being heated by the interaction with forward shock or from dust formation in a CDS, but it is most likely from a heated CSM by the radiation from the forward shock and CSM interaction (Van Dyk, 2013). When the forward shock hits the CSM, kinetic energy can be converted to radiation, and this could explain why type II_n are some of the most luminous SN detected (Mauerhan & Smith, 2012).

5 Possible progenitor stars

There are several possible progenitor stars for type II_n SNe and for type II SNe in general. Since the type II_n classification is purely based on the lines that appear in the spectrum, it is not necessarily a definition of the physical nature of the explosion, whether it is thermonuclear or a core-collapse (Leloudas et al., 2013). Type II_n is thought to be a core-collapse events with progenitor stars suffering from mass loss before the explosion (Leloudas et al., 2013) (Stritzinger et al., 2012). Mass loss has a significant influence on the late evolutionary stages of massive stars. Mass loss has an effect on the mass of the star, the convective core, temperature of the core and luminosity over time (Smith & Owocki, 2006). Because of the temperature and luminosity effect, mass loss influence where the star is found on the HR-diagram before SN explosion. Late time stellar evolution thus have an effect on the type of SN explosion that occur, and a study of the different CCSN and their remnants therefore lead to more knowledge on their progenitor stars (Arcavi et al., 2010). Some of the possible progenitor stars for type II events are RSG, LBV and WR-stars which are all massive stars.

It is sometimes hard to determine the properties of high mass stars, and determine the correct progenitor because massive stars move at almost a constant track on the HR-diagram and may be at very different evolutionary phases even though they appear at almost the same point in the HR-diagram (Smith, Vink & de Koter, 2004). Two important consequences of mass loss in massive stellar progenitors are that it affects the evolution of the star and it chemically enriches the ISM through stellar winds (Lamers, 2013).

Generally the difference in the different types of SN spectra and light curves are due to the properties of the progenitor stars, such as the mass, the radius or chemical composition of the star and envelope (Langer, 2012). Furthermore the explosion energies and geometries of the ejecta is also thought to be dependent on the progenitor star properties, such as the rotation, the mass and the magnetic field of the star (Langer, 2012). Below is given a description of three types of possible progenitor stars for CCSN.

5.1 Red Super Giant

Supergiant stars are defined as stars in the luminosity class I in the MK system (Langer, 2012). The luminosity is a way to divide stars into different classes in the Hertzsprung-Russel (HR) diagram. On Fig. 6 stars at different stages on the main sequence is divided into different classes according to luminosity. The most massive and luminous of stars are supergiants and they are further divided into e.g. RSG, Blue supergiants, LBV and WR stars (Langer, 2012). Fig. 6 only show star with masses up to $10M_{\odot}$, but the evolutionary track is similar to that of stars with higher masses. The higher mass stars have a flatter HR-diagram curve and the stellar lifetimes become shorter with increasing mass. The flatter HR-diagram curves can e.g. be seen on Fig. 7.

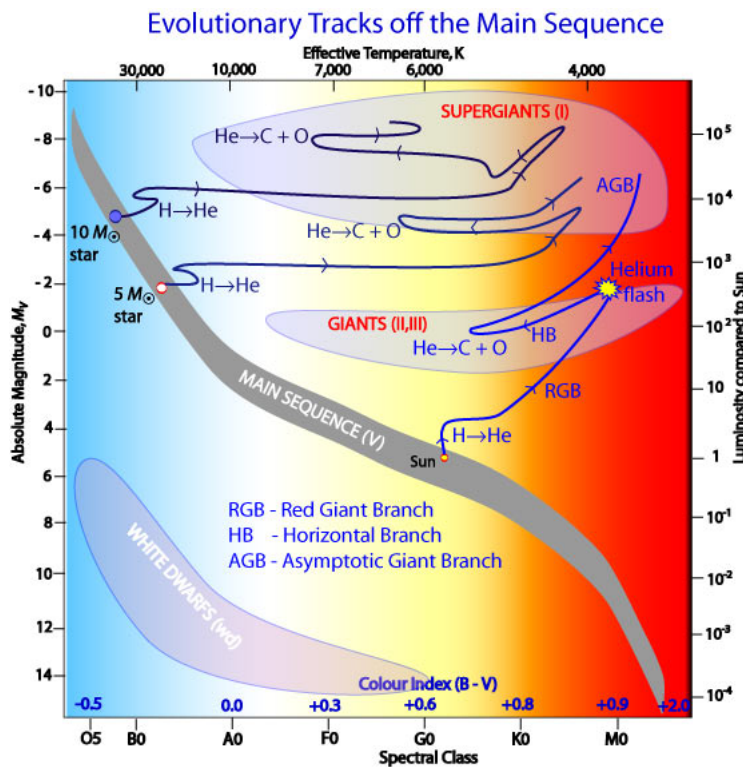


Figure 6: This figure shows the evolutionary track of the sun, a $5M_{\odot}$ star and a $10M_{\odot}$ star. Figure source: Australian Telescope National Facility (2014)

Stars with masses between $8 - 30M_{\odot}$ are thought to become RSG stars at the

end of their lives (Smartt, 2009) (Groh, Meynet & Ekström, 2013). This is the stars that at near solar metallicity are below the lower mass limit for LBV stars (Langer, 2012).

There is a problem with the mass range for RSG stars and there is a lack of RSG with masses between $17 - 30M_{\odot}$ when comparing with the stellar population of the Local Group (Smartt, 2009). One solution to this could be that the stars above $17M_{\odot}$ form type IIn, II-L and Ib/Ic SN and therefore the stars above this mass move on in the H-R diagram to become LBV or WR stars, as seen on Fig. 7. RSG stars are often associated to be the progenitor stars of type II-P SNe, described in section 4.2.1 (Smartt, 2009). If the pre-supernova mass loss was severe enough, the RSG star could, however, be a possible progenitor for type IIn SNe (Smith, Hinkle & Ryde, 2009). The star VY CMa is an example of a RSG that could be a possible progenitor for type IIn SN. VY CMa is a well-studied example of a RSG with severe mass loss and therefore with an unusually dense CSM, which makes it a candidate progenitor for type IIn SN (Smith, Hinkle & Ryde, 2009). The dense CSM in VY CMa is thought to have formed over the last 1000yrs by massive eruptions (Smith, Hinkle & Ryde, 2009). The wind speeds of RSG stars are of tens of km yr^{-1} and they have a mass loss rate around $\leq 10^{-5}M_{\odot}\text{yr}^{-1}$ (Kiewe et al., 2012). The RSG phase is thought to last for about 0.4Myr for a $25M_{\odot}$ star and around 2Myr for a $10M_{\odot}$ star (Gall, Hjorth & Andersen, 2011).

5.2 Luminous Blue Variables

The most massive stars will at some point pass through a LBV phase. Theoretically all stars above $8M_{\odot}$ become RSG, blue super giants (BSG) or WR stars (Groh, Meynet & Ekström, 2013). Some theories states, that RSGs evolve to eventually become WR stars, but very high mass stars ($40 - 50M_{\odot}$) and luminosities of $\log(L_{\star}/L_{\odot}) = 5.8$ does not reach the RSG phase, as seen on Fig. 7. Instead undergo a phase with severe mass loss where the star loose most or all of its hydrogen envelope. This phase is the LBV phase (Smith & Owocki, 2006) (Smartt, 2009). In other words, the LBV phase is often suggested to merely be a a transitional phase to WR stars (Groh, Meynet & Ekström, 2013). More generally stars with masses above $20M_{\odot}$ undergo the LBV phase (Gall, Hjorth & Andersen, 2011).

LBV's are characterized by powerful and massive eruptions and show S-Doradus variability. The mass loss rates of LBVs are of $\sim 10^{-2}M_{\odot}\text{yr}^{-1}$ (Kiewe et al., 2012). LBV's are phenomenologically determined (Groh, Meynet & Ekström, 2013). During the mass loss, most of their hydrogen, and at times also their helium shell, is ejected (Smartt, 2009) (Smith & Owocki, 2006). During the phase where the stars throw off H or He layers, and thus throw of a lot of mass, they might show unpredictable variability, and are observationally defined to be hot, unstable and suffer irregular eruptions, much like S-Dor, AG Car, P-Cyg or η Car (Langer, 2012) (Smartt, 2009) (Crowther, 2007) (Bohannon, 1997). LBVs are therefore also called S-Doradus stars or Hubble-Sandage variables (Smith, Vink & de Koter, 2004) (Langer, 2012) (Smartt, 2009). Because LBV stars show strong mass eruptions,

they will create an often widespread CSM (Smartt, 2009)(Langer, 2012). LBV's are thought to be progenitors of type IIIn SN because of their CSM and the possibility that the forward shock collides with the CSM (Smith, Mauerhan & Prieto, 2014). LBV stars have furthermore observationally been suggested to be progenitors of type IIIn events (Groh, Meynet & Ekström, 2013).

When the core of a massive star is hydrogen exhausted it often expands to the supergiant branch or rather the red supergiant branch. Some luminous stars may reach their Eddington limit² before they are completely hydrogen exhausted, which would happen when they were expanding towards a cooler surface temperature (Langer, 2012). When stars reach their Eddington limit while evolving on a thermal time scale, it is thought that the stars then undergo mass loss events, and this is generally the idea of what happens to LBV stars, because they are very close to the Eddington limit in the HR-diagram (Langer, 2012).

LBV's usually have luminosities of around $5.5 < \log(L/L_{\odot}) < 6.0$ (Smartt, 2009). The largest of this type of stars will have initial main sequence masses of $80 - 120M_{\odot}$ (Smartt, 2009). It is their position on the HR-diagram that suggests that they are either H or He burning stars, which have evolved off the main sequence (Smartt, 2009). Fig. 7 shows an H-R diagram where RSG, LBV's and WR stars are seen in their different evolutionary stages.

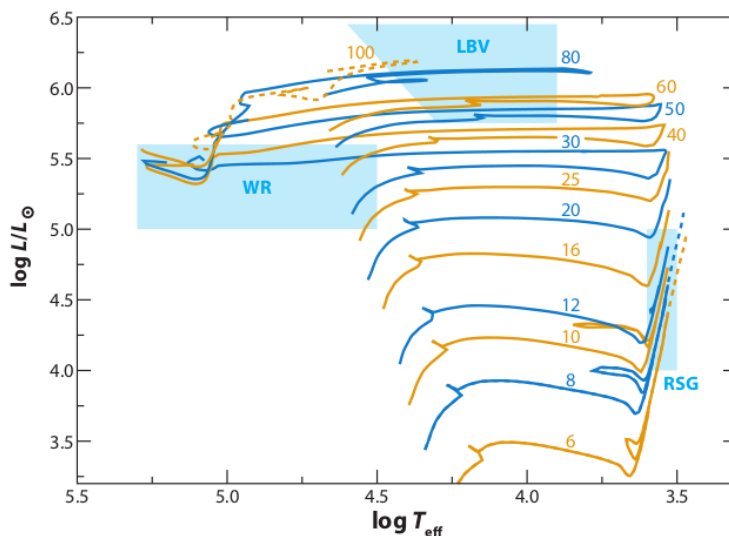


Figure 7: This figure shows an H-R diagram where Red Super Giants, Luminous Blue Variables and Wolf-Rayet stars are shown. It can be seen that the most massive stars appear to become LBV's, and WR stars and the least massive RSG. Figure source: Smartt (2009).

Their evolution and mass would suggest that LBV's collapse into black holes at a supernova explosion, given that they do not evolve further to becoming WR-stars (Smartt, 2009). In more recent years there have been several observations of

²The Eddington limit is the maximum luminosity a star can obtain and still be in hydrostatic equilibrium (Maeder et al., 2012).

very bright supernovae which were observed to have a CSM or a "photosphere-like" medium surrounding them that were of order 150AU in radius and had a mass of $10 - 20M_{\odot}$ (Smartt, 2009). This CSM or photosphere is too large to originate from a RSG and it is therefore thought that it may arise from eruptions of an LBV (Smartt, 2009).

The possible steps taken from a main sequence star to a SN, that it thought to have the LBV phase as progenitor, is the following two. It is for stars of masses $M_{\star} = 20M_{\odot}$ and $M_{\star} = 25M_{\odot}$:

- $20M_{\odot} := 7.5V \rightarrow BSG \rightarrow RSG \rightarrow BSG/BHG \rightarrow LBV \rightarrow SN$ (Groh, Meynet & Ekström, 2013)
- $25M_{\odot} : O6V \rightarrow OSG \rightarrow RSG \rightarrow OSG/WNL \rightarrow LBV \rightarrow SN$ (Groh, Meynet & Ekström, 2013)

Where BHG is a blue hypergiant and OSG is an O-supergiant, and the WNL is a late time WN star, which is a type of WR-stars (Groh, Meynet & Ekström, 2013).

5.3 Wolf-Rayet stars

WR stars are evolved massive stars that does no longer have any envelopes of H or He. These have been lost during radiatively driven winds or through LBV like outbursts (Smartt, 2009). They therefore have a high mass-loss rate and are thought to arise from stars of $M_{\star} = 25 - 30M_{\odot}$ or of higher mass (Smartt, 2009) (Gall, Hjorth & Andersen, 2011). WR stars can be divided into several subtypes that depend on the lines present in the spectra of the star. If nitrogen is present, then it is a WN-star and if carbon is present it is a WC star (Langer, 2012). It was previously thought that all WR star were completely hydrogen deficient, but it has recently become clear that very luminous and massive main sequence stars may be late time WR stars, with a Helium surface that is not enhanced, and therefore still containing some hydrogen (Langer, 2012). WR stars may become type IIb SN or Ib/c SN (Smartt, 2009) (Gall, Hjorth & Andersen, 2011). Another possibility is, that the neutrino driven and core-bounce driven explosions are not possible for stars above $25M_{\odot}$ and they therefore just quietly collapse to form a black hole without a SN explosion (Smartt, 2009). It is however not entirely well known which type of SN the WR stars become since they have not been observed directly as progenitors of SN (Groh, Meynet & Ekström, 2013). The WR phase last for about 10^5 yr (Gall, Hjorth & Andersen, 2011).

6 Dust

Dust in the universe is what essentially determine the type of stars formed. Dust controls the physics and chemical conditions in the interstellar medium (ISM) and the formation of stars in molecular clouds (Kozasa et al., 2009). Astrophysical dust is a mixture of particles that have different sizes, shapes and compositions, and it

accounts for only about 1% of the total interstellar mass (Elias-Rosa et al., 2007). There are two possible main dust producers namely AGB stars and SN (Gall, Hjorth & Andersen, 2011). In the local universe the AGB stars have long been known to produce dust during their late stellar phases, but there is, however, a problem with the AGB stars when looking at dust formation in the early universe. AGB stars have lifetimes of order of 10^9 yr, just as our sun (Freedman, Geller & Kaufmann, 2011). The problem with AGB stars is therefore, that their long life times means that they cannot be dust producers in the early universe, at high redshift, thus more massive stars with shorter lives must be the main dust producers (Van Dyk, 2013). Massive stars end their short lives in great explosions as SN, and they are possible dust producers at high redshift, but also in the current universe (Gall, Hjorth & Andersen, 2011) (Smith et al., 2012). SN as early dust producers also fit with the initial mass function (IMF) which is biased towards high mass stars (Gall, Hjorth & Andersen, 2011). This is why SNe are interesting to examine, both at high redshift, but very much so also in our local universe.

6.1 Dust formation

Different types of SNe forms dust in very different ways (Gall, Hjorth & Andersen, 2011). All CCSN types have in common that the majority of dust production happens at the end of their evolution and after the supernova explosion (Gall, Hjorth & Andersen, 2011). SN 1987A was one of the first SN where emission line symmetries were observed developing and where dust formation was proved (Mauerhan & Smith, 2012). Dust in CCSN have been observed, however, it is only small amounts of dust that is observed, it may even be less than or around $1.0 \cdot 10^{-3} M_{\odot}$. This is less than what is expected and needed to contribute to the amount of dust in the ISM (Kozasa et al., 2009).

The amount of dust and what kind of dust is created and ejected into the ISM by the SN or pre-SN star depends on the formation of dust in the ejecta and on the interaction and destruction of dust in the SN remnant and by the forward and reverse shock in the CSM (Kozasa et al., 2009). Dust can form through different chemical reactions where molecules and atoms in the gas phase combine, and the molecular composition is what determines the kind of dust formed (Gall, Hjorth & Andersen, 2011). Dust forms in cold gas, which is, in the case of SN, in the out-flowing region, or possibly between the reverse and forward shock (Kozasa et al., 2009).

There is one problem with dust formation in the local universe, and the types of SN typically present. The most common CCSN is type II-P and this type is only observed to have formed $4 \cdot 10^{-5} M_{\odot}$ dust, where the needed amount is closer to be of order $\approx 1 M_{\odot}$, which is why types such as IIIn are interesting to examine, and why it is interesting to examine characteristics of the dust produced. For the Galactic dust, the MRN distribution states a dust size of $a = 0.005 - 0.25 \mu m$ or $a = 0.025 - 0.25 \mu m$ depending on the dust type (Asano et al., 2014) (Mathis, Rumpl & Nordsieck, 1977).

6.1.1 Sign of dust formation

There are a few signs of new dust formation in SNe. One is that IR excess from thermal emission from hot or warm dust is possible or there may be a systematic blueshift of the emission lines (Smith et al., 2012). There may also be a damping of the red wing of lines such as the $H\alpha$ line (Stritzinger et al., 2012). This line can be seen on Fig. 8 for SN 2005ip.

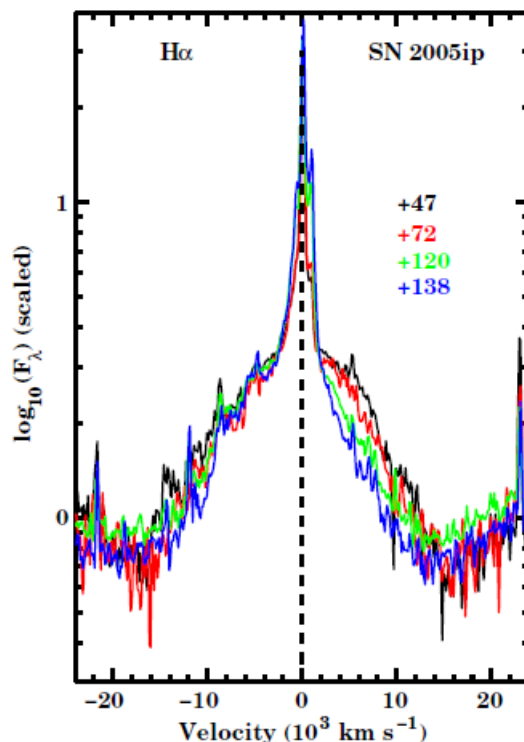


Figure 8: This figure shows the $H\alpha$ line for SN 2005ip, where it can be seen, that with passing time the blue line becomes more and more damped whereas the red line does not change. Figure source: Stritzinger et al. (2012).

The first two of the possible dust formation signs may also come from pre-existing dust in the CSM (Smith et al., 2012). The attenuation of the red wing is caused by being formed around the SN. The $H\alpha$ line arise by the CSM and around the shock wave, and if dust is formed behind the forward shock wave, then the light that is seen moving towards us will have gone through a layer of dust and is then suppressed as in Fig. 8. The possible place that this dust form is in a CDS, between the forward and reverse shock (Smith et al., 2012). The dust could also have formed in the ejecta of the SN (Smith et al., 2012), and both possibilities could block the receding side of the CSM (Smith et al., 2012).

There is a possible alternate explanation for the damped red wing. It is possible that it was due to electron scattering which is responsible for the broadening of the lines and which could lead to the asymmetry of the line profile (Fox et al., 2011). But it is still very likely that it is ongoing dust formation that is the reason for the suppression of the red wing.

6.1.2 Where and when is dust formed?

Type II_n supernovae are thought to produce dust, and this type of SN might even show indications of very early dust formation (Stritzinger et al., 2012). One theory for where this early dust is formed is in a CDS which is just behind the forward shock, and right after the reverse shock has propagated through the medium (Stritzinger et al., 2012) (Fox et al., 2011) (Smith et al., 2012). An overview of where dust formation would take place is shown in Fig. 9.

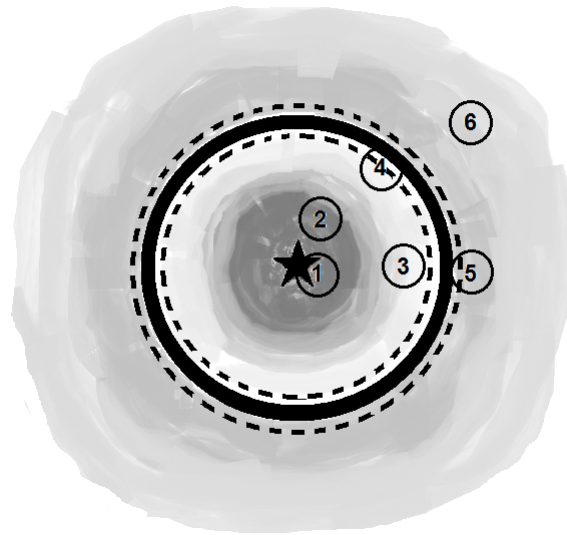


Figure 9: This figure shows the CDS in the SN environment. The numbers described the different parts of the post SN environment. 1) is the remnant of the SN, 2) is the SN ejecta, 3) is the reverse shock, 4) is the CDS, 5) is the forward shock moving out through the CSM and 6) is the unshocked CSM. The lines observed originate from different places in the SN. the broad lines come from the ejecta, the intermediate lines are from between the shock fronts, from the CDS, and the narrow lines come from the unshocked CSM.

There have been observed newly formed dust in most SN ejecta, although of different masses, but there have not been observed any dust in type Ic SN, and it is also very unlikely that it has been observed in type Ia SN (Smith et al., 2012). Dust in the CDS could possibly be formed very early, which have been observed in type II_n SN, e.g 2005ip, 1998S, 2006jd, 2006tf and 2010jl (Stritzinger et al., 2012) (Smith et al., 2012) (Gall et al., 2014). In some of the II_n SN the dust formation is very early, as early as 30 days, which is similar to what is seen for SN 2005ip, where dust formation is around 55 days (Stritzinger et al., 2012) (Smith et al., 2012). Dust formation would otherwise only happen approximately 100 days after SN explosion, because the regular dust theory is that dust forms in the ejecta, and it needs to be cold enough for dust formation to happen. It does, however, seem that a dense radiative shock provides a mechanism for rapid cooling, which would explain the dust formation in the CDS (Smith et al., 2012). The dust that is formed in SN have been found to be around $10^{-4}M_{\odot}$ for hot dust (500-1000K), but there is also the large amounts of cold dust ($< 50K$) that have been observed (Gall, Hjorth & Andersen, 2011). When the dust grains have formed, they may suffer from both erosion and destruction in the gas between the forward and reverse shock, and it

is this process that will eventually determine how much dust will reach the ISM (Kozasa et al., 2009).

6.1.3 Shock physics and CDS

When a SNe explodes it creates a forward propagating shock wave which interacts with the surrounding CSM, and there will thus presumably be created a reverse shock wave (Kiewe et al., 2012) (Mauerhan & Smith, 2012). Between these two, it is possible for dust to form, because the interaction slows down the blast wave and a dense shell is then formed (Kiewe et al., 2012). To understand what happens after and when a shock wave goes through a medium it is crucial to understand what a shock wave is and how it affects its surrounding environment.

A Shock wave can be defined to be a disturbance often propagating through a medium, where it has a faster speed than that of the medium it goes through (Draine, 2011). The shock wave leads to irreversible changes, e.g. increase in entropy, which means that heat is induced into the system of the collision between the shock wave and the medium (Draine, 2011). For a SNe this would mean that the surrounding media and the mass cast of in the SN process is heated when the shock wave propagates through. Early dust formation is a possibility because the very high density in the radiative post-shock layers allow the gas to cool very rapidly and thus allow for early dust formation to occur (Smith et al., 2012). For a shocked medium to cool radiatively the shock needs to be steady and propagate long enough, so that the medium is able cool (Draine, 2011).

Dust formed in CDS have been directly observed in types IIn and Ib SN (Kozasa et al., 2009). Dust formation in the ejecta can still occur in type IIn SN, but it will be at a later time (Kozasa et al., 2009). So the dust formed in a CDS is a possible explanation for the early dust production in type IIn SN (Mauerhan & Smith, 2012) (Smith, 2013). The CDS, SN ejecta and the forward and reverse shock is sketched in Fig. 9.

6.2 Interstellar extinction

The presence of interstellar dust was first recognised because of its reddening effect on the light from distant stars (Tielens, 2005). The colour excess is given as the difference between the extinction in two different photometric bands (Tielens, 2005). It is often the B and V band that is used, which is also what is used through this thesis. The colour excess is given by (Tielens, 2005):

$$E(\lambda_1 - \lambda_2) = A_{\lambda_1} - A_{\lambda_2} = A_B - A_V = E(B - V) \quad (1)$$

It is the Johnson photometric system that is used here. Extinction will generally increase as the wavelength decrease, and it is therefore called reddening. The total-to-selective extinction is defined by Tielens (2005):

$$R_V = \frac{A_V}{E(B - V)} \quad (2)$$

The mean value of R_V in the Milky Way is $R_V = 3.1$ (Tielens, 2005), and it is generally the case, that if $R_V \approx 3.1$ then the grain sizes of the dust examined corresponds to a diffuse ISM, and if $R_V \approx 4 - 6$ then it corresponds to dense molecular clouds (Tielens, 2005). R_V is not a direct measure of the dust grain size (a). It is a measure of the inclination of the extinction curves. However, high values of R_V give shallow extinction curves and low values of R_V gives steep inclinations of extinction curves. Steep extinction curves are believed to indicate small dust grains.

7 SN 2005ip

In the following sections the light curve data for SN 2005ip have been examined and different models have been fitted in order to find the total-to-selective extinction ration, R_V , which is then calculated for each of the models.

SN 2005ip is a type II_n supernova that show clear evidence of narrow line emission (Smith et al., 2009) (Stritzinger et al., 2012). SN 2005ip was discovered on 2005 November 5.2 UT in the Scd galaxy NGC 2906, with a Julian date of discovery of 2453679.66JD (Boles, Nakano & Itagaki, 2005) (Smith et al., 2009) (Stritzinger et al., 2012). The luminosity distance to the galaxy is found to be 29.7Mpc or equivalent to an apparent redshift of $z = 0.007$ (Smith et al., 2009). It is suggested that the SN exploded about 8-10 days prior to discovery, but it is by no means certain (Stritzinger et al., 2012). The galaxy and SN can be seen on Fig. 10 and the SN is indicated by the red markers.

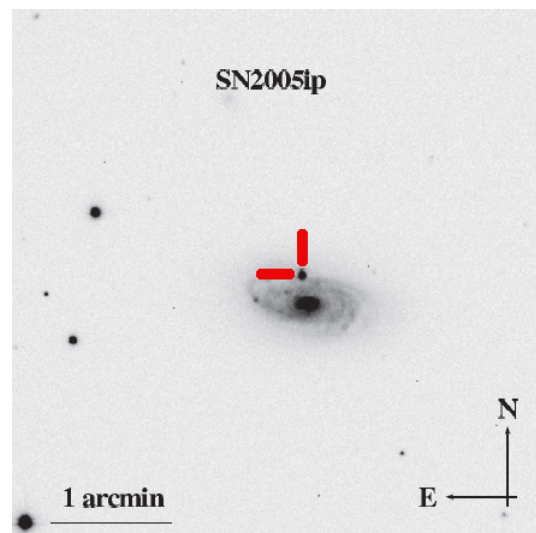


Figure 10: The images shows SN 2005ip indicated in the host galaxy NGC 2906. The image is taken with Swope telescope in the V-band. Figure source: Stritzinger et al. (2012).

The progenitor star of SN 2005ip is very likely a LBV, but it is not certain, since the progenitor was not observed prior to the explosion. The progenitor could thus also be a RSG or any other star where mass loss occurs before explosion (Stritzinger et al., 2012) (Gall, Hjorth & Andersen, 2011). There are, however, some things that

point to an LBV as the progenitor. The wind speed measured from the P-Cygni profile is around 100kms^{-1} and this correspond to LBV eruption wind speeds (Fox et al., 2010). Another possible progenitor is RSGs, but these only have wind speeds of around $20 - 40\text{kms}^{-1}$, which is too low in the case of SN 2005ip (Fox et al., 2010). SN 2005ip appeared to show similarities with SN 1988Z like objects, as described in section 4.2.3 (Stritzinger et al., 2012). This means that the SN shows similar early and late time spectra to SN 1988Z (Stritzinger et al., 2012). SN 1988Z also showed interaction between the SN and the CSM (Stritzinger et al., 2012). Through the interaction between the SN and CSM dust formation in a CDS may occur as described in section 6.1.2 and 6.1.3. This is thought to be the case for SN 2005ip, because early dust formation, as early as 55-60 days, have been confirmed (Stritzinger et al., 2012) (Fox et al., 2011) (Smith et al., 2009).

7.1 Light curves

The light curves of SN 2005ip originate from the Carnegie Supernova Project (CSP) (Stritzinger et al., 2012). SN light curves display the evolution of the energy release by the SN. On Fig. 11 the light curves of 2005ip are seen, and all have a drop off at $t \approx 50$ days after discovery, which is where dust is believed to form, see section 7 (Stritzinger et al., 2012) (Smith et al., 2009). Another evidence of dust is described in section 6.1.1, which is the suppression of the $H\alpha$ lines, which show a damping between 47-72 days after discovery (Stritzinger et al., 2012). The light curves presented are broadband UV, optical and NIR photometry, which means that they represent the u , B , g , V , r and i -bands (Stritzinger et al., 2012). SN 2005ip was observed over a period of 5.3 years from about 4 days after discovery (Stritzinger et al., 2012).

The overall evolution of the light curves seem to be dominated by a sharp drop in luminosity very early on, before 20 days, after which a more constant luminosity period follow. At around 55-60 days there is a drop in luminosity, thought to origin from new dust forming. The drop off continues until 150-200 days after discovery. Almost at present time there are only very few data points and it is thus not clear how the light curves behave from 200 days to present time. The full light curves are shown in appendix 12.3. The phenomena where the light curves drop off is expected to be due to new dust forming in a CDS (Stritzinger et al., 2012). The bump on the light curves could either be photometric errors or something to do with the structure of the SN explosion. The bumps does not appear to be due to a full moon, so it may be due to the SN sending "shells" of material out from the SN centre. It is, however, not certain what causes the bumps. **TJEK with the moon position!**

It should be noted that one point have been removed from the bands B , g , V , r and i . This is because for this specific point, at the time of 3815.62JD, there is no data for the u -band. Since all the bands at all times are needed for the following models, this point, for the remaining bands, have been left out. In appendix 12.8 the missing points are seen for the various bands. It is seen overplotted with a linear fit to both the data used, and the data including the otherwise missing point, and

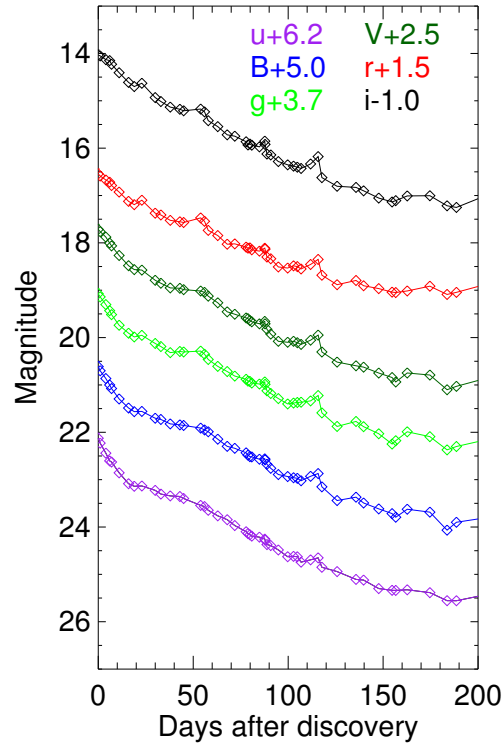


Figure 11: This figure show a plot of the light curves of SN 2005ip in the six bands, u , B , g , V , r and i . It is seen that the light curves have a drop in magnitude after about 55 days, and that this is most prominent in the u -band and least in the i -band. This drop off is thought to occur due to dust formation.

this does not give any difference in the linear fit, and would therefore not give any difference in the final calculation of R_V , because, as the next sections will describe, the fit is used to find R_V . R_V is the total-to-selective extinction ratio as described in section 6.2.

The following sections will be a description of how dust formation can be examined from looking at light curves, and a discussion of different models, that assume how the light curves would evolve had there been no dust, and therefore no drop off around 55-60 days, is shown.

8 Extinction curve calculation for SN 2005ip

If dust was not formed, it is assumed that there would not be a drop in the light curves, and the light curves might have continued as before $t \approx 50$ days with a different evolution, e.g. a linear decline. Assuming a model for how the light curve would appear, had no dust formed, may give an idea about the dust that is formed and an idea about the SN evolution. If a model for no dust production is assumed and fitted to the light curve, it may be used to calculate the extinction and R_V , which is an indirect measure of the dust grains size. Different models and the results they yield are presented in the following sections.

8.1 Linear fit

The light curves are examined by making a fit to $25 \leq T \leq 45$ days after discovery, where T is the time after SN discovery. The fit is made to these times because those are the times just before the light curves drop off, and thus assumed to be an indicator of how the light curves would behave without dust formation. This fit is then extrapolated to continue over all days. The first model that will be assumed here is a linear model. With this model it is assumed that the light curve would simply fall off with a linear decline, had there been no new dust formation to obscure the light. The equation used for the fit is eq. 3.

$$M = p_1 + p_2 \cdot T^B \quad (3)$$

In eq. 3, p_1 and p_2 are free parameters. The third parameter, B , is set to be $B = 1$ for a linear model. The B parameter is chosen to be introduced, so that the same formula for the fit may be used with a different B value for different models. The B parameter is always a fixed value. B determines how steep the decline is, a low B means a decline that bends of. The linear fit to the light curves are shown on Fig. 12, and light curves for different B models is seen in Appendix 12.5.

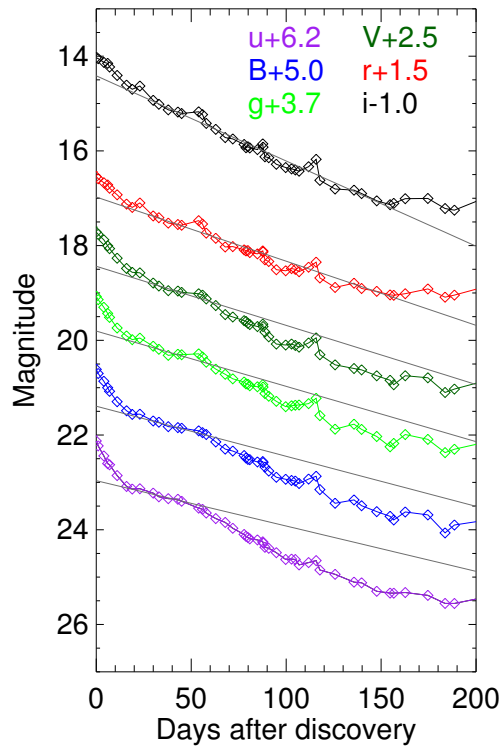


Figure 12: This figure shows a linear fit ($B = 1$), grey line, to each of the six photometric bands used. There have been added numbers to each of the bands, so that they do no overlap. There have been fitted to $25 \leq t \leq 45$.

On Fig. 12 it is seen, that the fit to the light curves remains above the light curves for the blue bands, but for the red bands, a linear fit is not optimal since it falls below the light curves. It is also seen on Fig. 12 that for the red bands the

linear fit only matches up to about 150 days past discovery, and then it becomes so steep, that it falls below the light curve which will mean a negative extinction, which is not physically possible. This is why only the first 200 days past discovery is examined. A figure showing the light curves plotted over a larger time interval can be seen on Fig. 40 in Appendix 12.3. Fig. 12 show the light curves without any observational errors. To find the proper errors for the fit and for the following calculation of the SN extinction, Monte Carlo simulation has been used.

8.1.1 Monte Carlo simulation

Monte Carlo simulations is used for re-sampling data sets around the original data, to give an estimate of errors through out the following sections and calculations. The Monte Carlo Method is structured so that there is a data set for which fitted parameters are known, and it is known how this data set evolves (Press et al., 2001). Within the parameters known for the data set, the data is re-sampled and simulated by creating random numbers from the same distribution as is known for the original data set and which describe how the original data evolve (Press et al., 2001). If the specific parameters for the data set is not known, it is not possible to use a regular Monte Carlo method, but instead a simpler and quicker method, the Bootstrap method is used (Press et al., 2001). The Bootstrap method uses the original data set with a number, N , of data points, and then generate a number, n , of synthetic data sets of N points, in a distribution around the original data set (Press et al., 2001). The Bootstrap method uses replacement so that the original data is not the only data set found in the re-sampling (Press et al., 2001).

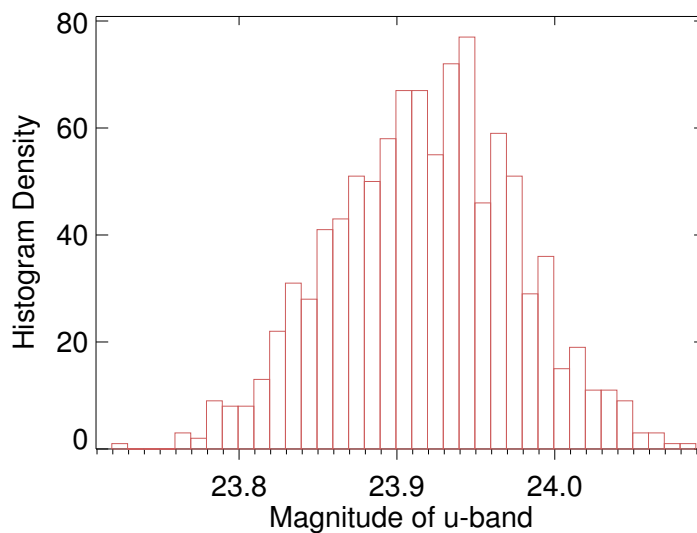


Figure 13: This figure shows the histogram of the re-sampled light curve fit at 99 days after discovery in the u -band. On the figure it is seen that it is the full, within 3σ , distribution, that is re-sampled, and it appears to be approximately normally distributed. The median point, when points outside of 1σ is removed, is 23.92, and the minimum and maximum values are 23.86 and 23.98 respectively.

For the light curve data points, there is not enough knowledge of the evolution

of the light curves to use regular Monte Carlo, so the Bootstrap method is used. The N data points in each of the light curves are re-sampled $n = 1000$ times. The n number of synthetic data is simulated by creating random numbers in a distribution around the original data set. The distribution assumed is a normal distribution, and the confidence limit is chosen to be 3σ , which means that the synthetic data is simulated within 3σ in a normal distribution around the original data. This normal distribution, for the u-band at 99 days past discovery, is seen in Fig. 13. The re-sampled light curves, re-sampled within 3σ , with the corresponding linear fits are shown in Fig. 14.

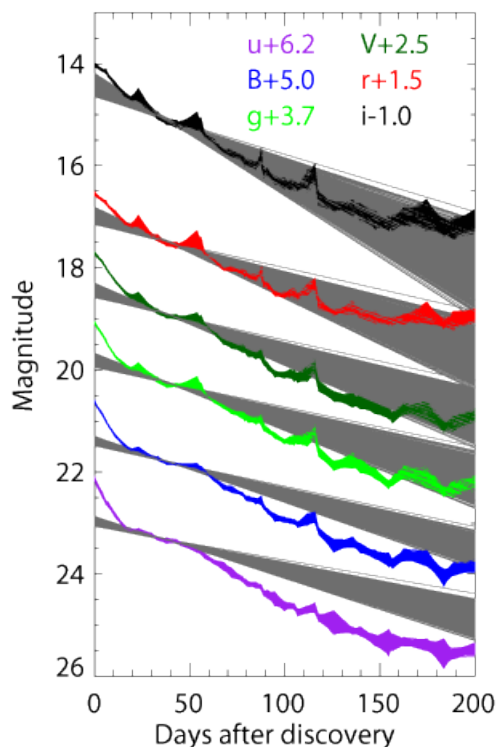


Figure 14: This figure shows the light curves re-sampled $n = 1000$ times, and the corresponding fits, which is also $n = 1000$ fits, within 3σ . The figure again shows the linear fit with $B=1$.

In Fig. 14 it is clearly seen how the data is now normally distributed. When the extinction is calculated in the next sections, then there is calculated n extinction curves and the distribution of these curves are equivalent to the error on them, again within a 3σ limit.

8.1.2 Extinction curves

The extinction curves over time of SN 2005ip in the six different photometric bands are created from the difference between the light curve data and the fitted model, in this first case the linear fit. Eq. 4 shows the equation used to find the extinction for the SN.

$$A_\lambda = \text{Light curve} - \text{fit} \quad (4)$$

The extinction curves are a measure of how much light is removed by a dusty media between the light source and the observer (Draine, 2011). In 1910 it was realised that some stars were dimmed by a medium absorbing light (Draine, 2011). The extinction is a term for both scattering and absorption of light from a source (Draine, 2011). In Appendix 12.5.1 the extinction vs. time is shown with an artificial spacing to show the full range of the light curves extinction for all bands examined.

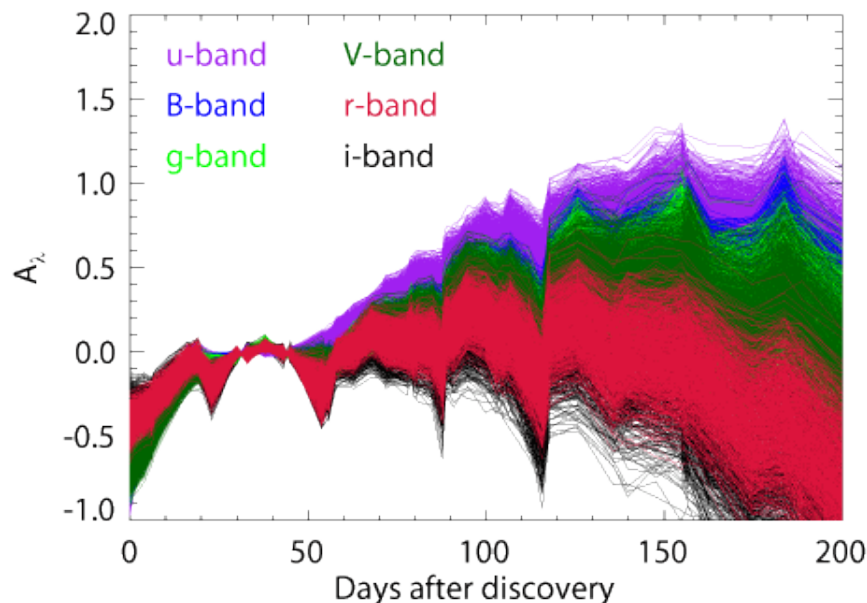


Figure 15: This figure shows the extinction data over time. It is seen that the extinction is overlapping a lot. Here it is for the linear model with $B = 1$.

On Fig. 15 the extinction data over time is seen. The extinction is about zero and below up to 50 days after discovery, where the extinction begins to increase. All the bands increase until after about 150 days, where the initial fit made to the light curves is no longer a good fit, and the extinction therefore decrease. It is expected that the extinction grows with time, and when it falls of after some time this may be because the fit to the light curves are not optimal, and it is therefore relevant to examine other possible fitting methods. These are examined in section 8.2. The data are affected by the dust in the MW. The extinction calculated therefore needs to be corrected for the Galactic reddening. The Galactic reddening comes from dust in the Galaxy, the Milky Way (MW), and this can be corrected for as described in the following section 8.1.3.

8.1.3 Galactic reddening

For the SN 2005ip the Galactic colour excess, reddening, is $E(B - V)_{MW} = 0.047\text{mag}$ (Stritzinger et al., 2012). There have been observed Na I D absorption lines in the host galaxy of SN 2005ip, which suggest that the extinction of the host galaxy is negligible, and so only the MW extinction is taken into account (Stritzinger et al., 2012). This means that the total reddening that needs to be corrected for

is based on the MW having a total-to-selective extinction ratio of $R_V = 3.1$ and $A_V = 0.15\text{mag}$ for the observations (Stritzinger et al., 2012). A mean extinction law is found by Cardelli, Clayton & Mathis (1989), henceforth the CCM model, which can be used to calculate the colour excess and de-redden observations (Cardelli, Clayton & Mathis, 1989). In the CCM model the extinction laws are parametrized by using $R_V = \frac{A_V}{E(B-V)}$, described in section 6.2 (Cardelli, Clayton & Mathis, 1989). The model used in CCM was a good linear fit to $A(\lambda)/A(V)$, which is given as the following linear representation in eq. 5.

$$\langle A(\lambda)/A(V) \rangle = a(x) + \frac{b(x)}{R_V} \quad (5)$$

The coefficients $a(x)$ and $b(x)$ is described by a 7th degree polynomial, as seen in eq. 6 and 7, which are for the Optical or NIR in the wavelength range $1.1\mu\text{m}^{-1} \leq x \leq 3.3\mu\text{m}^{-1}$ and $y = (x - 1.82)$ (Cardelli, Clayton & Mathis, 1989).

$$a(x) = 1 + 0.17699y - 0.50447y^2 - 0.02427^3 + 0.72085y^4 + 0.01979y^5 - 0.77530y^6 + 0.32999y^7 \quad (6)$$

$$b(x) = 1.41338y + 2.28305y^2 + 1.07233y^3 - 5.38434y^4 - 0.62251y^5 + 5.30260y^6 - 2.09002y^7 \quad (7)$$

And the values for u , B , V , r and i bands are shown in Fig. 16.

COEFFICIENTS AND EXTINCTION AT STANDARD OPTICAL/NEAR-IR WAVELENGTHS						
FILTER	$x(\mu\text{m}^{-1})$	$a(x)^a$	$b(x)^a$	$A(\lambda)/A(V)$ for $R_V = 3.1$		
				$a(x) + b(x)/R_V$	SM79 ^b	RL ^c
<i>U</i>	2.78	0.9530	1.9090	1.569	...	1.531
<i>B</i>	2.27	0.9982	1.0495	1.337	1.322	1.325
<i>V</i>	1.82	1.0000	0.0000	1.000	1.000	1.000
<i>R</i>	1.43	0.8686	-0.3660	0.751	0.748	0.748
<i>I</i>	1.11	0.6800	-0.6239	0.479	0.484	0.482
<i>J</i>	0.80	0.4008	-0.3679	0.282	0.281	0.282
<i>H</i>	0.63	0.2693	-0.2473	0.190	...	0.175
<i>K</i>	0.46	0.1615	-0.1483	0.114	0.123	0.112
<i>L</i>	0.29	0.0800	-0.0734	0.056	0.052	0.058

^a Derived from eqs. (2) and (3).

^b From Savage and Mathis (1979) for their adopted R_V of 3.1.

^c From Rieke and Lebofsky (1985) for their adopted R_V value of 3.1.

Figure 16: This table show the values for $a(x) + \frac{b(x)}{R_V}$ for the u , B , V , r and i -bands. Figure source: Cardelli, Clayton & Mathis (1989).

If there is need for de-reddening IR bands, then the $a(x)$ and $b(x)$ would be calculated in eq. 8 and 9, in the wavelength range of $0.3\mu\text{m}^{-1} \leq x \leq 1.1\mu\text{m}^{-1}$.

$$a(x) = 0.574x^{1.61} \quad (8)$$

$$b(x) = -0.527x^{1.61} \quad (9)$$

The values in this thesis is in the optical and NIR bands, so equations 6 and 7 are the ones used to find $a(x)$ and $b(x)$. The value for the g -band is, however, not calculated in the paper by Cardelli, Clayton & Mathis (1989), this is instead calculated here. The calculation is carried out in the following way.

The wavelengths of the bands are from the webpage for the CSP (The Carnegie Supernova Project, 2011) and for the g -band it is $\lambda = 4765.1\text{\AA}$, and in μm^{-1} the wavelength is $2.09\mu\text{m}^{-1}$ and this is then put into the equation for y , so $y = (2.09 - 1.82)$ and this is put into the eq. 6 and 7 to find the values for $a(x)$ and $b(x)$ and this then becomes the values needed to put into eq. 5, and then this gives a correction value of

$$\frac{A_\lambda}{A_V} = 1.1888$$

It is again known, that the mean R_V value for the MW is $R_V = 3.1$ (Cardelli, Clayton & Mathis, 1989). The actual correction then comes, when the extinction calculated in the previous section is what corresponds to A_λ , and this is then corrected by subtracting $A_V \cdot K$, where K is the part of the equation that is $a(x) + b(x)/R_V$, which is a constant. The following is then the correction of the extinction of the different bands, which is subtracted.

$$\begin{aligned} A_u \text{ correction} &= 0.15\text{mag} \cdot 1.569 \\ A_B \text{ correction} &= 0.15\text{mag} \cdot 1.337 \\ A_V \text{ correction} &= 0.15\text{mag} \cdot 1.000 \\ A_r \text{ correction} &= 0.15\text{mag} \cdot 1.751 \\ A_i \text{ correction} &= 0.15\text{mag} \cdot 1.479 \\ A_g \text{ correction} &= 0.15\text{mag} \cdot 1.888 \end{aligned}$$

Here 0.15mag is the magnitude for the V band for the Galaxy (Stritzinger et al., 2012), and the A corrections are the ones used to correct the extinction for the SN in individual bands for the extinction contribution from the MW.

8.1.4 R_V calculation

When the corrected extinction for the SN is found, the total-to-selective extinction ratio, which is described in section 6.2, is then calculated. This is found by examining the B and V bands, and is calculated over all times. On Fig. 17 the extinction for 99 days after discovery is shown, but here only for a re-sample of $n = 10$.

On Fig. 17 it is seen, that the lines are not evenly distributed, that the re-sampled data is crossing. This means that if it is attempted to use the data values for the calculation of R_V then there may be obtained very high or very low and unrealistic values. What is done instead is that a fit to the extinction data is made, and the values for the B and V band from the fit is then used. The equation for the fit is seen in eq. 10. It should be noted that on Fig. 17 the points from the right is u , B , g , V , r and i .

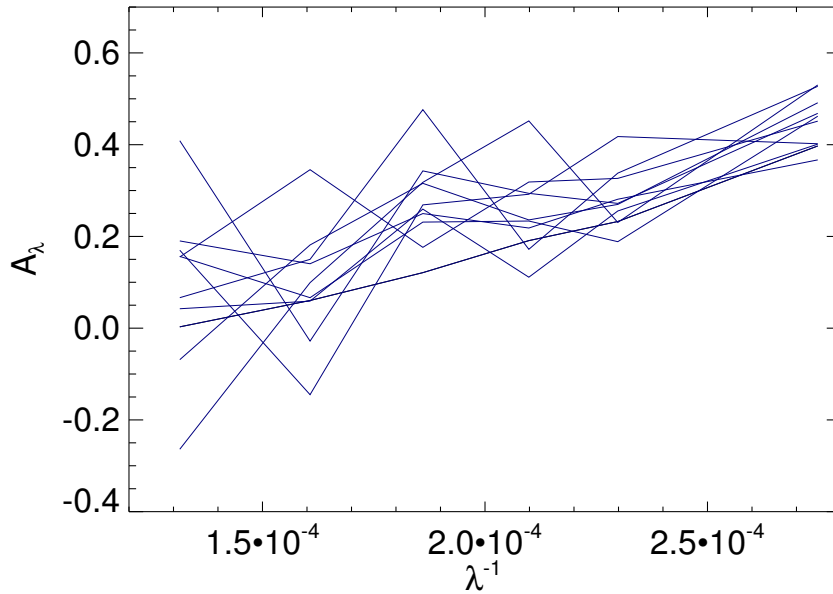


Figure 17: This figure shows the 10 first re-sampled extinction curves. It is seen that the curves are crossing. It is for a time of 99 days after discovery and for the linear model, $B = 1$.

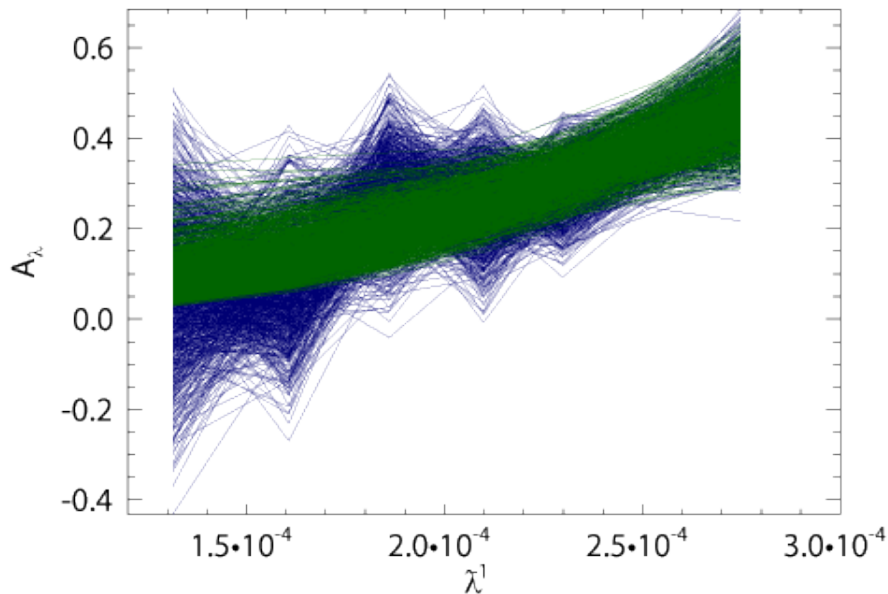


Figure 18: This figure shows the total re-sampled, $n = 1000$, extinction curve at 99 days past discovery. It is clearly seen that the fits (green curve) gives a more smooth distribution of the extinction compared to the data (blue curves) which were also seen in the previous figure.

In Fig. 18 the full re-sampled extinction data set, $n = 1000$, is plotted over λ^{-1} . The blue part of the figure is the re-sampled data and the green part is the fit made to the data. The fit is a power law and is described by:

$$A_\lambda = a \cdot \lambda^\alpha \quad (10)$$

Where λ is the wavelength of the different bands, A_λ is the extinction data, a is a fitting constant set to be positive, and α is also a free fitting constant. It should be noted that the value for α is always negative. α is set to be within $[-3.5; -0.000001]$ where the last number is set so that it is very close to zero. α is set to be in this range because the fit generally converge in this range, and to ensure that the R_V values does not become too physically unrealistic. The wavelengths used is

$$[3639.3, 4350.6, 4765.1, 5375.2, 6223.3, 7609.2]\text{\AA}$$

for the u , B , g , V , r and i band in this order, and it comes from the CSP (The Carnegie Supernova Project, 2011). Before R_V is calculated using the re-sampled data, it is examined what the connection between the R_V and α , from eq. 10 is, to give an example on how the values are connected. This can be shown to be fairly reasonable because the extreme values give very extreme values of R_V , which are not physically realistic. The values are analytically calculated by finding the relation between R_V and α . R_V is then found by the following equation, also stated in eq. 2 in section 6.2.

$$R_V = \frac{A_V}{A_B - A_V} = \frac{a\lambda_V^\alpha}{a\lambda_B^\alpha - a\lambda_V^\alpha} = \frac{\lambda_V^\alpha}{\lambda_B^\alpha - \lambda_V^\alpha} = \frac{5375.2^\alpha}{4350.6^\alpha - 5375.2^\alpha} \quad (11)$$

If the extreme values that are the limits for α is then put into eq. 11, then the range that R_V is within is $[0.912; 4.7 \cdot 10^6]$, where the last number is absolutely not physically relevant, since the values for the MW is $R_V = 3.1$ and for molecular clouds it is around $R_V = 4 - 6$ (Tielens, 2005), see section 6.2. I would therefore expect that the values found is roughly around these values.

The R_V is found for the entire range of 3σ . After these values are found, 1σ deviation have been extracted to give the final error on the total-to-selective extinction ratio. Fig. 44 in Appendix 12.5.2 show two histograms, one with the 3σ re-sampling and one where all outside 1σ have been removed.

The median value of R_V when 1σ have been found is around $R_V = 1.5$. This is a much smaller value of R_V than the value for the MW of $R_{V_{MW}} = 3.1$. It would suggest small dust grains are produced in the CDS of SN 2005ip. Fig. 19 is a plot of R_V over time with error bars that show the area R_V is possibly found within.

Fig. 19 shows reasonably good error bars for most of the points. There are a few outlying points on the figure for R_V , for this model ($B = 1$), but otherwise it is a reasonably constant curve. There are only a very limited number of points, because the fit to the extinction curve vs. λ^{-1} does not converge at all times. This happens because the fit is set, so that it is positive, and always above zero, the a value is always above zero. Therefore when the i -band is lower than zero, as it is for a number of days of the linear model, it is not possible for the fit to converge and it is therefore zero. This fit is seen in Fig. 41 in Appendix 12.4.

The corresponding α values to the R_V values are shown in Fig. 43 in Appendix 12.5.1. The α values and their error bars fit with the ranges for the R_V values. The α

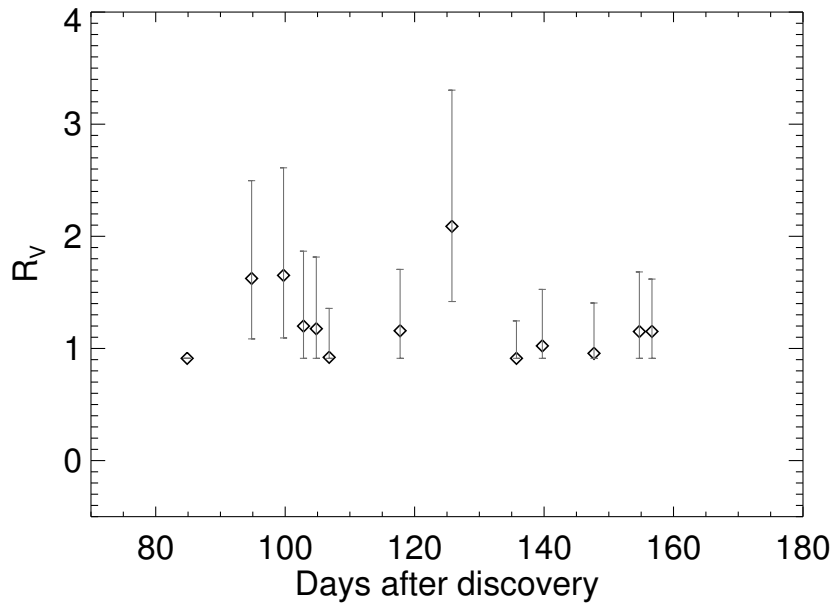


Figure 19: This figure shows the R_V values over different times with the corresponding error bars to each day. Here for the linear model of $B = 1$.

values therefore control the values that is calculated for R_V and the median values fit with what is found for R_V . The connection between R_V and α is shown in eq. 11.

Is it possible to minimize the errors on R_V and to create a more smooth extinction curve, so that all the data points may be used, and so that the negative points and bumps on the curves are avoided? In the following section different models are tried to see what difference it makes compared to the linear model ($B = 1$), and to see how R_V depends on the fitting model used.

8.2 Different B values

Different values for B give different fits, as already mentioned. The method above have been conducted for $B = [1, 0.9, 0.8, 0.7, 0.6, 0.5, 0.2]$. The end of this section the B values and the results are then shown and discussed, and further plots are shown in Appendix 12.5.

It should be noted, that R_V is not calculated for all times. It is calculated between times of 77-200 days after discovery, and then some times between 77-200 days are removed. On the light curves there are some bumps, and the data that correspond to these bumps are removed when examining the extinction. This is because the extinction becomes negative at this point. The fits, from eq. 10, to the extinction curves would not converge and create a fit to these times. It is the i - and r -bands that become negative.

8.2.1 Range of B values

The range of B give different values of R_V (See section 12.5.7 for discussion of $B = 0.5$), and the values are correlated, which will be shown and discussed in this section. On Fig. 20 the R_V values for the different B values are shown over the time range of 77-200 days after discovery, which is the time range that the extinction curves were positive for.

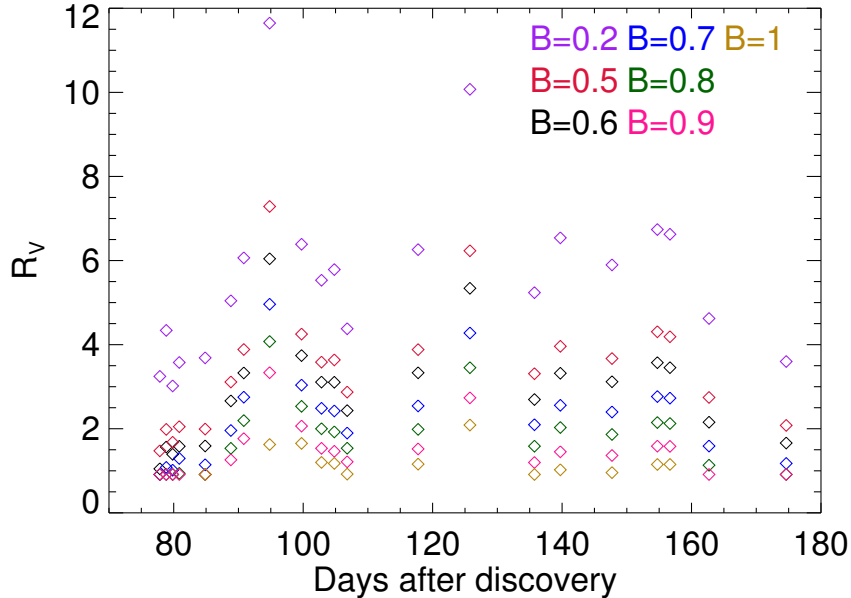


Figure 20: This figure shows all the values for R_V for the models including a B values, which is plotted over time. The values are seen to be approximately constant over time, with some outlying times, and with a spacing depending on the B values.

The R_V value over time is more or less constant. The values for R_V is seen to vary with the different values of B here. It is seen that the lower the B value the higher the R_V values.

The same can be seen on Fig. 21. Here it is even clearer that for lower values of B the R_V value is higher, and it looks to be periodically higher. $B = 1$ is a bad fit as has already been discussed, but if the values $B = [0.9, 0.8, 0.7, 0.6, 0.5, 0.2]$ are the ones examined, then it is clear, that the values for R_V has a range of possible values. Fig. 21 shows the median values for each model with B values. Here the points show the median values found over all times for each specific B value model. The error bars are found in the same way, by finding the median of the maximum and minimum values possible for each of the B models. In Appendix 12.5 plots of R_V vs. time is shown, and on these figures it is clear that there are two outlying points for all models. Those points have been removed when the median is found.

If the root mean square (RMS) of the points on Fig. 59, for $B = 0.5$, excluding the two outlying points, is calculated, it then give $RMS = 3.58$, which is a value a little higher than the mean value of R_V for the MW. It is much higher than the

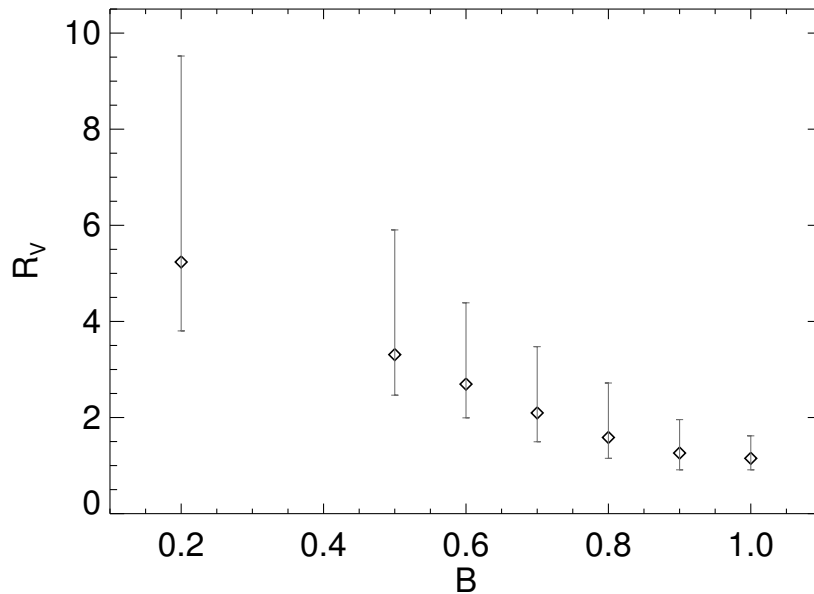


Figure 21: This figure shows R_V vs. the B parameter. It is seen that the values for R_V becomes more spread out and larger for smaller B values.

value found for the linear model. The RMS value does not fully correspond with the median value of all the points or with the error bars. There are some points that fit fairly well with the RMS, and then there are some where the value is at one of the extremes of the error bars, or some point where the RMS value is completely off. That it does not fit over the entire range means that there may be some systematic error or a systematic way that the fit works, which can also be seen as the B value. These values mean that all the points are correlated, and that when the value is changed, the points all move on the R_V value axis correspondingly. The lower the B parameter the higher the R_V value. So the points on Fig. 59 is not completely independent. They are all correlated due to the fit on the light curves, and therefore the B value have a huge influence on what the value of R_V becomes.

Another way to look at the evolution of the B value and the evolution over time is to look at the extinction value of the V -band, A_V . These can be seen on Fig. 22 and Fig. 23. On the figures the two latest dates of time is off in comparison to the rest of the times. It is seen on Fig. 23 that the value for A_V is increasing for most of the bands. For Fig. 22 it is again seen that the R_V values over B is more spread out the lower the B value and the higher the value for R_V also become.

The variety of R_V and B values that all give different results shows that R_V and B is indirectly linked, and that the fits to the light curves controls the calculated R_V values, just as it controls the extinction values, e.g. A_V . But what is the best fit and the right value for R_V ? Intuitively there are a few things that can characterize a good fit. 1) The R_V should not fall off, it should remain constant over small periods of time. 2) Over a long period of time it would make sense that the dust

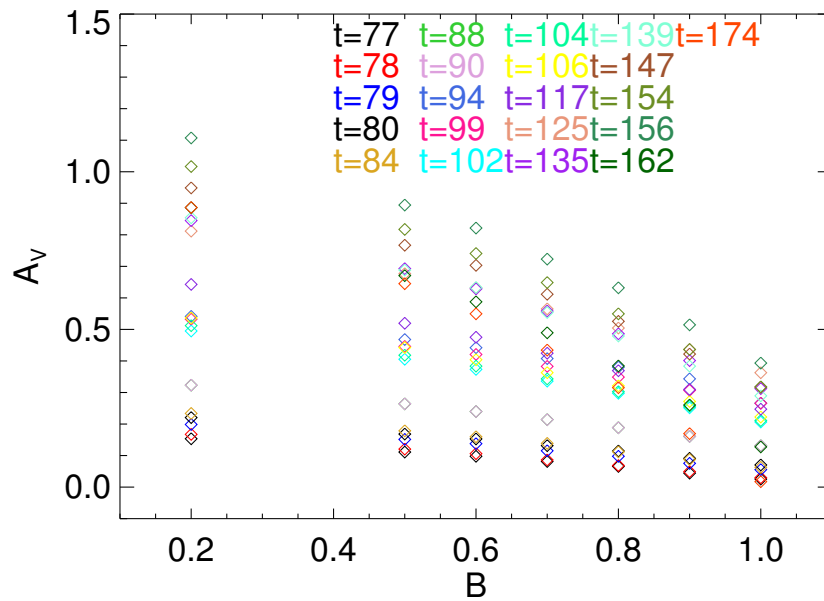


Figure 22: On the left figure A_V is shown vs. B and on the right A_V vs. times. The A_V value is seen to increase with time.

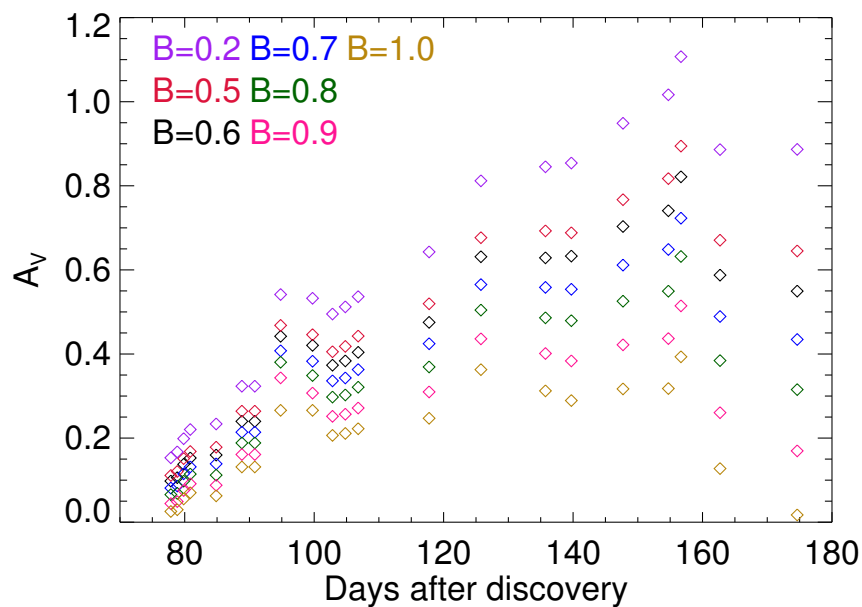


Figure 23: On the left figure A_V is shown vs. B and on the right A_V vs. times. The A_V value is seen to increase with time.

grows over time and becomes larger grains, and therefore R_V would grow. 3) A_V should increase. The extinction should increase as the dust grains grow and as there is formed a larger amount of dust. Larger amount of dust thus larger extinction value. But how much should R_V and A_V increase? This is hard to determine and give a good and qualified guess for, since the values in the previous sections are

not evenly distributed. The curves may be more smooth with a polynomial fit to the extinction vs. time. With a smooth curve the values of R_V and A_V over time should also become more smooth and thereby making it easier to examine exactly how the values develop.

8.3 Polynomial fitted model

To create a more smooth extinction vs. time curve, and thus a more constant results for R_V , a polynomial equation is fitted to the extinction. The polynomial that is found to be a reasonably good fit is a 5th degree polynomial as shown in eq. 12

$$y = c_1 + c_2 \cdot x + c_3 \cdot x^2 + c_4 \cdot x^3 + c_5 \cdot x^4 + c_6 \cdot x^5 \quad (12)$$

The polynomial is fitted to the extinction curve vs. time, as seen in Fig. 24, where the the red curve is the 5th degree polynomial fit to the extinction, which is calculated from the original fits from sections 8.1 and 8.2. The figure shows the fit to the extinction calculated for $B = 1$ in the u -band, and it appears that the polynomial fit is a reasonably good representation of the original extinction, but without the bumps from the light curve. This is then expected to give more continuous distributions of R_V and A_V .

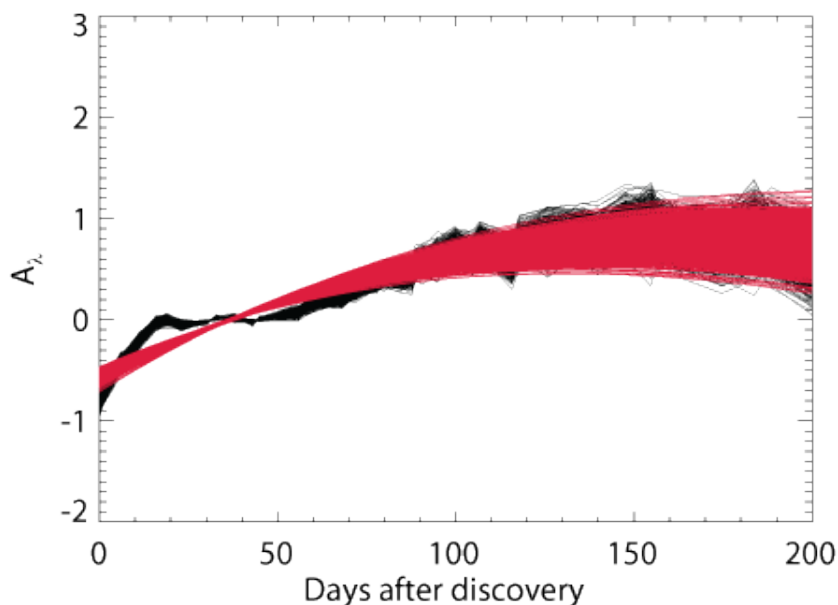


Figure 24: This figure is the polynomial fitted to the u -band for $B = 1$ model.

The resulting polynomial extinction over time is seen on Fig. 25. The extinction is seen to be very dependent on the B value, and indeed much more positive for $B = 0.5$.

The polynomial have been fitted to all the bands, and therefore also to all the extinction curves, which creates more positive extinction, and it is thus also seen that the fit to the extinction, as described in eq. 10, already at $B = 1$ becomes a

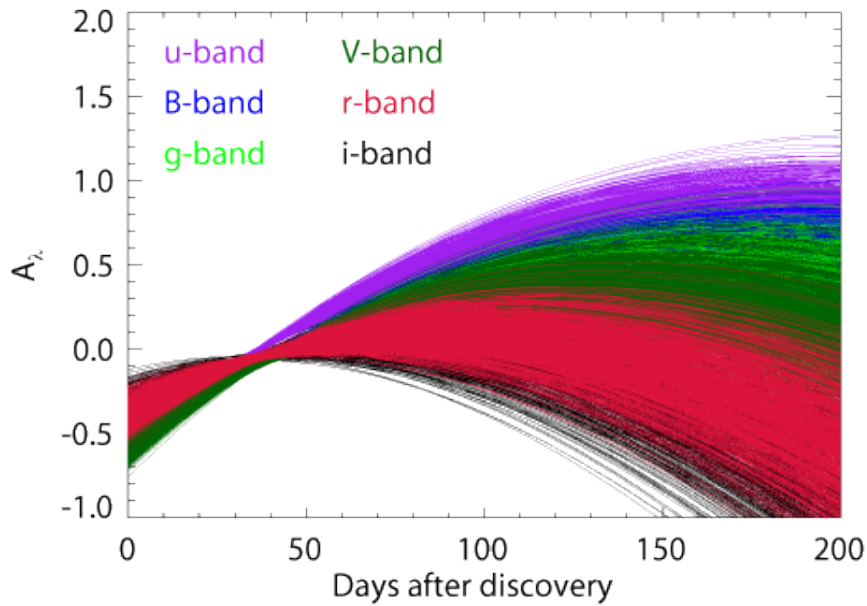


Figure 25: On the left figure the extinction vs. time is shown for $B = 1$ for all the bands.

better fit, which means that it fits over all times. This is because the i -band have more positive points over most of the times, and therefore the fit can converge, which was previously a problem with the linear fit. The fit to the polynomial fitted extinction curves for $B = 1$ and $B = 0.5$ is to be found in Appendix 12.6.1. From the fit to the extinction, found by the polynomial fit, R_V is then found from eq. 2, and is shown in Fig. 26. The corresponding α values is found in Appendix 12.6.1.

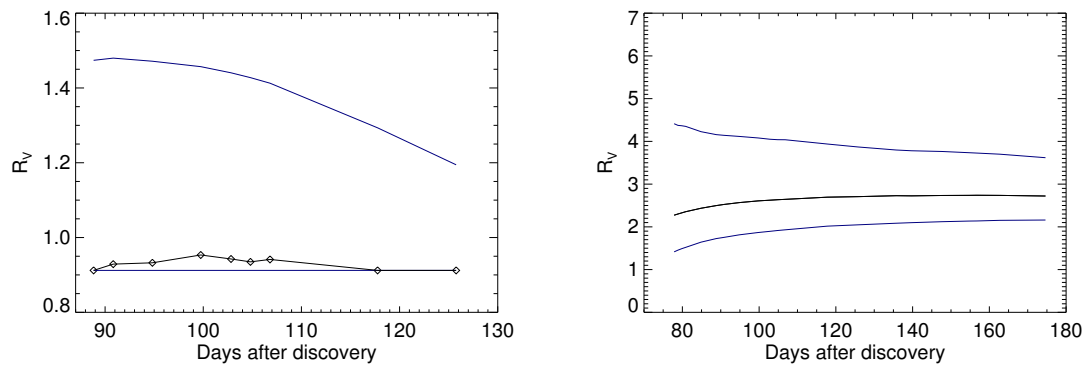


Figure 26: The left figure shows the R_V for the polynomial fits for $B = 1$, where the errors are indicated by the blue curves and the median values for R_V is indicated by the black line. The same is for the right figure, but here for $B = 0.5$.

On both the figure for R_V and for α the errors are shown by the blue curves, because the polynomial fit give continuous values for R_V . It should be noted, that the value for R_V seems to be higher for the polynomial fit that for the fit in section 8.1 and 8.2. It should also be noted that the errors on R_V and the median values are much more evenly distributed, the errors does not have the big outliers as before and the errors are more correlated due to the polynomial fit. It is not only the

values for R_V that is correlated with the B values, but the errors are also correlated with the polynomial fit. Again, the rest of the plot for the different B values are shown in Appendix 12.6.

R_V over time and over B is shown in Fig. 27 and Fig. 28, and again the R_V values are spread over a larger range of values for smaller B , but they are also shown to be almost constant if examined over time. Fig. 28 is found in the same way as for Fig. 21.

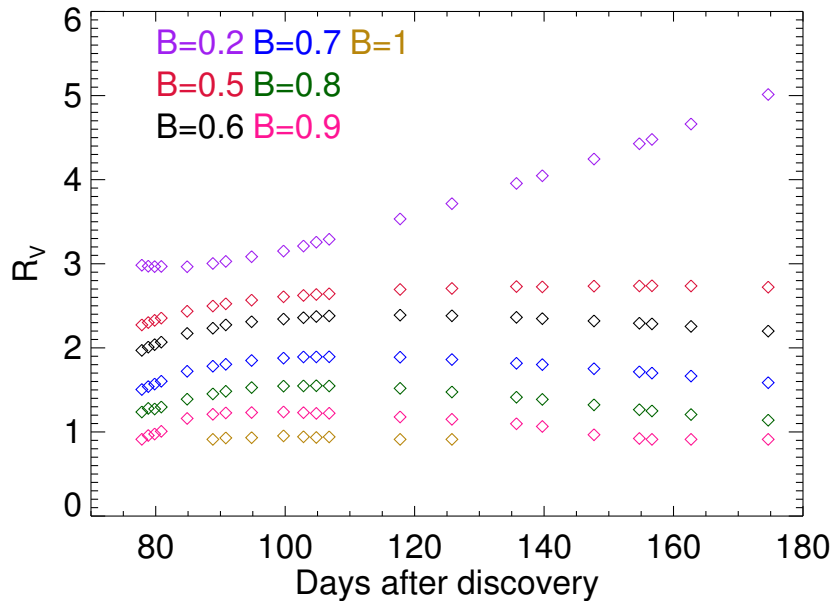


Figure 27: This figure shows the values for R_V over time and B . The first B values seems to be either falling off or becoming constant, or for $B = 0.2$ increase.

To examine which fits are good and which values of B are good, and give a physically reasonable result, then A_V for the polynomial fit needs to be introduced as well. A_V vs. time and B is seen in Fig. 29.

On both Fig. 27, Fig. 28 and 29 it is seen that the only curves that remain constant for R_V and increase for A_V is $B = [0.2, 0.5, 0.6, 0.7]$. The value of $B = 0.7$ does not increase for A_V , but seems to become positive and perhaps even start to bend of a little. If the total-to-selective extinction ratio is examined instead, then from Fig. 27 and Fig. 28, the B values that make R_V increase is $B = [0.2, 0.5, 0.6]$, and thus not $B = 0.7$. To be absolutely sure of how the A_V values develop the logarithm have been taken for A_V and T , as shown in Fig. 75 in Appendix 12.6.7. Examining the logarithm to the A_V plots give the same conclusion for the good B values as before. The values that are credible for B is $[B = 0.2, 0.5, 0.6, 0.7]$ although $B = 0.7$ is again debatable, because the extinction, A_V , becomes more or less constant and not increasing. Under the demands made previously, it is likely that good fits would be $B = 0.6$ and 0.5 and below. But how much or how little should A_V increase? It is not an easy question to answer since there are only very

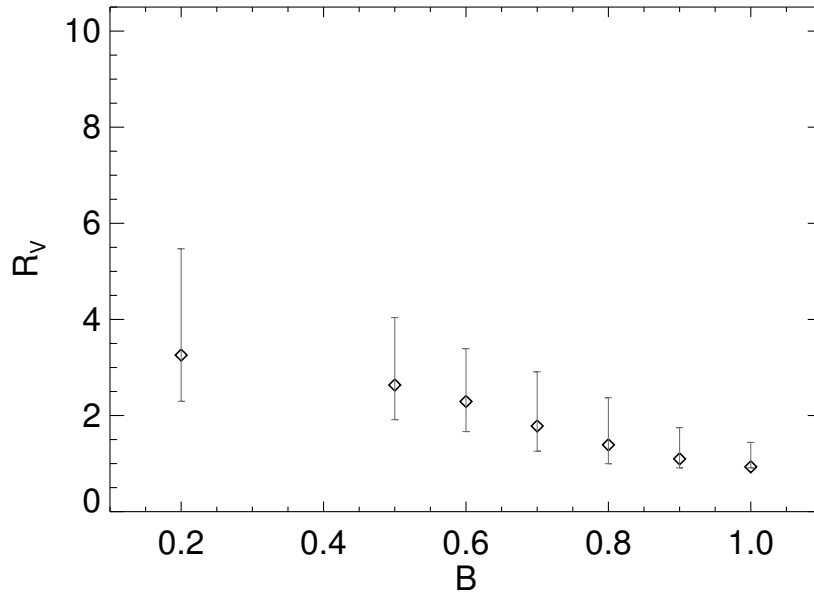


Figure 28: This figure shows the values for R_V over time and B . The first B values seems to be either falling off or becoming constant, or for $B = 0.2$ increase.

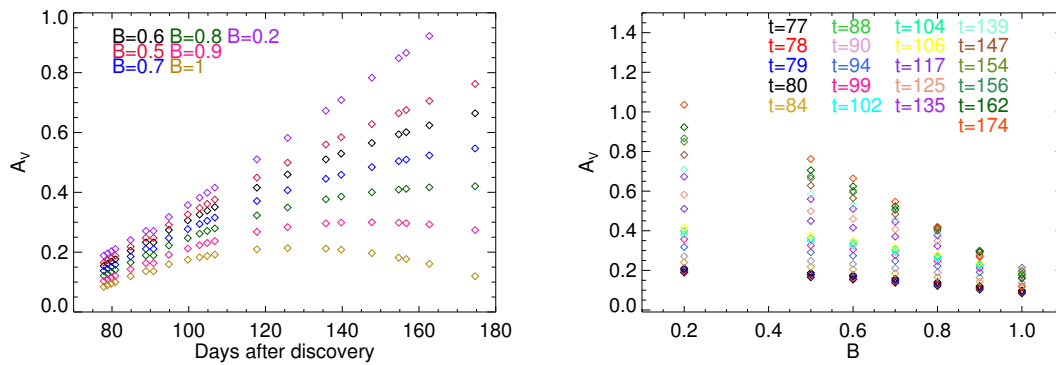


Figure 29: The figures show the extinction for the V -band over time and B values. A_V appears to be increasing for B below $B = 0.8$ and falling off at values above $B = 0.8$.

few calculations of R_V around and since the exact nature and evolution of SNe are not entirely known.

8.3.1 Other polynomial degrees

It is here examined what the difference is, if instead of a 5^{th} degree polynomial it is a 4^{th} or a 6^{th} degree polynomial that is used. The 4^{th} and 6^{th} degree polynomials are shown in eq. 13 and 14 respectively.

$$y = c_1 + c_2 \cdot x + c_3 \cdot x^2 + c_4 \cdot x^3 + c_5 \cdot x^4 \quad (13)$$

$$y = c_1 + c_2 \cdot x + c_3 \cdot x^2 + c_4 \cdot x^3 + c_5 \cdot x^4 + c_6 \cdot x^5 + c_7 \cdot x^6 \quad (14)$$

The method for finding R_V is then exactly the same as above, and the results for R_V is shown in Fig. 30.

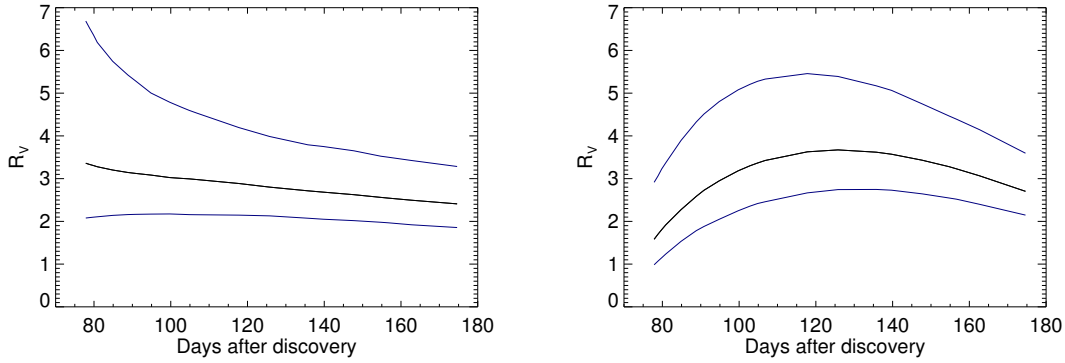


Figure 30: The left figure is for 4 degree polynomial fit, and the right is for the 6 degree polynomial fit. This is also for the model where $B = 0.5$ which is chosen because the value is shown in a previous section to be a fairly good fit.

It is seen, that the 4th degree R_V plot on Fig. 30 has some of the same characteristics as the 5th degree on Fig. 26. The 4th degree is, however, slightly declining, and the errors are larger and more declining at early times. When looking at the 6th degree polynomial then R_V first grows and then falls off, and therefore does not show a good fit to the extinction according to the previous restrictions where R_V was thought to be constant or increase. It should, however, be noted that Fig. 30 is only for the $B = 0.5$ model, and so the values for R_V could be thought to increase if the B value was lower, perhaps $B = 0.2$. Both, 4th, 5th and 6th degree polynomials give approximately the same value for R_V at late times. But at early times there is a difference. The 5th degree polynomial has been chosen because it appeared to be a better fit. Compared to the fits without polynomials, the R_V values are still higher, for all three degrees.

8.4 Logarithmic fit

8.4.1 The light curves

Another possible model to fit the light curves with would be if it is assumed, that they would fall off logarithmically. This comes from the magnitudes being a logarithmic relation if the flux falls off exponentially with time, so

$$F = at^{-b} \quad (15)$$

Then the logarithm is taken and this gives

$$\log(F) = \log(a) - b\log(t) \quad (16)$$

And to find the magnitude, all is multiplied with -2.5 , so

$$-2.5\log(F) = -2.5\log(a) + 2.5b\log(t) \quad (17)$$

and because the apparent magnitude is $M = -2.5\log(F)$, then

$$m = A + B \cdot \log(t) \quad (18)$$

Eq. 18 is the equation used to fit with a logarithmic law to the light curves, where m is the magnitude found and A and B are constants that are free parameters in this case. The fit to the light curves is seen on Fig. 31.

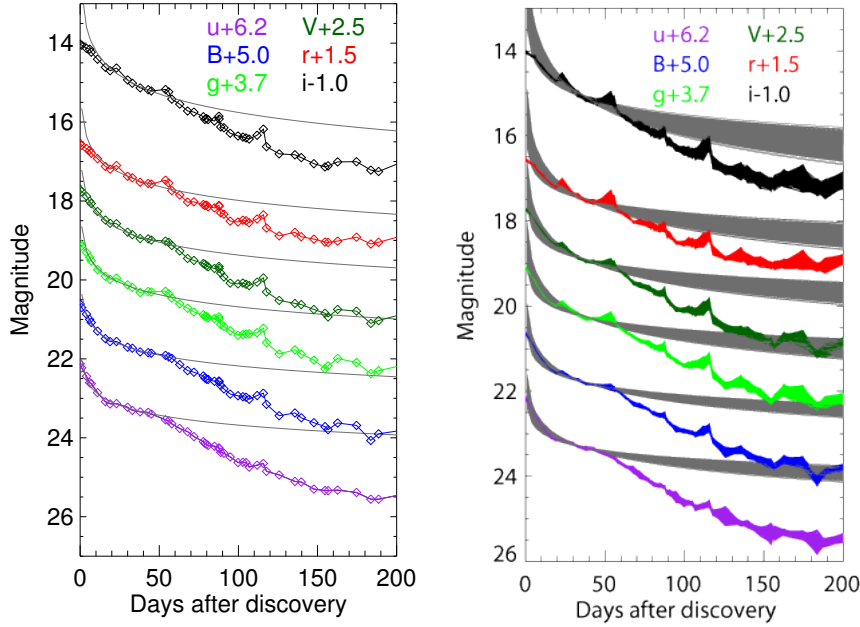


Figure 31: This shows the fit to the light curves for the logarithmic fit. The right fit shows the entire range of 3σ re-sampled data.

On the light curves for the logarithmic fit it is seen that the fit is positive over all times beyond 50 days past discovery. The logarithmic fit is even positive for all the days for the i -band, and it is generally placed very much higher than the fits for the model containing the value B . This means that the extinction will be somewhat higher for some of the optical bands. The extinction and the following total-to-selective extinction ratio is calculated and examined in the following sections.

8.4.2 Extinction and R_V

The extinction over time is seen on Fig. 76 in Appendix 12.7. This figure shows that the bumps and irregularities are on the light curve just as above, and R_V will therefore in the end also have varying values, with varying α parameter values. However, the extinction is mostly positive over time, from early on, and this would suggest a higher value of R_V since all the bands are positive, then the fit values, to the extinction vs. wavelength, will also become higher, thus resulting in a higher value for R_V . R_V is found in exactly the way as before from eq. 2, and there will arise corresponding α values. R_V is seen on Fig. 32.

On the R_V plot it is seen, that for one of the values the error bar is very high. This is the same point that is an outlier for almost all the models, and it has to do with the bumps in the light curve. R_V for the logarithmic fit is very much higher

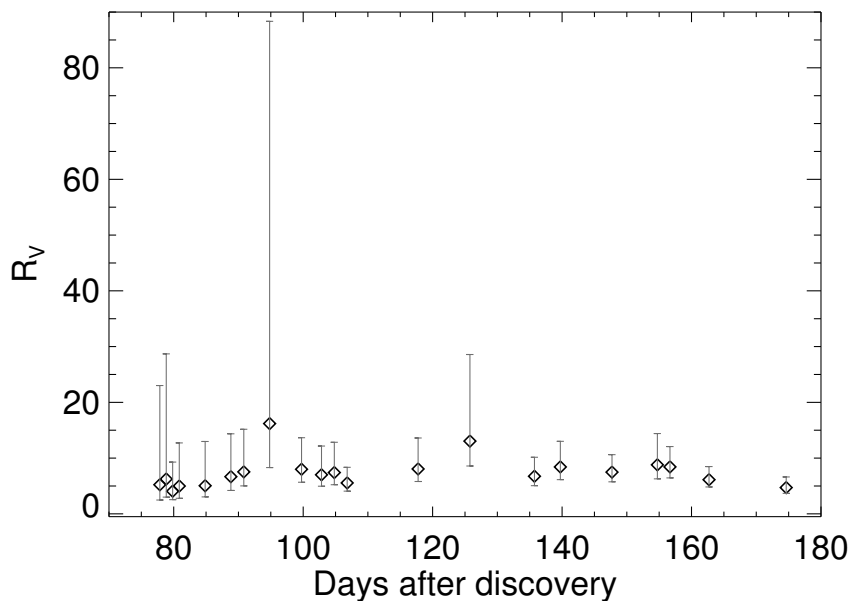


Figure 32: The left figure shows the R_V values and corresponding error bars for the logarithmic fit.

than for the other fitting model to the light curves. This model give most values well beyond $R_V = 5$, which is more similar to R_V for a molecular cloud, than for the MW. The α parameters should also be noted to be in the high end. None of the α values hit the minimum extreme of -3.5 , whereas α was more spread out for the other model, for all B values. The α values are seen on Fig. 77 in Appendix 12.7.

The A_V value, seen on Fig. 33, is here within the expectation previously described. A_V is increasing with time, although it does appear to fall of for the last two points.

So the first impression is that this is a model that also fulfil the demands that was set up for a good model. The results here are, however, very different. To take a closer look, a 5 degree polynomial have again been fitted to the extinction vs. times, and it is described below in section 8.4.3.

8.4.3 Polynomial fit

The polynomial fit, in this case to the u -band is shown in Fig. 78 in Appendix 12.7.1, which shows a good polynomial fit to the extinction over time. The same 5th degree polynomial is chosen as previously, from eq. 12. The polynomial fit then creates the extinction over time for all the bands which is seen on the right side of Fig. 78. The extinction is again seen as very high, but as before expected to have a more limited range of R_V . Those values for R_V is seen on Fig. 34.

The values are indeed more confined, but the R_V value is still very much higher than found by the previous models, and the same for the values for α which are seen in Appendix 12.7.1. R_V here show a sign of this not being an entirely good

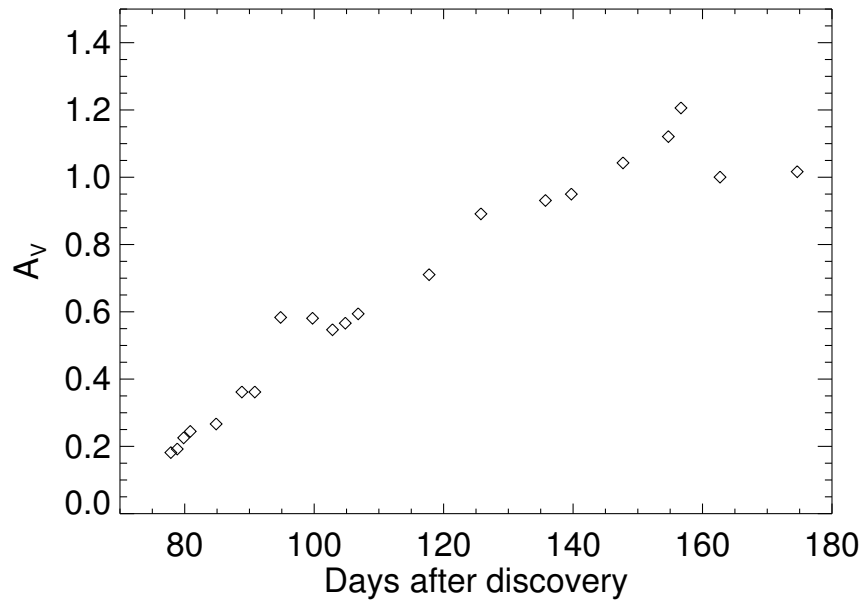


Figure 33: This figure shows A_V over times, and here it is also seen that A_V increase over time for the logarithmic model.

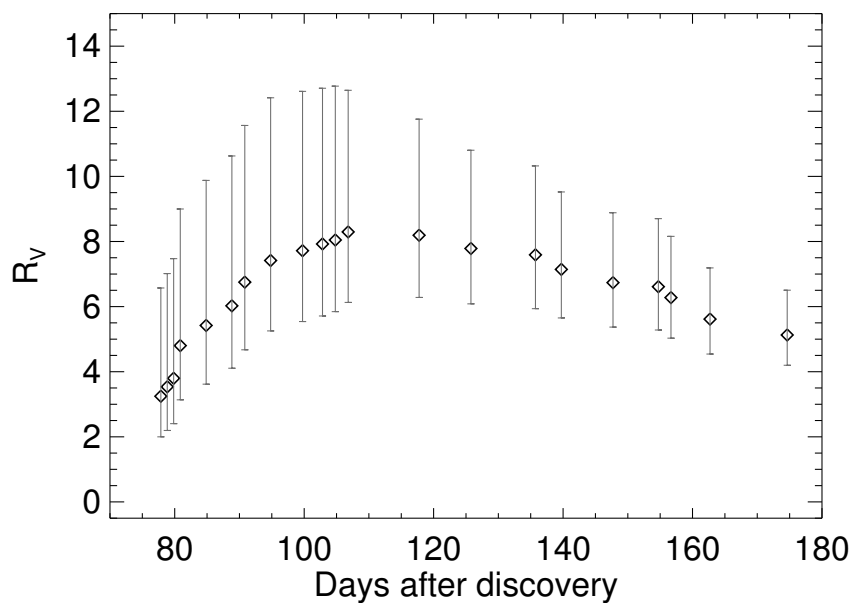


Figure 34: The left figure shows the R_V values over time for the polynomial fitted logarithmic model and the right figure shows the corresponding α values. Both with error bars.

model. In section 8.2.1 some expectations that were to be fulfilled for the fit to be satisfactory was made. Here it was stated that R_V should be constant or increasing, and the same for A_V . Neither of them are increasing.

On Fig. 35 A_V vs. time is shown. A_V turns off towards 200 days and becomes constant, and R_V fall of quite sudden, and R_V thus does not only violate the

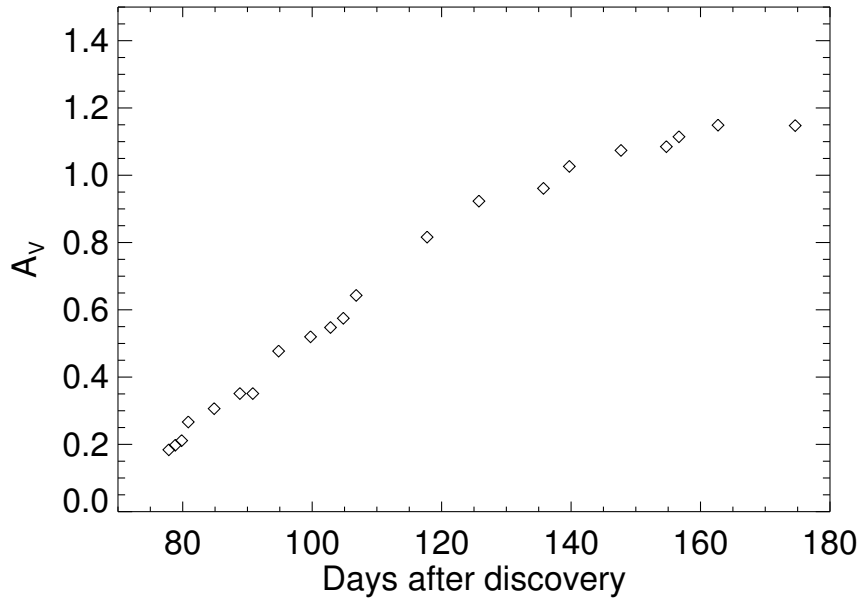


Figure 35: This figure shows the A_V values over time, which is again shown to be increasing for most times, but appears to become constant in late times.

expectation that it should be constant or increasing, but also the expectation that R_V should not change dramatically over a short period of time. This suggests that it is not a very good fit after all, since it does not meet the expectations for R_V and A_V .

8.5 No r -band

The r -band is dominated by the $H\alpha$, which means that the r -band is suppressed compared to the other bands. The $H\alpha$ lines is at a wavelength of around $\lambda_{H\alpha} = 6562.8\text{\AA}$. If the r -band is removed, does this then have an effect on the values for R_V ? Fig. 36 shows R_V values for a model with $B = 0.5$ where the r -band has been removed, and the values found have error bars larger than the ones on the original fit, but the median values are more or less the same as for the data from previous sections. It does therefore make a huge difference whether or not the the r -band is included or not. The error bars does, however, become larger. Therefore the r -band has been included.

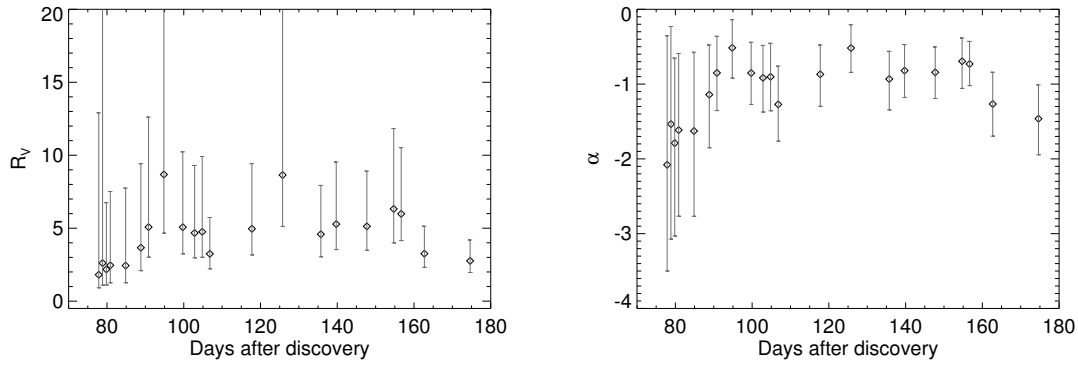


Figure 36: This figure shows the R_V for $B = 0.5$ to the left and the corresponding α to the right for a trial, where the r -band is removed. This is for a non-polynomial fitted method.

9 Results

The different models tried out in the previous sections give a variety of different R_V values. For the linear model, $B = 1$, without a polynomial fit, R_V is much lower than what is expected for a process that could form the dust found in the MW, if the dust is assumed to be similar to the MW dust. The values for R_V are around $0.9 - 2.6$ and only for one point is it possible, according to the error bars, for R_V to reach 3.3 , and thus a value similar to R_V for the MW.

If B then becomes a lower value then the extinction has more positive points in all the bands, and the R_V values increase with respect to this value. In Fig. 21 and Fig. 28 the values of R_V over B values are shown. It is seen that the lower B values give a higher R_V value. To find R_V values that are similar to the R_V values for the MW, $R_{V_{MW}} = 3.1$, LMC, $R_{V_{LMC}} = 3.41$, or SMC, $R_{V_{SMC}} = 2.76$, would need B values of $0.7 - 0.2$. This is both for the polynomial and non-polynomial fitted models (Gordon et al., 2003).

The logarithmic model yields much higher values of R_V , around $R_V = 5 - 10$, and some of the points with a possibility of R_V up to 80 , which is not a physically possible value. The logarithmic model with a polynomial fit is, however, not reasonable because A_V and R_V decrease, which was not expected. This is because it is known that dust is produced in SN (Gall, Hjorth & Andersen, 2011) and that dust would most likely grow and not be destroyed when dust formation is occurring.

It has already been mentioned what the R_V values are for the MW, SMC and LMC, but to take a closer look at the three galaxies R_V values their extinction curves are fitted to the extinction curves for some of the models described above. This is seen in section 9.1.

9.1 MW, SMC and LMC

On Fig. 37 and Fig. 38 the MW, LMC and SMC extinction curves have been recreated in the range of the extinction curves found from the models with $B = 1$

and $B = 0.5$ respectively. It is done using the CCM model (Cardelli, Clayton & Mathis, 1989). The R_V values for the MW, LMC and SMC are found in the paper by Gordon et al. (2003).

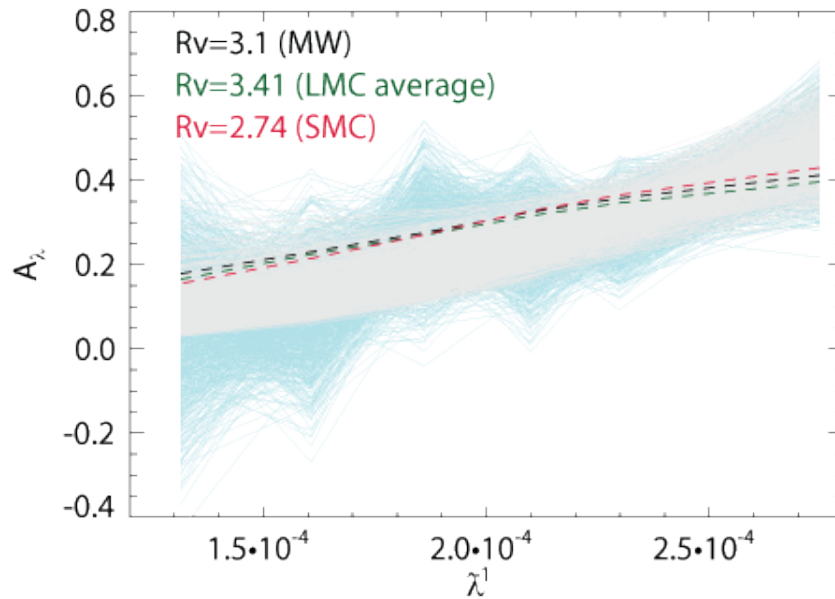


Figure 37: This figure show the extinction curve for $B = 1$ overplotted with the extinction curves for MW, SMC and LMC, for the non polynomial figure and for a time of 99 days after discovery.

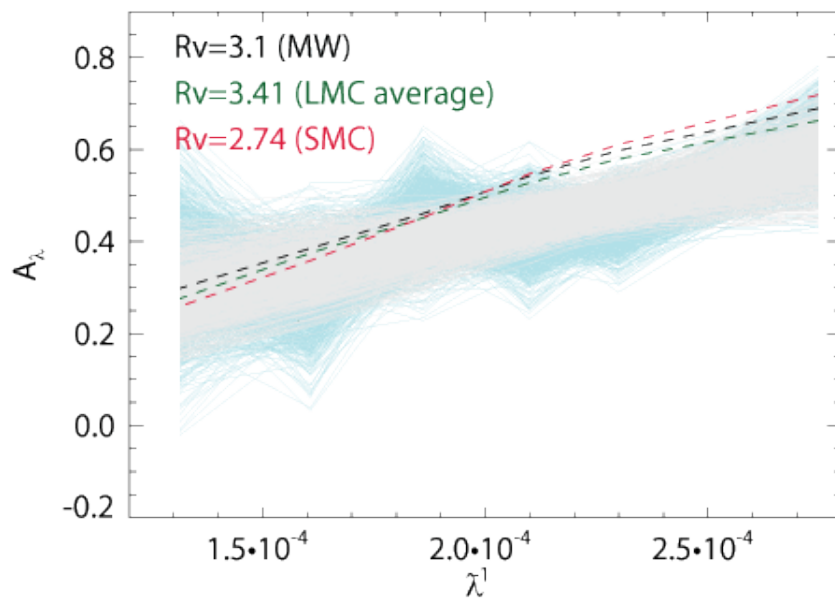


Figure 38: This figure show the extinction curve for $B = 0.5$ overplotted with the extinction curves for MW, SMC and LMC. Here it is again for the non polynomial figure and for a time of 99 days after discovery.

On Fig. 37 and Fig. 38 it is seen that neither of the MW, LMC or SMC models are perfect fits for the extinction of $B = 1$ or $B = 0.5$ at a times of 99 days after

discovery, and without a polynomial fit. For $B = 1$ the increase in MW, LMC and SMC is not as large as for the model fit, and for $B = 0.5$ the increase is a little too big. This has to do with the values for R_V . R_V is only about 1.6 at 99 days after discovery, and this is much smaller than the values for MW, LMC and SMC. The small R_V values yields a steeper slope for the extinction curves, and larger R_V values yield more shallow extinction curves. For $B = 0.5$ R_V is about 4.2 which is larger than for the MW, LMC and SMC. The extinction curves will therefore fit with the points that have an R_V value closer to their values, e.g a times of 135 days after discovery for $B = 0.5$, where for $B = 1$ all R_V values are smaller than the MW, LMC and SMC values, and their extinction curves are therefore not similar in increase or decline at any time.

10 Discussion

The results from the fits to the light curves for both the non polynomial, polynomial and logarithmic fits are very different. The values for R_V over times is seen on Fig. 21 and Fig. 28. The results vary from a median value of the fits with $B = [1.0 - 0.2]$ is $R_V = [1.15 - 5.24]$ and for the polynomial fitted model R_V is $[0.93 - 3.26]$, for both models, the smallest value is for $B = 1$ and the highest value is for $B = 0.2$, and the values for the rest of the B values are within these values as seen on Fig. 21 and Fig. 28. The values for the logarithmic model is $R_V = 5 - 10$ magnitudes, and for the polynomial fitted logarithmic model varies between about $R_V = [3 - 9]$ magnitudes. All the values from the three different main models are very much dependent on the values for B , and they therefore does not give a final value for the total-to-selective extinction ratio for SN 2005ip. The total-to-selective extinction values are completely dependent on the B values and thus of the fits to the light curves in the different photometric bands.

The method used for finding R_V is only theoretical and a very basic method. The values obtained in this thesis for R_V and A_V is therefore not necessarily the correct values since these are not known, and there are only very little knowledge of R_V for type II SN to compare with. The values found here is very much dependent on the B values, thus the fits to the light curves, and the values for R_V is therefore only valid for the specific model. The results of this thesis is therefore not independent and it gives a range of possible R_V values that could be possible for SN 2005ip. The results of this thesis thus does not show one final result for the total-to-selective extinction, and thereby for the dust formed in the CDS of SN 2005ip, but it is different model values and thus an examination for which model might be a good way to describe the evolution of SN light curves had there been no dust formed. It is also a possible interpretation on how dust evolves, and which size dust grains are formed. The results are, however, not entirely conclusive.

The best possible model is a debate about which value for B is best. There have already been set 3 expectations that can determine this. 1) R_V should remain constant over short periods of time, 2) R_V is expected to increase over longer periods of time and 3) A_V should increase. These three are also stated in section 8.2.1. This rules out quite a few of the models as discussed in section 8.2.1, where only the models with $B = 0.6$ and below seems to fit the expectations both for the polynomial and non-polynomial method. For the logarithmic method it is seen, that only for the non-polynomial fit R_V stays fairly constant, and A_V increase except for the last two points. However, the polynomial fit to the logarithmic extinction curves are not fulfilling the expectations. Both R_V decrease and A_V seems to turn more or less constant, and stop increasing, as seen on Fig. 34 and Fig. 35. This model therefore does not appear to fit the expectations no matter if there is a polynomial fitted or not, whereas the B model does. When looking at the non-polynomial and polynomial B models, then it is also a discussion about how much A_V should actually increase, because it is seen on Fig. 22, 23 and 29 that there is a big difference between $B = 0.6$ and $B = 0.2$ in how much A_V increase, and it is particularly clear in the polynomial fitted model.

There are some possibilities for examining whether any of the models are any good for the R_V and A_V , and thus for recreating the light curve if no dust was formed, and thus a model for SN evolution. This is to look at similar studies, or rather similar R_V values for other SN. Below the method and values found for SN 2005ip is compared to R_V values for SN Ia and type II In SN 2010jl.

There are only a few papers where R_V have been found, and in most cases R_V is found for type Ia SN. The type Ia SNe are not comparable to SN 2005ip. Ia SNe typically occur in environments where dust is scarce, such as elliptical galaxies, and they presumably occur from a completely different explosion mechanism, a thermonuclear explosion (Elias-Rosa et al., 2007) (Rosswog & Brüggen, 2007). Dust in type Ia SN is highly debated. It does not appear to be a significant dust producer, and the values for R_V seems to be found from a circumstellar medium interacting with the SN explosion, or it may be an illumination of clouds that exist further away from the SN, and it is thus not dust formed in situ for the SN, but it may be pre-existing dust (Gall, Hjorth & Andersen, 2011) (Elias-Rosa et al., 2007) (Goobar et al., 2014) (Goobar, 2008). R_V found for type Ia SN, no matter if it is for their host galaxy, the SN it self or for some material further away from the Ia SN, appear to be much lower than R_V found for the MW, $R_V = 3.1$. These values are around $R_V = 1 - 2$ and thus small values (Elias-Rosa et al., 2007) (Goobar et al., 2014) (Goobar, 2008).

If the results found for SN 2005ip is instead compared to other type II SN, which have a more similar evolution and dust formation method, then it is found that the values for 2005ip are low for most of the values. For instance, the values found for SN 2005ip could be compared to R_V found for SN 2010jl. SN 2010jl occurred in the galaxy UGC 5189 in November 2010, and has been shown that the progenitor was likely a LBV just as for SN 2005ip (Gall et al., 2014) (Smith et al., 2011). For 2010jl R_V is found to be $R_V = 6.4$ which is very much higher than what is found for SN 2005ip. The two SN are both type II In and both thought to origin from LBV stars, which would give them some of the same characteristics, and perhaps the same possibilities of forming new dust. For both 2005ip and 2010jl it is thought that the new dust formation is happening in a CDS, situated similar to what is seen in Fig. 9 (Gall et al., 2014) (Stritzinger et al., 2012). The difference might be due to difference in the amount of dust produced, but it is not known why there seem to be a difference. It may just be that the models used for SN 2005ip are not entirely correct, and that there needs to be implemented another model for the light curve evolution without dust formation.

If the two type II In SN were to have values corresponding to each other, then for SN 2005ip it would only be the models where $B = 0.2$, and not for the polynomial fitted model, that would yield values similar to that found for SN 2010jl. $B = 0.3$ may also be able to produce a similar value, but it is also seen, that the median value for $B = 0.2$ is still smaller, and it is only because this B value have high error bars that it is possible. This would, however, mean that the values for A_V

would increase much more sudden than would perhaps be expected, but it would increase, see Fig. 29. The values found for SN 2010jl indicates dust grain sizes which are much higher than the ones found in the MW and dust grain which are in the high end of what is found in dense molecular clouds. Perhaps this is needed for dust to survive in the extreme environments that SN are. But the majority of the values found in this thesis, and for the models that fitted with the expectations in section 8.2, $B = 0.6, 0.5, 0.2$ all show median value smaller than found for SN 2010jl, and for $B > 0.2$ show values much more similar to what is found for the MW.

The models are varying in values for R_V and A_V and it is difficult to know exactly which value is correct, and thus which model, $B = 0.6, 0.5, 0.2$ describe SN 2005ip's evolution without dust satisfactory. If compared to SN 2010jl then it is only the $B = 0.2$ model that is satisfactory, and models with lower B values.

No matter what the value for R_V is, it is certain that there is some dust formation that occur in both SN 2005ip and 2010jl. In both SNe dust is thought to be formed in the CDS around the remnant of the SN and both SNe are the same type, IIn. The R_V values would make sense to be alike, but the two SNe might also just create different types of dust and thus creating different R_V 's. The type IIn SN almost never have exactly the same light curves, and thus have the possibility of having very different progenitors and due to the differences in the progenitor stars and thus in the light curves. Since the extinction is found from the light curves in this thesis, and similarly for SN 2010jl, then the difference in the different IIn SN is a possible explanation for the difference in the R_V values. However, the it would still be plausible that the values were similar, and thus it would be possible to give constraint on the evolution models for the light curves without dust.

10.1 Future prospects

Some future prospects for this thesis and the method in this thesis may be to try and fit some other methods and see which R_V these yield, and to see if it would be possible to find a model that gave consistent results, and which was consistent with other calculations of R_V for other type IIn SN, such as SN 2010jl. This would of course mean that a more detailed analysis of the future observations of type IIn SN would be required, and that the past observed type IIn would need to be examined too, to find R_V values in generally for this type of SN. The only two SN which this has been found for, which has been found in connection to this thesis, is SN 2010jl, and then what is done for SN 2005ip in this thesis. It is always a wish to have more and better observations of the type of SN that is examined. The IIn SN is, however, fairly rare, and more observations of this is therefore not just something to come by. But better observations directed towards finding the extinction and thus finding R_V may be possible when the type SN occurs, is something to wish for.

It may be possible to find more consistent R_V values over time if a function is fitted to the light curves, which would smooth the bumps on the light curve. The

same procedure would then follow the same procedure as before, and the R_V values may be more consistent over time with less variations than there is now. This could be a method of improvement of the methods in this thesis.

11 Conclusion

There have been found values for the total-to-selective extinction ratio for three different main models, with different fitting values B . It is for a model with no polynomial fit to the extinction, with a polynomial fit to the extinction, and with a logarithmic fit to the light curves, including a polynomial fit to the extinction. The R_V values that are found vary over the different B values found, and the R_V values seems to have an offset according to the B values. The R_V values seem to almost increase linearly with lower B values as seen on Fig. 21 and Fig. 28. The values are smaller for all of the methods than for the SN 2010jl. There are possible values that can be compared to SN 2010jl, and the SN 2010jl is a possible way to set limits for a good fit, but it is hard to know if this is correct. The R_V values that fit with the values found for SN 2010jl is only for the values of $B \approx 0.2$. There is not found a completely confirmed single value for B and thus no final result for the evolution of the light curves for SN 2005ip if here were no dust formed, but different possible models have been tested and possible values, on the basis of astrophysical expectations and comparison to other SN have been discussed. This results in the model using the fit from eq. 3 being a possibly good fit, and $B = 0.6, 0.5$ and in particular $B = 0.2$ and smaller are very likely models.

References

- Anderson J. P., James P. A., 2008, MNRAS, 390, 1527
- Arcavi I. et al., 2012, ApJ, 756, L30
- Arcavi I. et al., 2010, ApJ, 721, 777
- Asano R. S., Takeuchi T. T., Hirashita H., Nozawa T., 2014, How do the extinction curves in galaxies evolve? <http://pos.sissa.it/cgi-bin/reader/conf.cgi?confid=207#session-3>, accessed: 15-04-2014
- Australian Telescope National Facility, 2014, Post-main sequence stars. http://www.atnf.csiro.au/outreach/education/senior/astrophysics/stellarevolution_postmain.html, accessed: 26-03-2014
- Bohannon B., 1997, in Astronomical Society of the Pacific Conference Series, Vol. 120, Luminous Blue Variables: Massive Stars in Transition, Nota A., Lamers H., eds., p. 3
- Boles T., 2005, JBAA, 115, 197
- Boles T., Nakano S., Itagaki K., 2005, CBET, 275, 1
- Cardelli J. A., Clayton G. C., Mathis J. S., 1989, ApJ, 345, 245
- Chandra X-ray Observatory, 2012, Pulsating variable stars and the hertzsprung-russell (h-r) diagram. http://chandra.harvard.edu/edu/formal/variable_stars/bg_info.html, accessed: 27-03-2014
- Chevalier R. A., 2003, in From Twilight to Highlight: The Physics of Supernovae, Hillebrandt W., Leibundgut B., eds., p. 299
- Christensen-Dalsgaard J., 2008, Stellar Structure and Evolution. Institut for Fysik og Astronomi, Aarhus Universitet
- Crowther P. A., 2007, ARA&A, 45, 177
- Draine B. T., 2011, Physics of the interstellar and intergalactic medium. Princeton university press
- Elias-Rosa N., Beckman J. E., Benetti S., Cappellaro E., Turatto M., 2007, in Supernovae: lights in the darkness
- Filippenko A. V., 1997, ARA&A, 35, 309
- Fox O. D., Chevalier R. A., Dwek E., Skrutskie M. F., Sugerman B. E. K., Leisenring J. M., 2010, ApJ, 725, 1768
- Fox O. D. et al., 2011, ApJ, 741, 7
- Fransson C. et al., 2013, ArXiv e-prints

- Freedman R. A., Geller R. M., Kaufmann W. J., 2011, Universe. W. H. Freeman and Company, New York, USA
- Gall C., Hjorth J., Andersen A. C., 2011, *A&ARv*, 19, 43
- Gall C. et al., 2014, To be published in *Nature*
- Goobar A., 2008, *ApJL*, 686, L103
- Goobar A. et al., 2014, *ApJ*, 784, L12
- Gordon K. D., Clayton G. C., Misselt K. A., Landolt A. U., Wolff M. J., 2003, *ApJ*, 594, 279
- Groh J. H., Meynet G., Ekström S., 2013, *A&A*, 550, L7
- Heger A., Woosley S. E., Baraffe I., 2005, in *Astronomical Society of the Pacific Conference Series*, Vol. 332, *The Fate of the Most Massive Stars*, Humphreys R., Stanek K., eds., p. 339
- Heger A., Woosley S. E., Fryer C. L., Langer N., 2003, in *From Twilight to Highlight: The Physics of Supernovae*, Hillebrandt W., Leibundgut B., eds., pp. 3–540
- Kiewe M. et al., 2012, *ApJ*, 744, 10
- Kozasa T., Nozawa T., Tominaga N., Umeda H., Maeda K., Nomoto K., 2009, in *Astronomical Society of the Pacific Conference Series*, Vol. 414, *Cosmic Dust - Near and Far*, Henning T., Grün E., Steinacker J., eds., p. 43
- Lamers H. J. G. L. M., 2013, in *ASPC*, Vol. 470, *370 Years of Astronomy in Utrecht*, Pugliese G., de Koter A., Wijnburg M., eds., p. 97
- Langer N., 2012, *ARA&A*, 50, 107
- Leloudas G. et al., 2013, *ArXiv e-prints*
- Maeder A., Georgy C., Meynet G., Ekström S., 2012, *A&A*, 539, A110
- Mathis J. S., Ruml W., Nordsieck K. H., 1977, *ApJ*, 217, 425
- Mauerhan J., Smith N., 2012, *MNRAS*, 424, 2659
- Press W. H., Teukolsky S. A., Vetterling W. T., Flannery B. T., 2001, *Numerical Recipes in Fortran 77, The art of scientific computing*. Cambridge University Press
- Rosswog S., Brüggen M., 2007, *Introduction to High-Energy Astrophysics*. Cambridge University Press, Cambridge, UK
- Sanders N. E. et al., 2014, *ArXiv e-prints*
- Schlegel E. M., 1990, *MNRAS*, 244, 269

- Siriwardane U., 2010, Atomic structure. <http://www.chem.latech.edu/~upali/chem481/Chem481c1.htm>, accessed: 30-04-2014
- Smartt S. J., 2009, *ARA&A*, 47, 63
- Smith N., 2013, *MNRAS*, 429, 2366
- Smith N., Hinkle K. H., Ryde N., 2009, *AJ*, 137, 3558
- Smith N. et al., 2011, *ApJ*, 732, 63
- Smith N., Mauerhan J. C., Prieto J. L., 2014, *MNRAS*, 438, 1191
- Smith N., Owocki S. P., 2006, *ApJ*, 645, L45
- Smith N. et al., 2009, *ApJ*, 695, 1334
- Smith N., Silverman J. M., Filippenko A. V., Cooper M. C., Matheson T., Bian F., Weiner B. J., Comerford J. M., 2012, *AJ*, 143, 17
- Smith N., Vink J. S., de Koter A., 2004, *ApJ*, 615, 475
- Stritzinger M. et al., 2012, *ApJ*, 756, 173
- The Carnegie Supernova Project, 2011, Filters. <http://csp.obs.carnegiescience.edu/data/filters>, accessed: 08-05-2014
- Tielens A. G. G. M., 2005, *The physics and chemistry of the interstellar medium*. Cambridge University Press, Cambridge, UK
- Van Dyk S. D., 2013, *AJ*, 145, 118
- van Marle A. J., Smith N., Owocki S. P., van Veelen B., 2010, *MNRAS*, 407, 2305
- Wikipedia, 2012, Supernova. <http://en.wikipedia.org/wiki/Supernova>, accessed: 26-03-2014
- Woosley S., Janka T., 2005, *Nature Physics*, 1, 147

12 Appendix

12.1 Poster for Nordic Physics Days 2013

UNIVERSITY OF COPENHAGEN

DUST IN TYPE II_n SUPERNOVA 2005ip

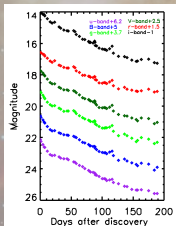
Ann-Sofie Bak Nielsen¹

¹Dark Cosmology Centre, Niels Bohr Institute, University of Copenhagen; asbn@dark-cosmology.dk

Dark Cosmology Centre

1. How is dust formed?

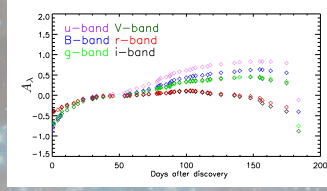
Cosmic dust is produced in two different ways, either by asymptotic giant branch stars or supernovae (SNe). One type of supernovae that produce dust is the core-collapse SN (CCSN), which can be a type II_n SN. This type of SN is characterized by its mass loss before the SN explosion, which could be a cause for efficient dust formation.



The SN2005ip is a type II_n SN, which is believed to have a luminous blue variable (LBV) as the progenitor star. The light curves for SN2005ip seems to fall off quickly after a period of 45-50 days after discovery. This indicates a quick dust production, which may be formed in a dense shell around the SN. In this poster I calculate the extinction curves for SN2005ip. Extinction curves have never previously been calculated for type II_n supernovae.

2. Method

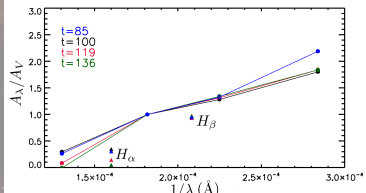
To examine dust formation, lines are fitted to the early light curves. The fits are then subtracted from the light curves, hereby calculating the extinction.

$$A_\lambda = \text{light curve} - \text{fit}$$


On the extinction curves it can be seen that the extinction becomes larger over time, but that it falls off in the i- and r-band, and around 150 days after discovery. This is where the light curves reach a constant level, and the linear fits stop describing the light curves.

3. Method & Results

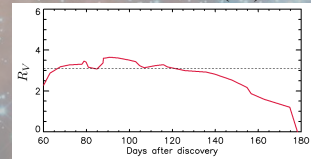
Points on the extinction curves are selected at different times, and normalized to the V-band. The normalized extinction curves are shown below, as a function of the inverse wavelength.



The extinction is increasing over wavelength, but there are a few outlying points seen on the figure. Those originate from the Balmer lines, H α in the r-band and H β in the g-band. This indicates that the light comes from a dense shell around the SN and not from the SN ejecta.

4. Results

The reddening of light from the SN is now examined by looking at the colour excess, the reddening law, and hereby examine dust properties.

$$E(B-V) = AB - AV \quad R_V = \frac{A_V}{E(B-V)}$$


It is here seen, that $R_V \approx 3$, which is similar to the value for the Milky Way. This indicates that the dust produced in this SN has the same grain size distribution as in the Milky Way. Further improvements on this project include analyzing the errors on the above curves, and a look at the dust compared to other known models for dust production.

References

Stritzinger, M. et al., "Multi-wavelength observations of the enduring type II_n supernovae 2005ip and 2006jd", *Aj* 756:173 (2012)

Gall, C. et al., "Production of dust by massive stars at high redshift", *A & Arv* 19:43 (2011)

Draine, B. T., "Physics of the interstellar medium and intergalactic medium", Princeton University press, 2011.

Acknowledgement

I would like to thank Jens Hjorth for good guidance and advice and Stritzinger et al. for data. I would also like to thank Anja C. Andersen and Marianne Vestergaard for inspiration to the poster design.

12.2 Comparative light curves

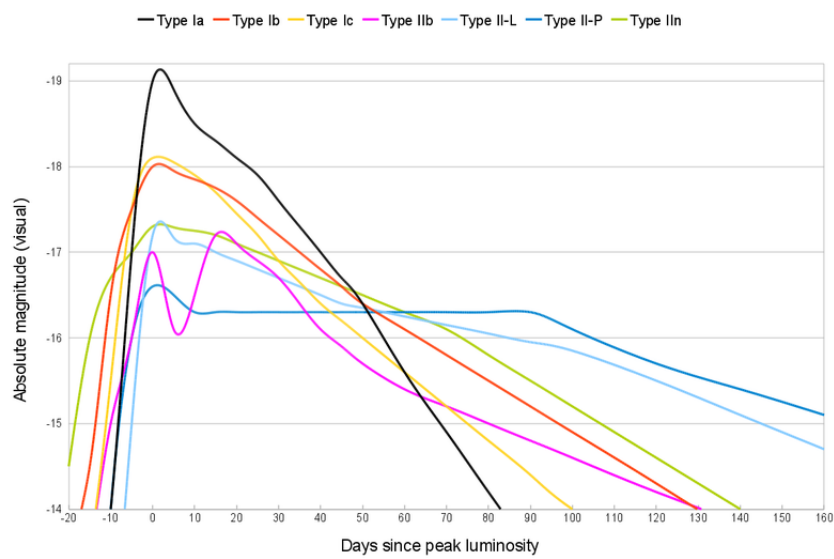


Figure 39: Sample light curves of 7 supernovae types are shown here. The type II-L and IIc have a late time peak and are often of a wide range of luminosities, and can be very luminous. IIb are instead of intermediate luminosity between II-P and IIc/II-L (Chevalier, 2003). Figure source: Wikipedia (2012).

12.3 Light curves over all time

On Fig. the light curves in the photometric bands u, B, g, V, r and i can be seen over all times, instead of only the first 200 days after discovery, as used in the thesis.

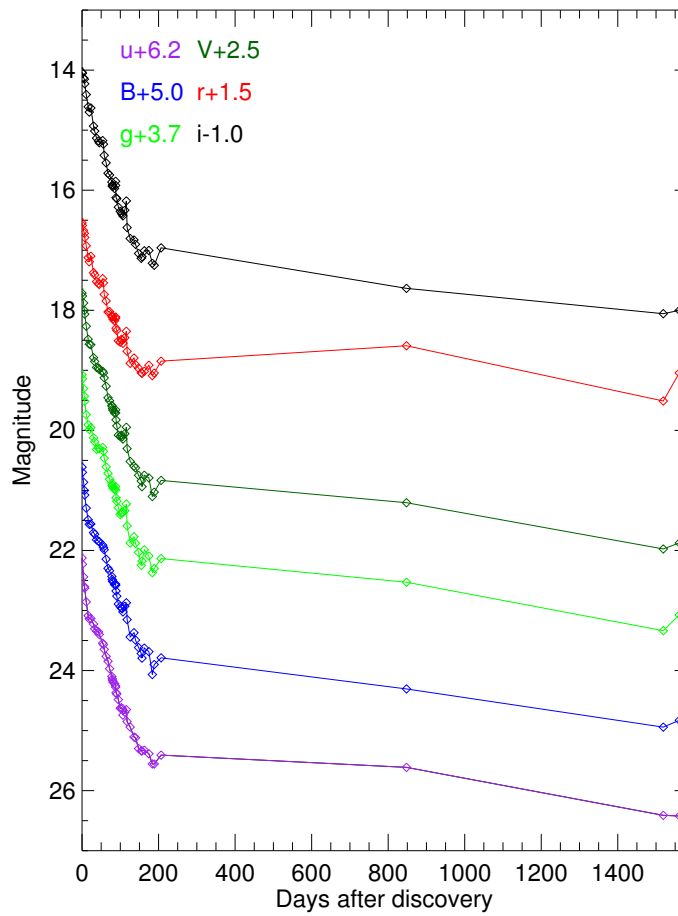


Figure 40: This figure shows all the photometric bands used over the entire observational time since discovery of the SN 2005ip.

12.4 Non converging fits

On Fig. 41 the linear model for a time of 79 days past discovery is shown. It is clearly seen that the fit does not converge, and is therefore zero. This is what the fit does at the points that are not on the figure for R_V for $B = 1$ but are there for $B = 0.5$.

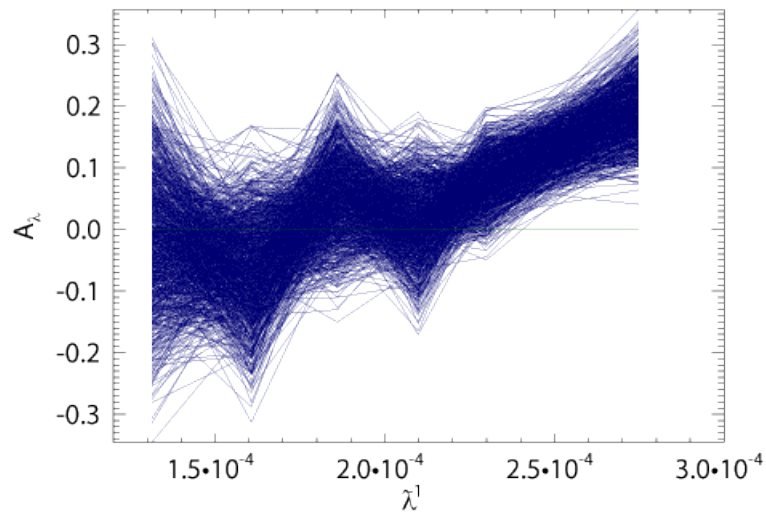


Figure 41

12.5 Plots for the B value model

12.5.1 Plots for $B=1$

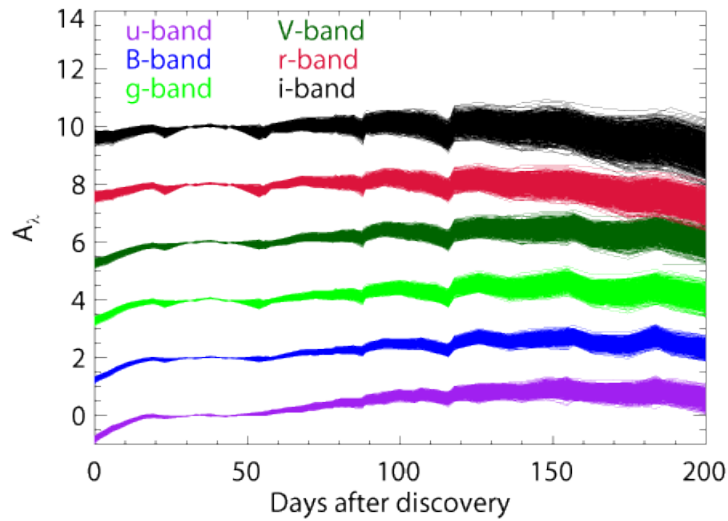


Figure 42: This figure shows the extinction curves for all six bands and for the linear model, $B = 1$. Here there have been added numbers to the bands, to separate them, so that the extent of each band is visible. The numbers that are added are: $u + 0$, $B + 2$, $g + 4$, $V + 6$, $r + 8$, $i + 10$.

On Fig. 42 extinction vs. time, for all n curves, are plotted, with an artificial spacing. The u -band has its original extinction value, but the rest of the bands have a number added, so that it is $B + 2$, $g + 4$, $V + 6$, $r + 8$ and $i + 10$ that is plotted. It is seen that the extinction curves are similar to each other, but that they have a different slope after about 120 days.

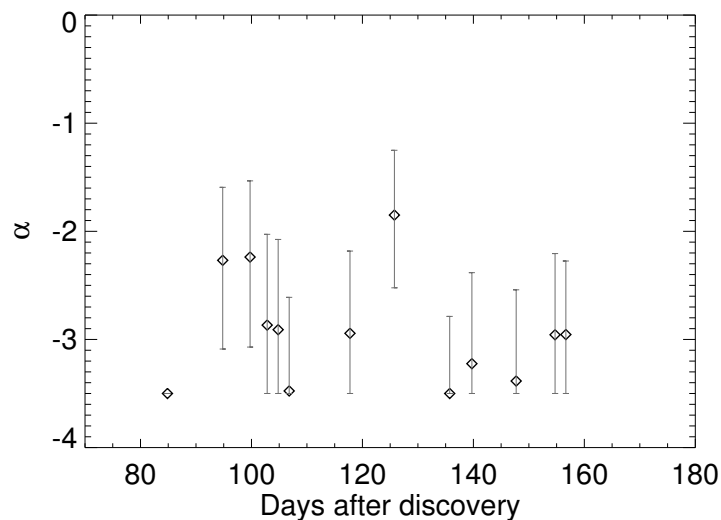


Figure 43: This figure shows the α values for the $B = 1$ model. The α values correspond to the R_V values in the previous plot.

12.5.2 Histograms $B=1$

The figure on the left shows a histogram of R_V found within 3σ and the one on the right shows a similar histogram, but when all the points lying outside of 1σ error have been removed.

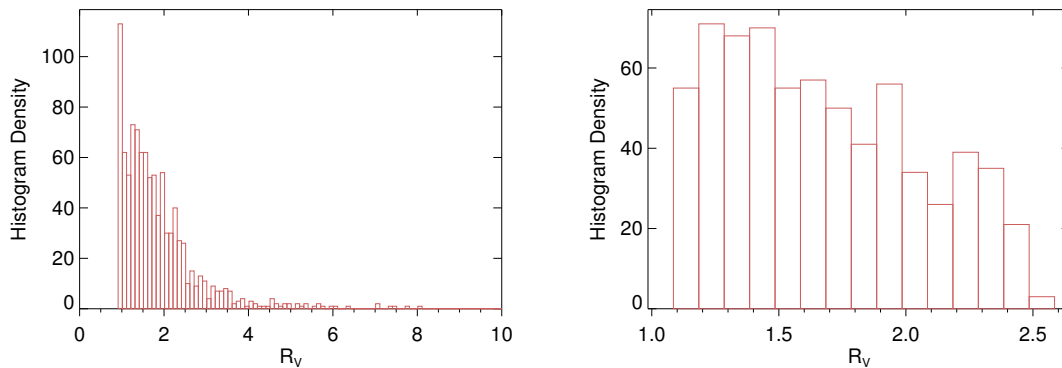


Figure 44: The left figure shows a histogram of R_V for the $B = 1$ model for the full array of 3σ and the right figure shows a corresponding histogram but now only for 1σ .

The two histograms do not resemble a normal distribution, which is because the values lies close to the maximum points for α , and is not normally distributed within the error bars for α .

12.5.3 Plots for $B=0.9$

The following figures in this Appendix section is the plots for $B = 0.9$ for the B model without a polynomial fit. The figures are the light curves, extinction curves and corresponding R_V and α values.

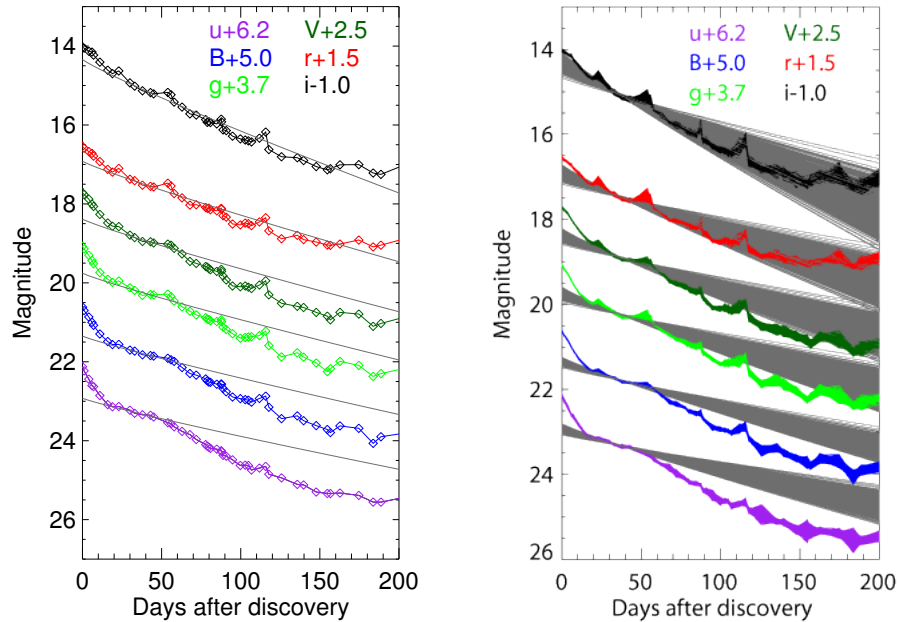


Figure 45: The figure show the light curves with a model fit of $B = 0.9$. The right panel is re-sampled within 3σ .

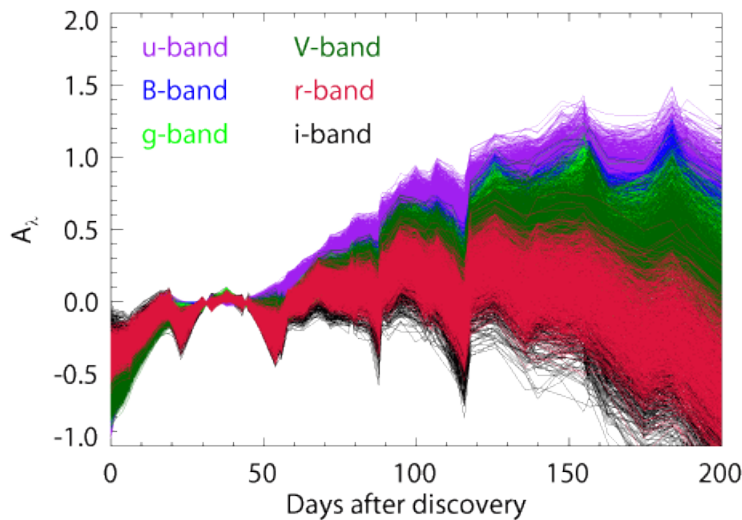


Figure 46: This figure show the extinction over time for the model of $B = 0.9$.

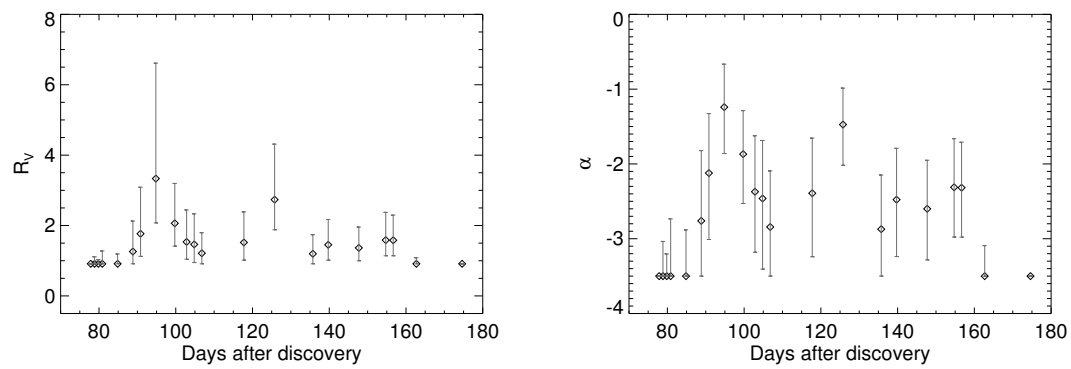


Figure 47: The left panel show the R_V values for $B = 0.9$, and the right panel show the corresponding α values.

12.5.4 Plots for $B=0.8$

The following figures in this Appendix section is the plots for $B = 0.8$ for the B model without a polynomial fit. The figures are the light curves, extinction curves and corresponding R_V and α values.

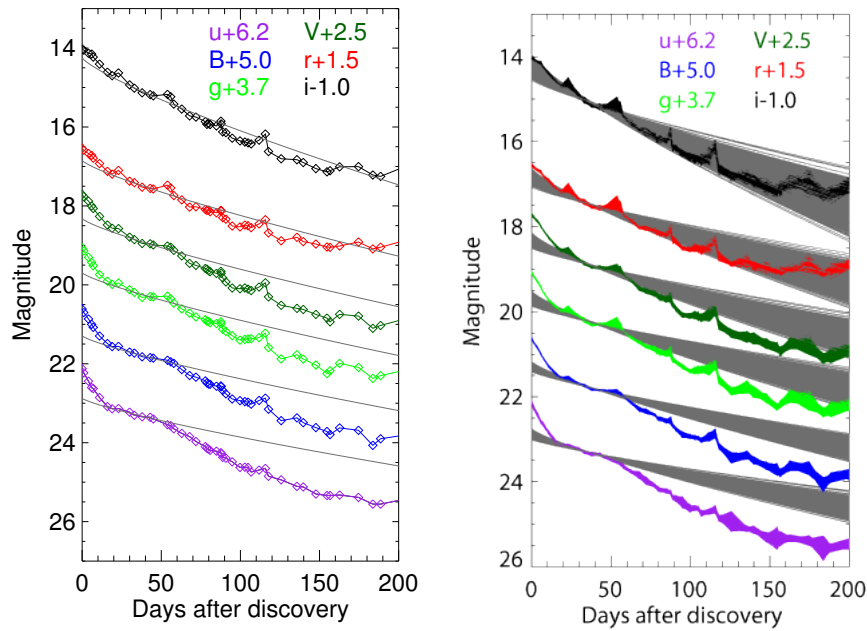


Figure 48: The figure show the light curves with a model fit of $B = 0.8$. The right panel is re-sampled within 3σ .

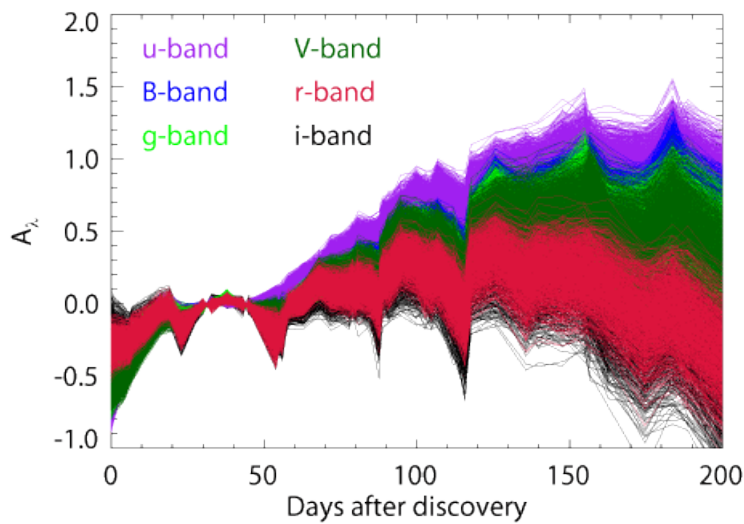


Figure 49: This figure show the extinction over time for the model of $B = 0.9$.

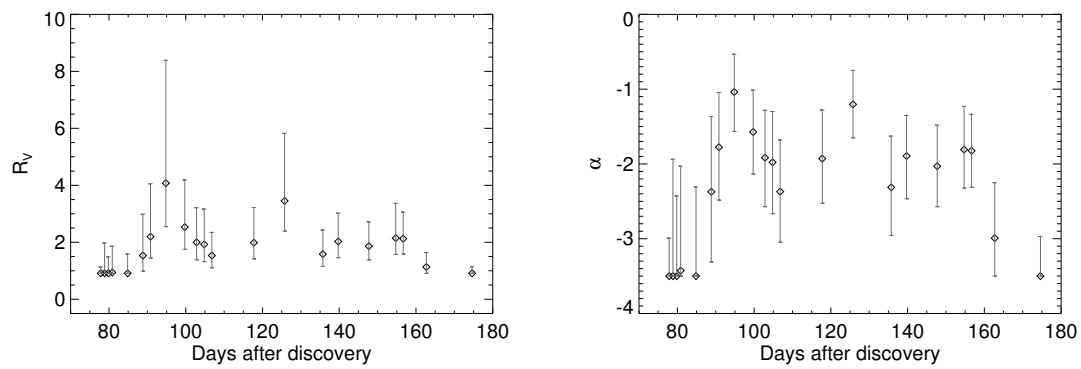


Figure 50: The left panel show the R_V values for $B = 0.9$, and the right panel show the corresponding α values.

12.5.5 Plots for $B=0.7$

The following figures in this Appendix section is the plots for $B = 0.7$ for the B model without a polynomial fit. The figures are the light curves, extinction curves and corresponding R_V and α values.

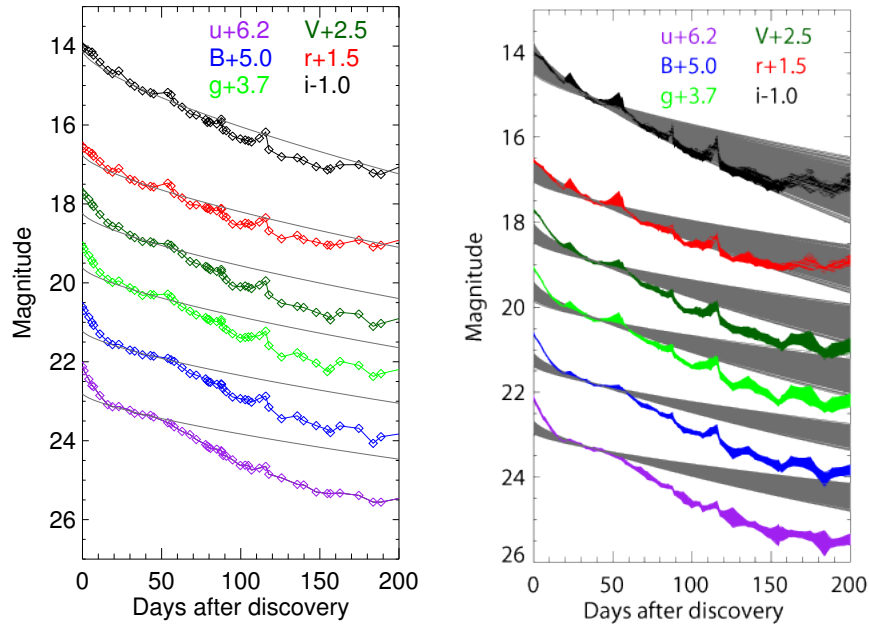


Figure 51: The figure show the light curves with a model fit of $B = 0.7$. The right panel is re-sampled within 3σ .

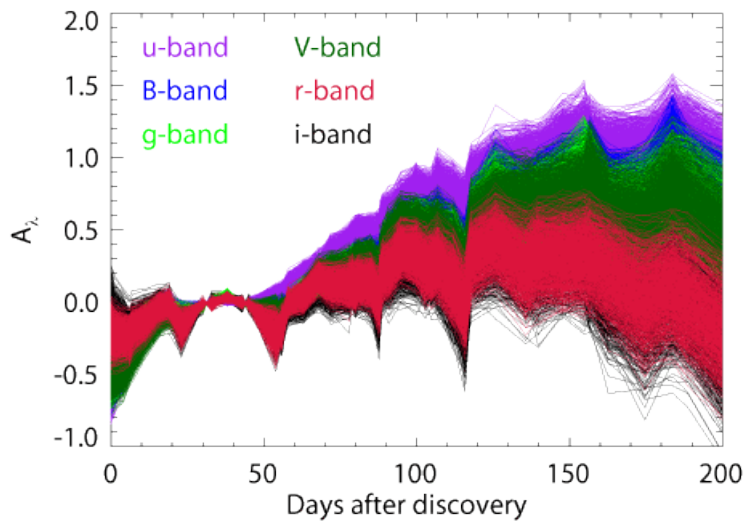


Figure 52: This figure show the extinction over time for the model of $B = 0.7$.

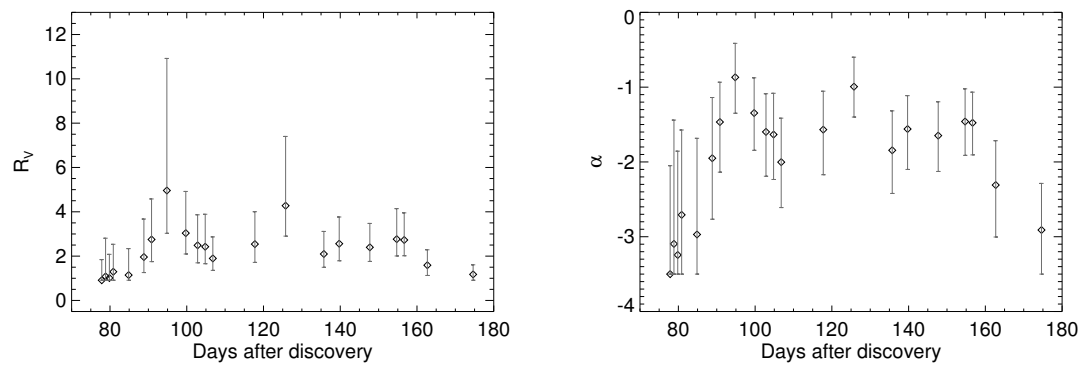


Figure 53: The left panel show the R_V values for $B = 0.7$, and the right panel show the corresponding α values.

12.5.6 Plots for $B=0.6$

The following figures in this Appendix section is the plots for $B = 0.6$ for the B model without a polynomial fit. The figures are the light curves, extinction curves and corresponding R_V and α values.

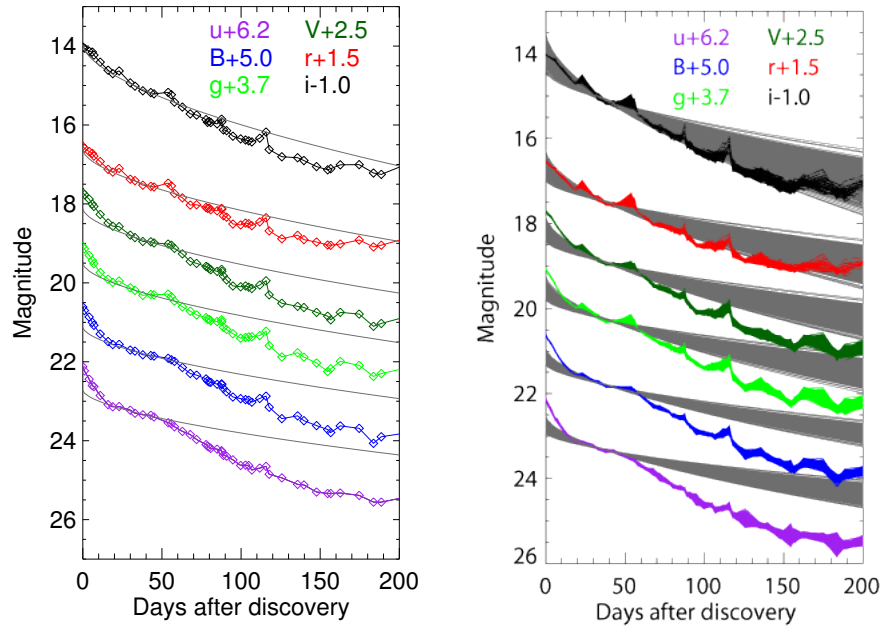


Figure 54: The figure show the light curves with a model fit of $B = 0.6$. The right panel is re-sampled within 3σ .

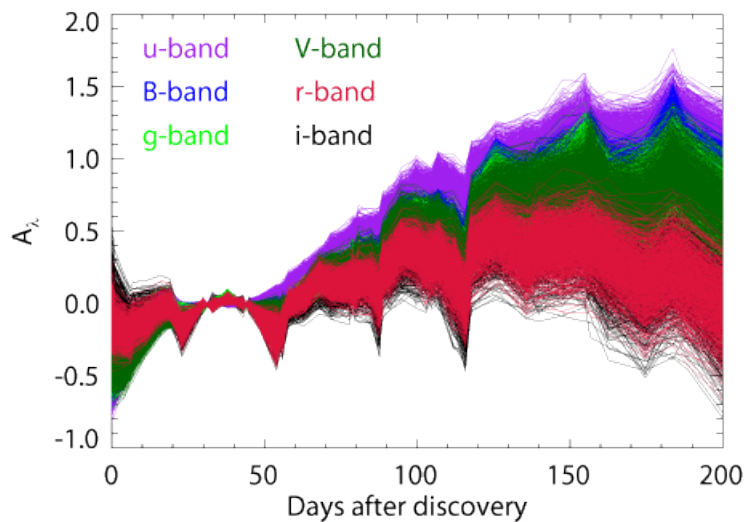


Figure 55: This figure show the extinction over time for the model og $B = 0.6$.

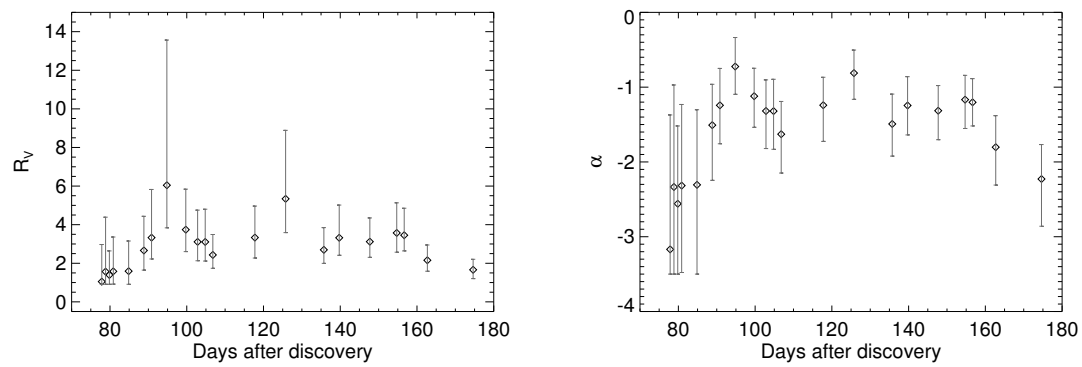


Figure 56: The left panel show the R_V values for $B = 0.6$, and the right panel show the corresponding α values.

12.5.7 Plots for $B=0.5$

The light curves with the $B = 0.5$ fit is shown in Fig. 57. It is here seen, that the light curves bend off instead of being a linear fit. This means that even for the i -band the fit does not go below the light curve before 200 days.

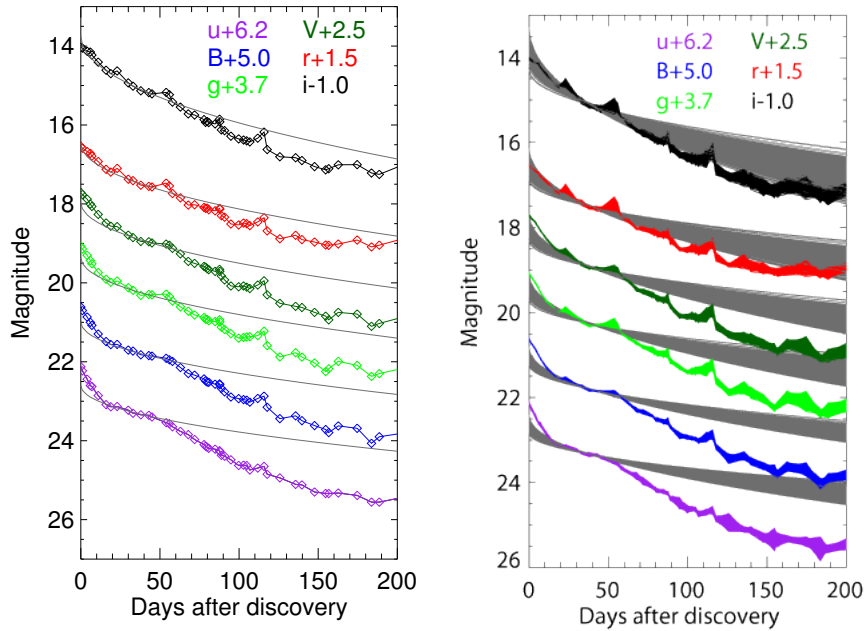


Figure 57: This figure shows the fits to the light curve, with $B = 0.5$. The left figure is the original light curves and the fit to just those, and the right is the re-sampled data and corresponding fits.

The fact that the fit bends off means that the extinction will also become more positive than it was with the linear model of $B = 1$. The extinction over time is shown in Fig. 58.

It is seen that the extinction is much more positive, even for the i -band. This essentially means, that when the fits to the extinction curves are made, as shown in Fig. 18 for $B = 1$, then all the fits to all the days between 77 – 200 days converge, and here are therefore found more points and values for R_V .

The values for R_V is shown in Fig. 59 and the corresponding α values are shown in Fig. ??.

The R_V values here have a somewhat higher value than for $B = 1$. The values here are about $R_V = 3$, but they can again vary within the error bars shown. There are again two points that are a bit outside of the general trend. This may be due to bumps in the light curves.

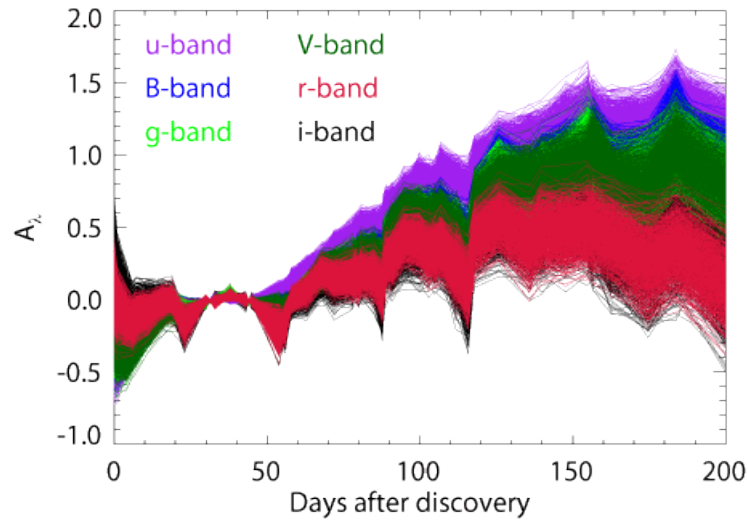


Figure 58: This figure shows the extinction vs. times for the $B = 0.5$ model. Here all six bands are seen, the u , B , g , V , r and i -band.

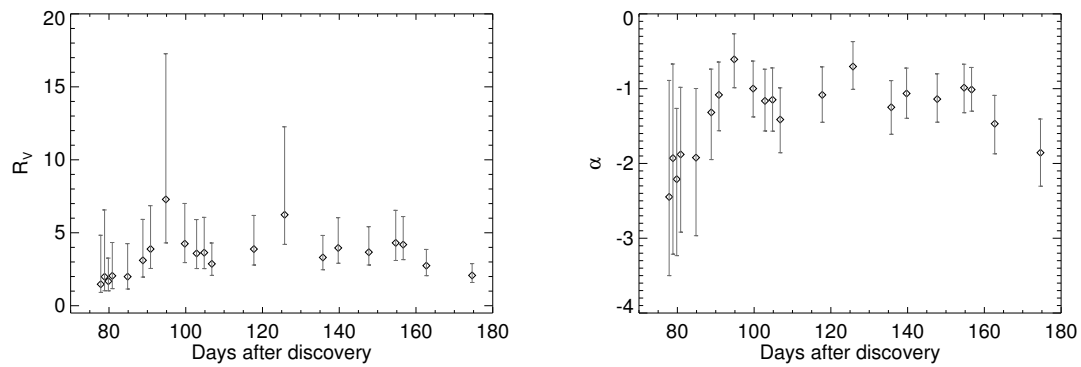


Figure 59: This figure shows the R_V values for the model of $B = 0.5$ with the corresponding error bars, and is over the selected time interval. The right panel of the figure shows the corresponding α values.

12.5.8 Plots for $B=0.2$

The following figures in this Appendix section is the plots for $B = 0.6$ for the B model without a polynomial fit. The figures are the light curves, extinction curves and corresponding R_V and α values.

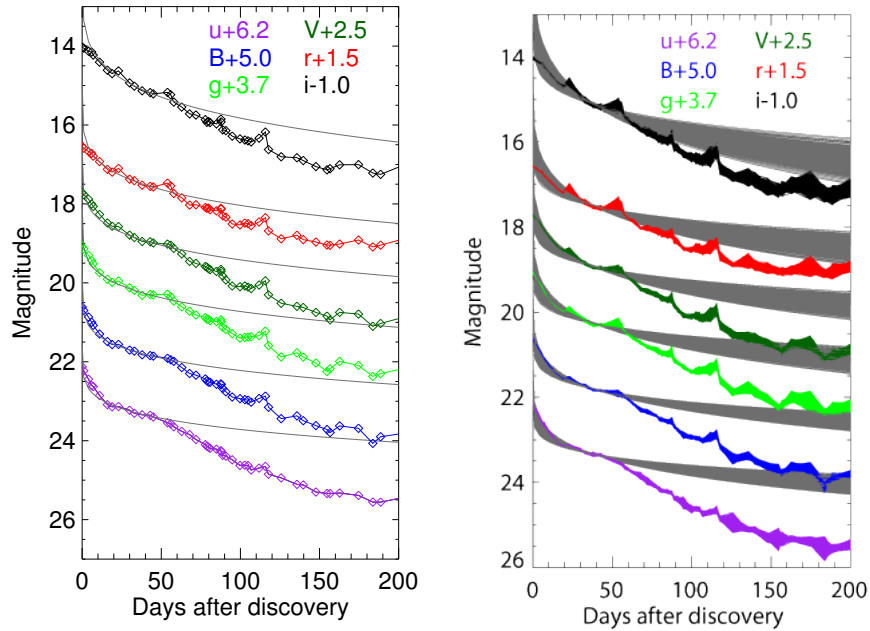


Figure 60: The figure show the light curves with a model fit of $B = 0.2$. The right panel is re-sampled within 3σ .

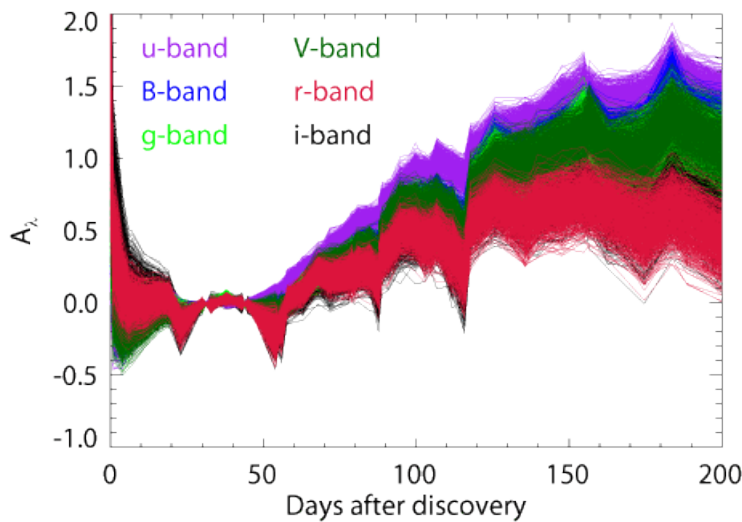


Figure 61: This figure show the extinction over time for the model og $B = 0.2$.

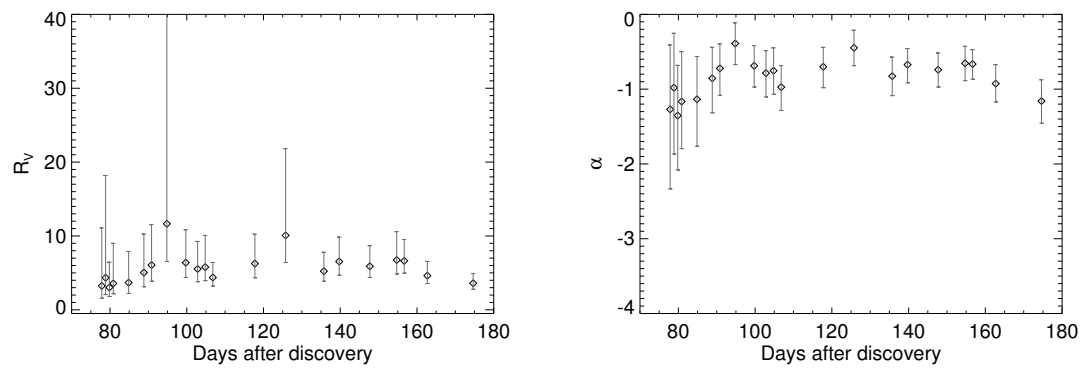


Figure 62: The left panel show the R_V values for $B = 0.2$, and the right panel show the corresponding α values.

12.6 Plots for Polynomial fits to B models

12.6.1 Polynomial model plots for $B=1$ and $B = 0.5$

This figure shows the polynomial fitted extinction curves over time, for $B = 1$ and $B = 0.5$.

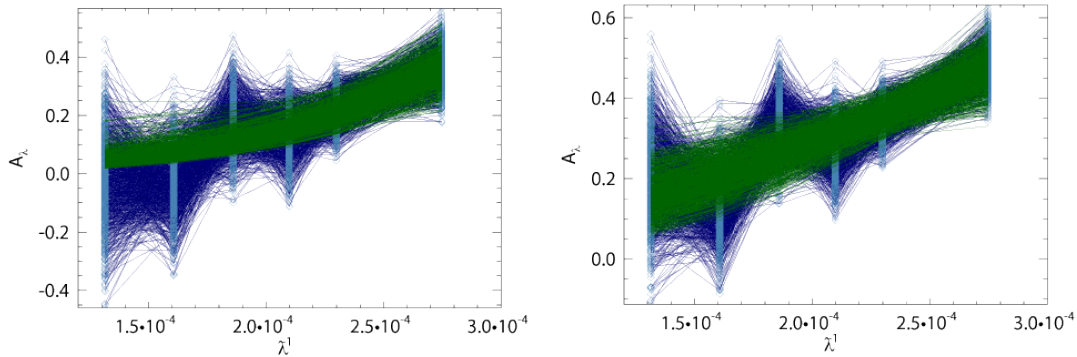


Figure 63: On the left figure the extinction curve for the polynomial fitted $B = 1$ is shown along with the fit, green curves, and the right curve shows the corresponding fits and extinction curve for $B = 0.5$. Both for a time of 99 days past discovery, and as previous plots, both within 3σ .

Fig. 63 shows the polynomial fit to the extinction curves, and even here it is seen, that for $B = 1$ the i -band is still mainly negative, whereas $B = 0.5$ is mostly positive.

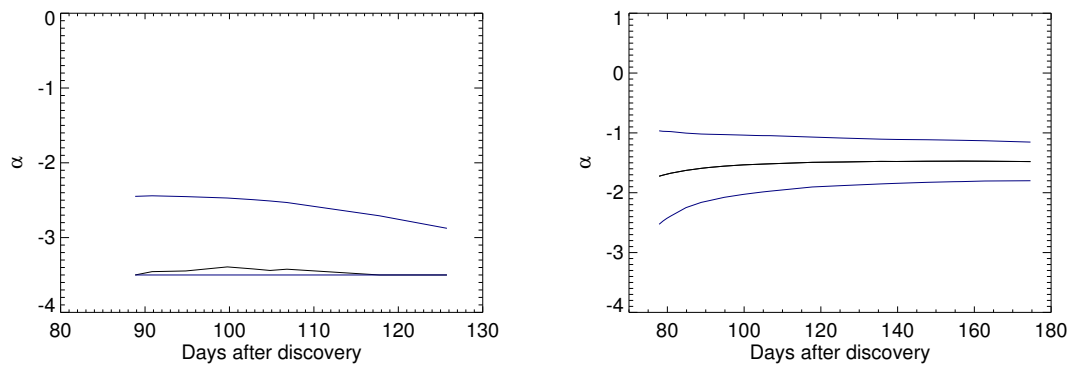


Figure 64: These figure are the corresponding α values for the R_V plots above, here the left is for $B = 1$ and the right is for $B = 0.5$. The blue lines indicate the errors and the black the median value for α .

12.6.2 Polynomial model plots for $B=0.9$

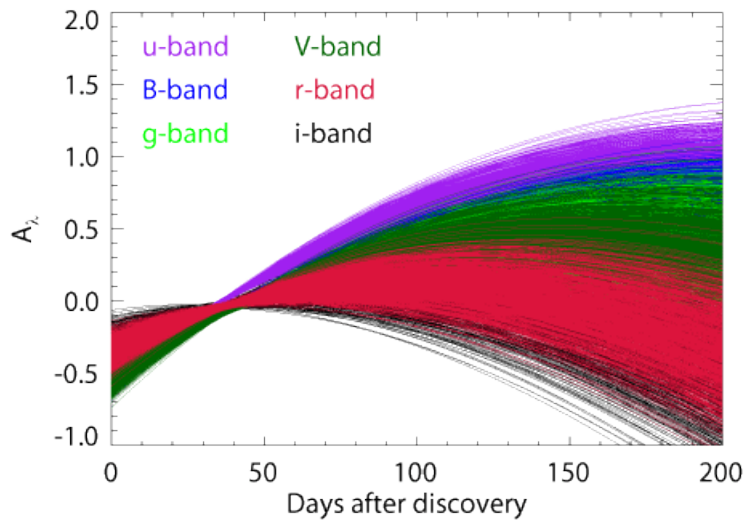


Figure 65: This figure shows the extinction over time for the polynomial fitted to the $B = 0.9$ model.

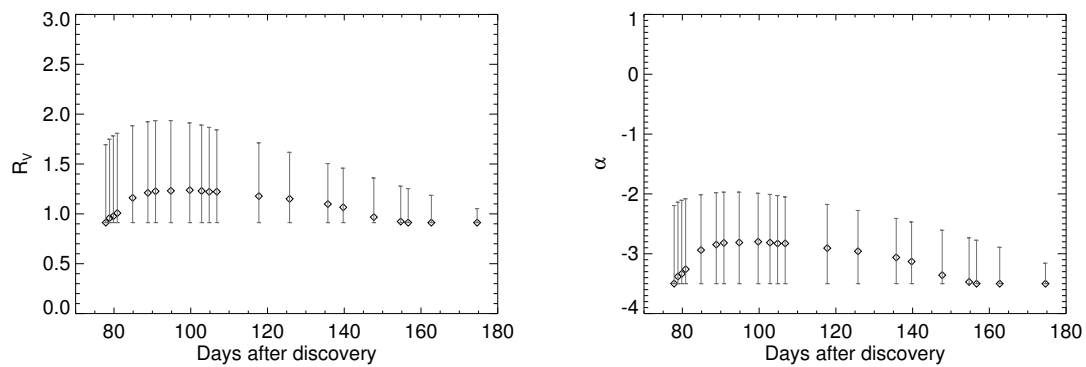


Figure 66: The left panel shows the R_V values for the polynomial fit to $B = 0.9$ model, and the right panel shows the corresponding α values. The figure have error bars, but it is basically the same as the blue lines on the figures in section 8.3.

12.6.3 Polynomial model plots for $B=0.8$

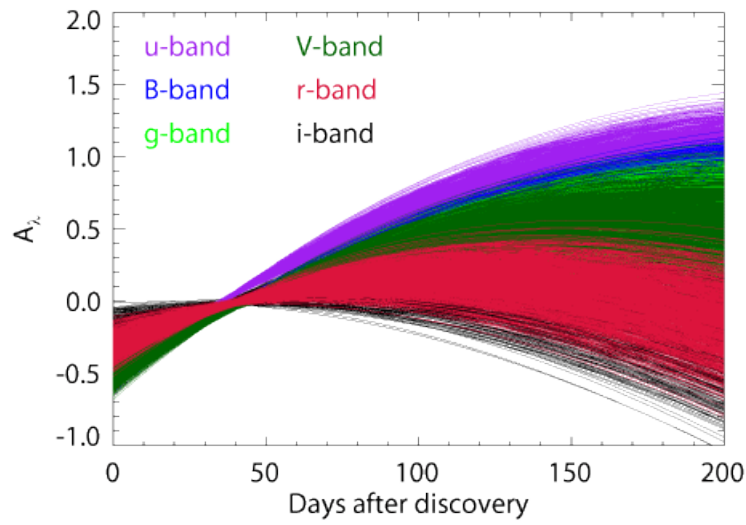


Figure 67: This figure shows the extinction over time for the polynomial fitted to the $B = 0.8$ model.

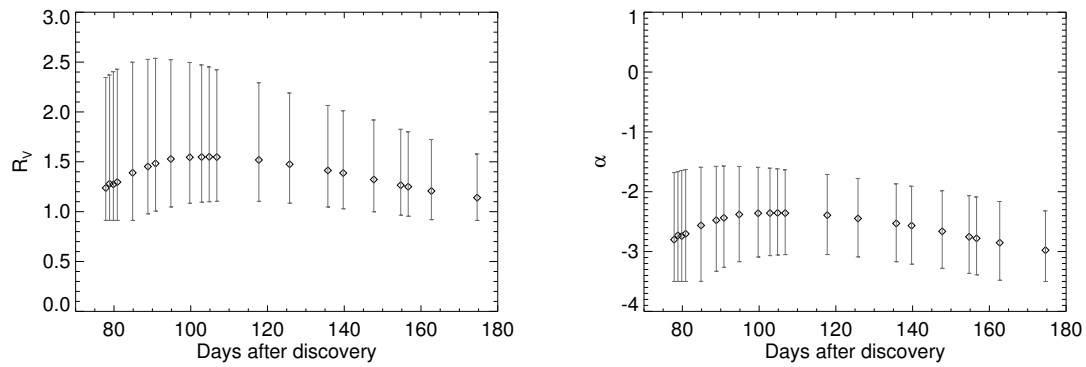


Figure 68: The left panel shows the R_V values for the polynomial fit to $B = 0.8$ model, and the right panel shows the corresponding α values. The figure have error bars, but it is basically the same as the blue lines on the figures in section 8.3.

12.6.4 Polynomial model plots for $B=0.7$

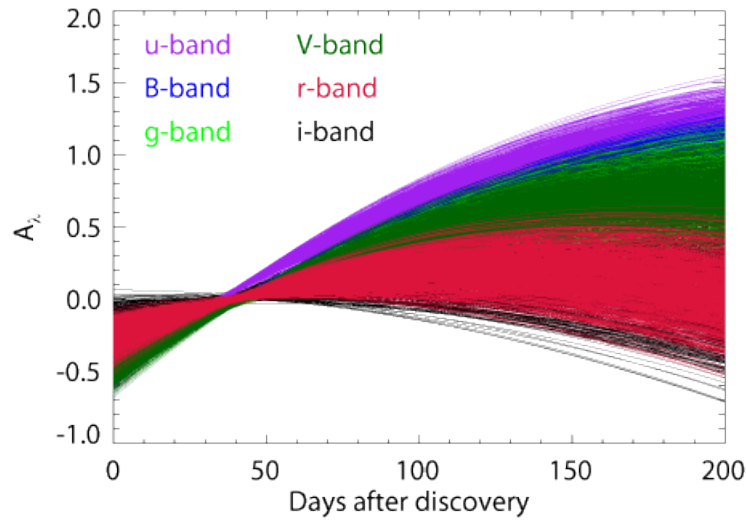


Figure 69: This figure shows the extinction over time for the polynomial fitted to the $B = 0.7$ model.

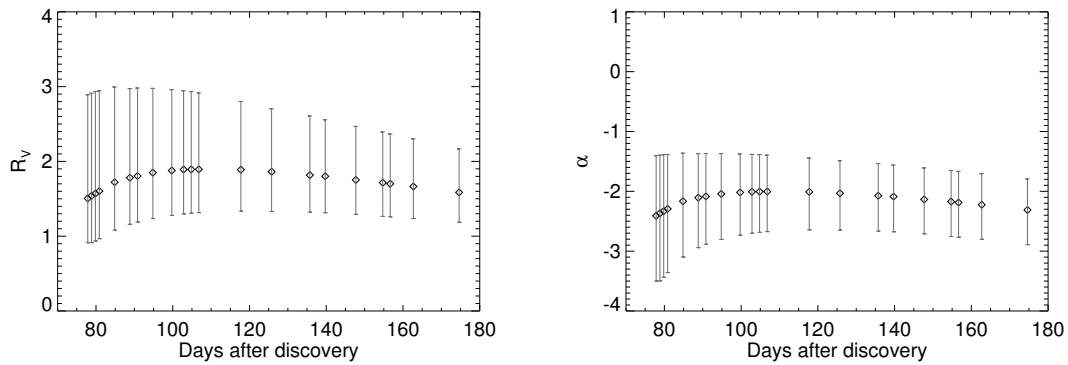


Figure 70: The left panel shows the R_V values for the polynomial fit to $B = 0.7$ model, and the right panel shows the corresponding α values. The figure have error bars, but it is basically the same as the blue lines on the figures in section 8.3.

12.6.5 Polynomial model plots for $B=0.6$

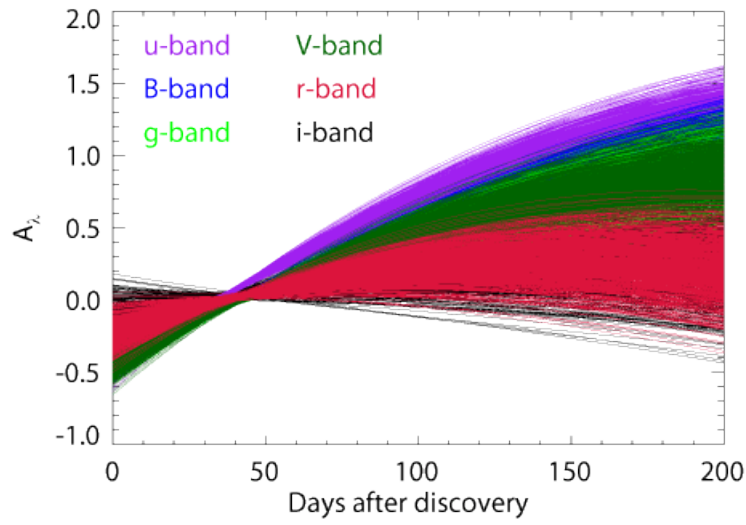


Figure 71: This figure shows the extinction over time for the polynomial fitted to the $B = 0.6$ model.

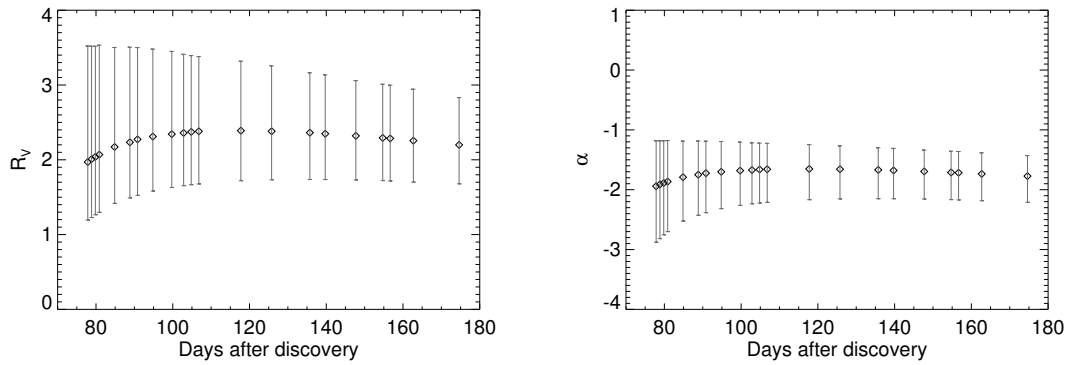


Figure 72: The left panel shows the R_V values for the polynomial fit to $B = 0.6$ model, and the right panel shows the corresponding α values. The figure have error bars, but it is basically the same as the blue lines on the figures in section 8.3.

12.6.6 Polynomial model plots for $B=0.2$

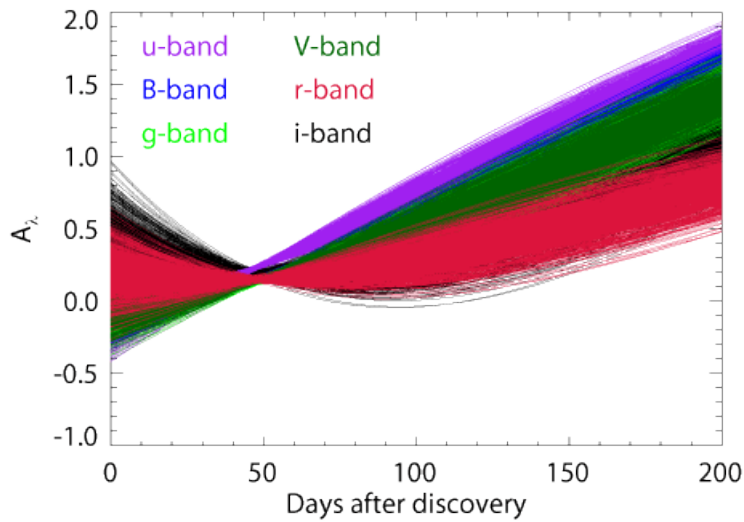


Figure 73: This figure shows the extinction over time for the polynomial fitted to the $B = 0.2$ model.

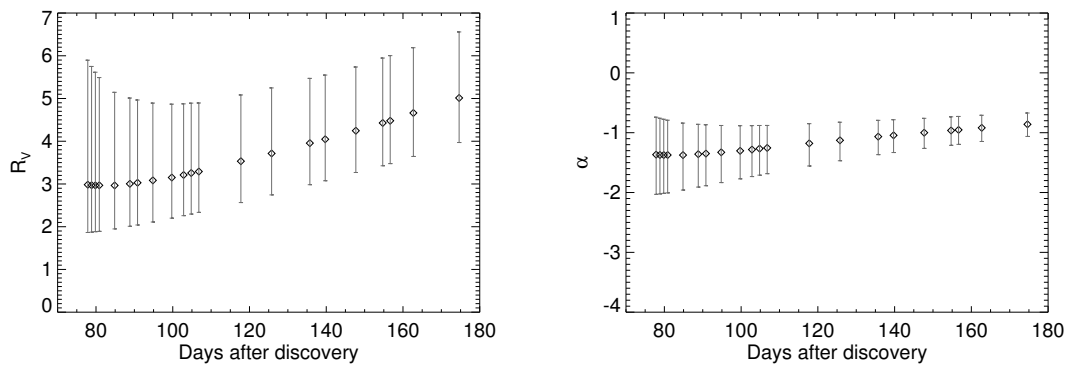


Figure 74: The left panel shows the R_V values for the polynomial fit to $B = 0.2$ model, and the right panel shows the corresponding α values. The figure have error bars, but it is basically the same as the blue lines on the figures in section 8.3.

12.6.7 Polynomial model - Entire range of B values

This figure shows the entire range of B values, here in the section for A_V vs. $\log(T)$ and $\log(A_V)$ vs. $\log(T)$.

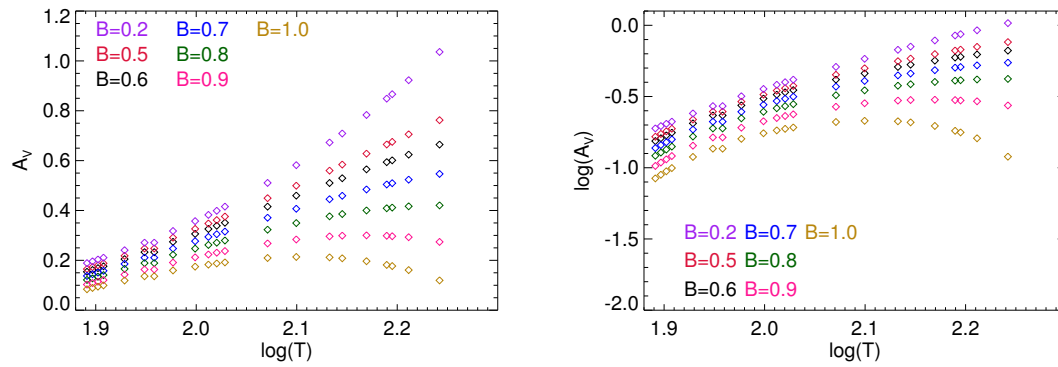


Figure 75: This figure shows the plots to the left of A_V vs. $\log(T)$ and to the right $\log(A_V)$ vs. $\log(T)$. The values for A_V is again seen to be increasing for values below $B = 0.8$ or $b = 0.7$, for both plots.

12.7 Logarithmic fit

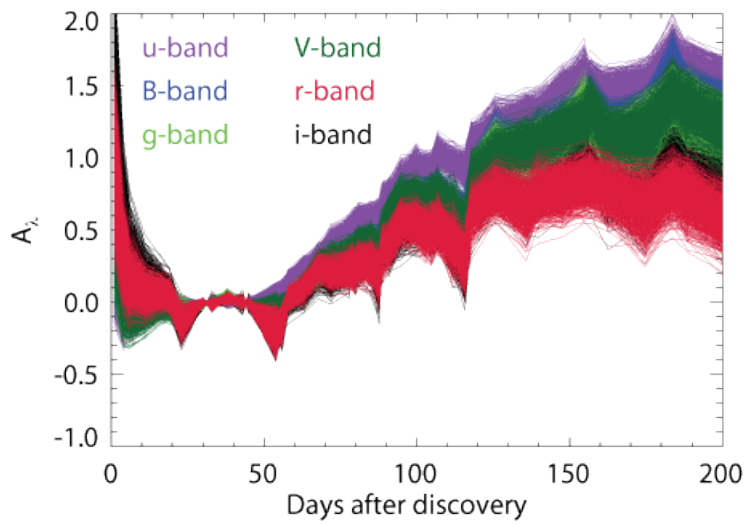


Figure 76: This figure shows the extinction over time for the logarithmic fit for all the bands.

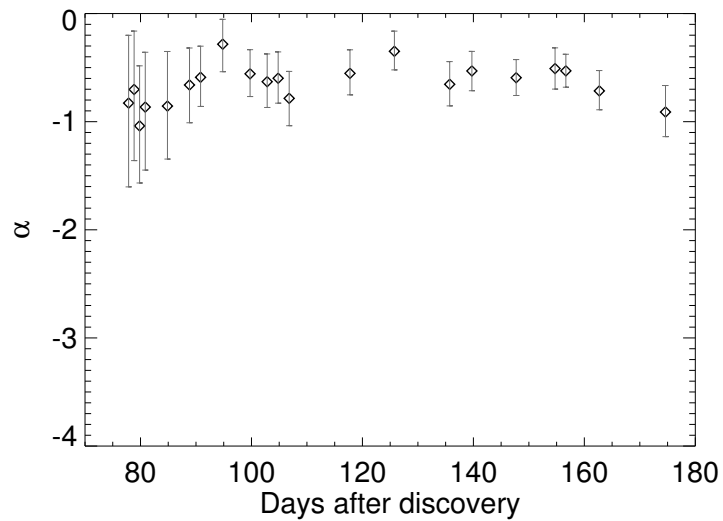


Figure 77: This shows the values of α corresponding to the R_V values from section 8.4.

12.7.1 Logarithmic model with polynomial fit

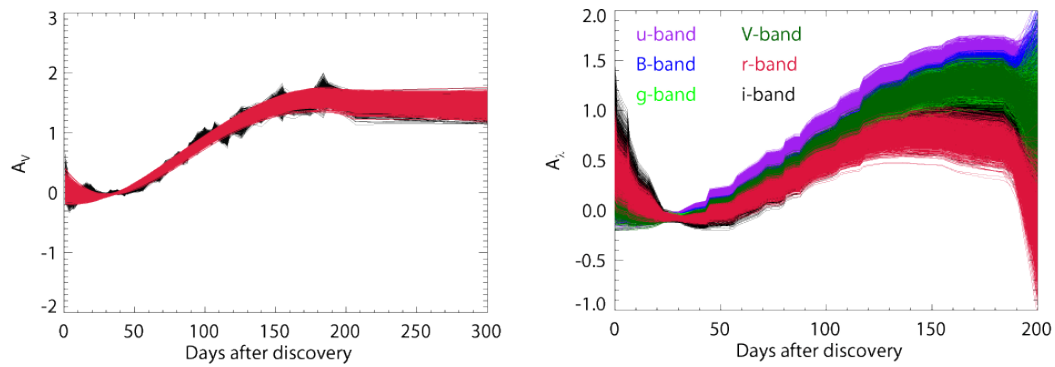


Figure 78: The left figure shows a 5 degree polynomial fit to the u -band of the logarithmic model. The right figure shows the extinction over time of this polynomial fit. Again, all curves until R_V is within 3σ .

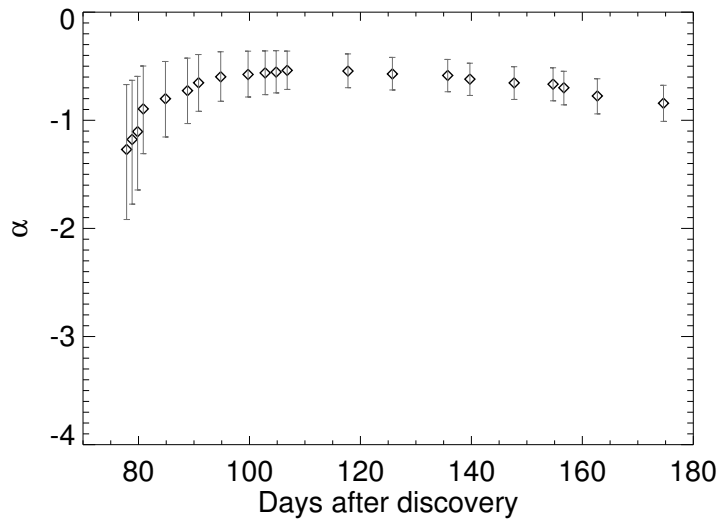


Figure 79: This shows the values of α corresponding to the R_V values from section 8.4. Here for a polynomial fitted to the logarithmic model.

12.8 The removed point

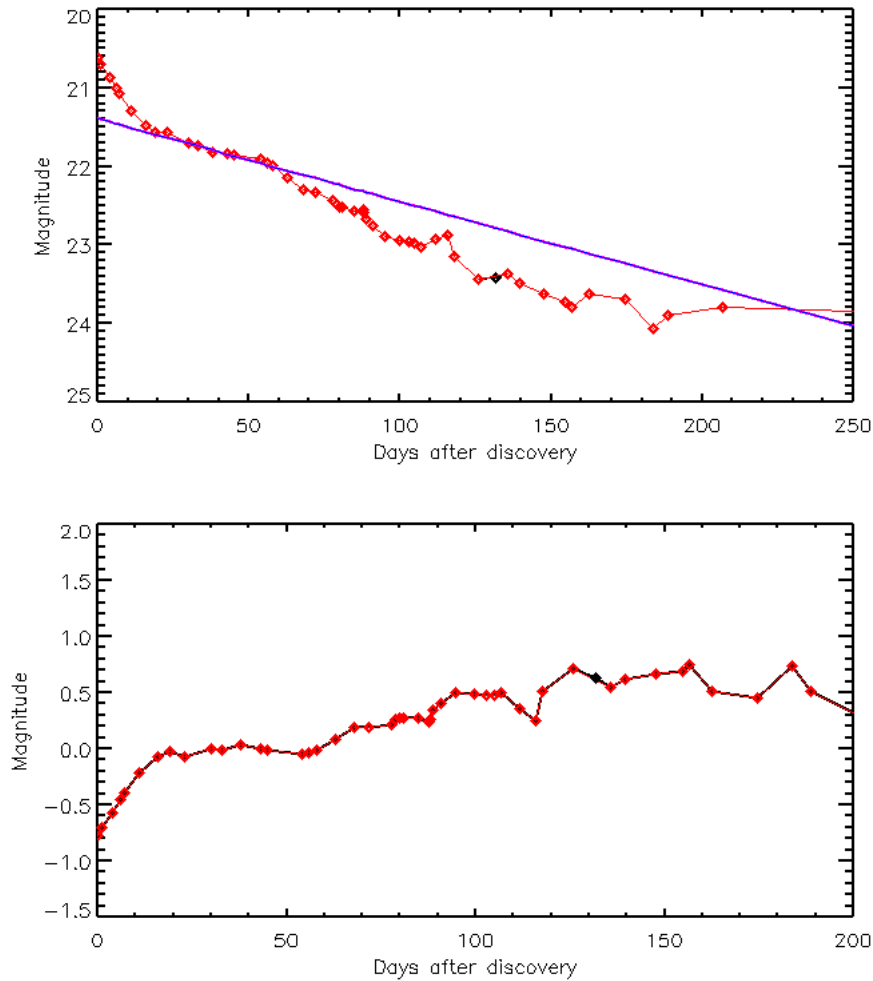


Figure 80: This figure show the B -band light curve with the extra point. The top panel shows the extra point, black point, and with the linear fit, and lower panel shows the extinction over time, with the extra point in black.

On the above figures it can be seen, that the red points and line is the data that is used in this thesis, and that the black point is the extra observation point which only exists for the B , g , V , r and i -bands. The pink and blue line is the linear fit to the data. The pink is the fit to the data used in this thesis and the blue is the fit to the data with the extra point. The pink line has been made thicker, so that it is possible to see it behind the blue line. It can be seen that the red and black point follow each other well, and that it is a very small difference, if any, that there is between the two curves. The two fits are, on the other hand, completely identical. The fits made are not based on the area where the extra point, is, because the fit is made to the dates 25-45 days after discovery, and the extra point is at 131.76 days after discovery.

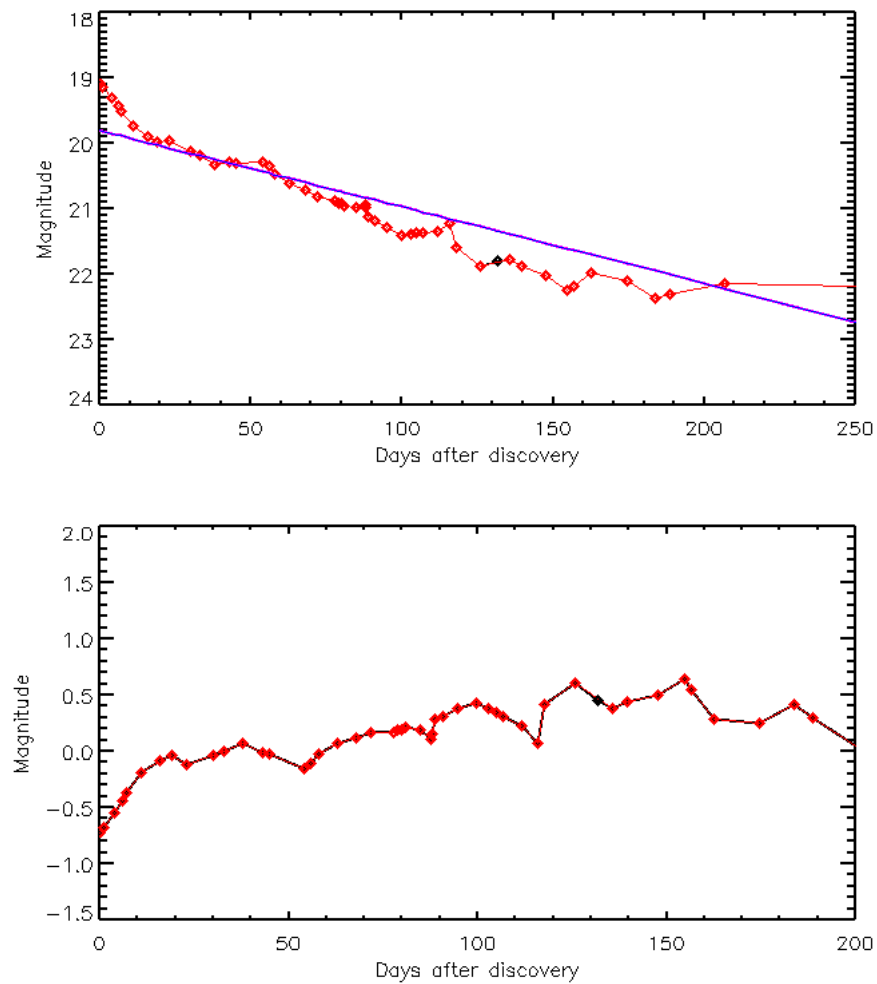


Figure 81: This figure show the g -band light curve with the extra point. The top panel shows the extra point, black point, and with the linear fit, and lower panel shows the extinction over time, with the extra point in black.

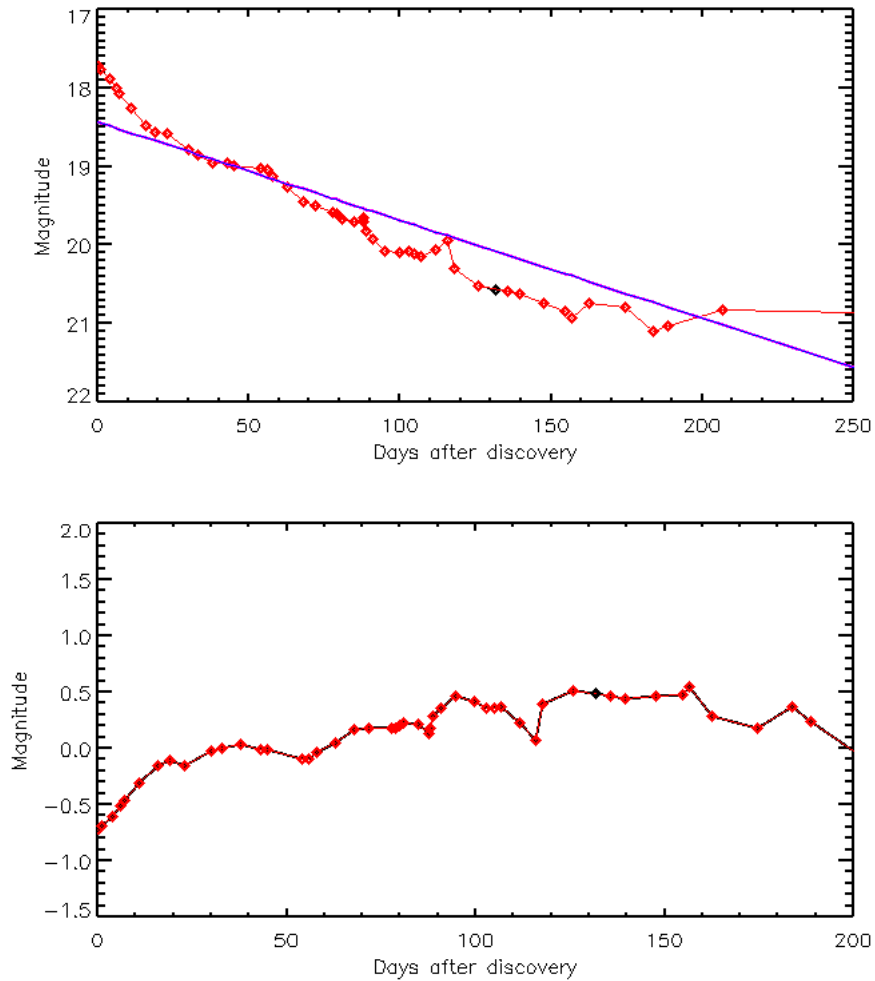


Figure 82: This figure show the V-band light curve with the extra point. The top panel shows the extra point, black point, and with the linear fit, and lower panel shows the extinction over time, with the extra point in black.

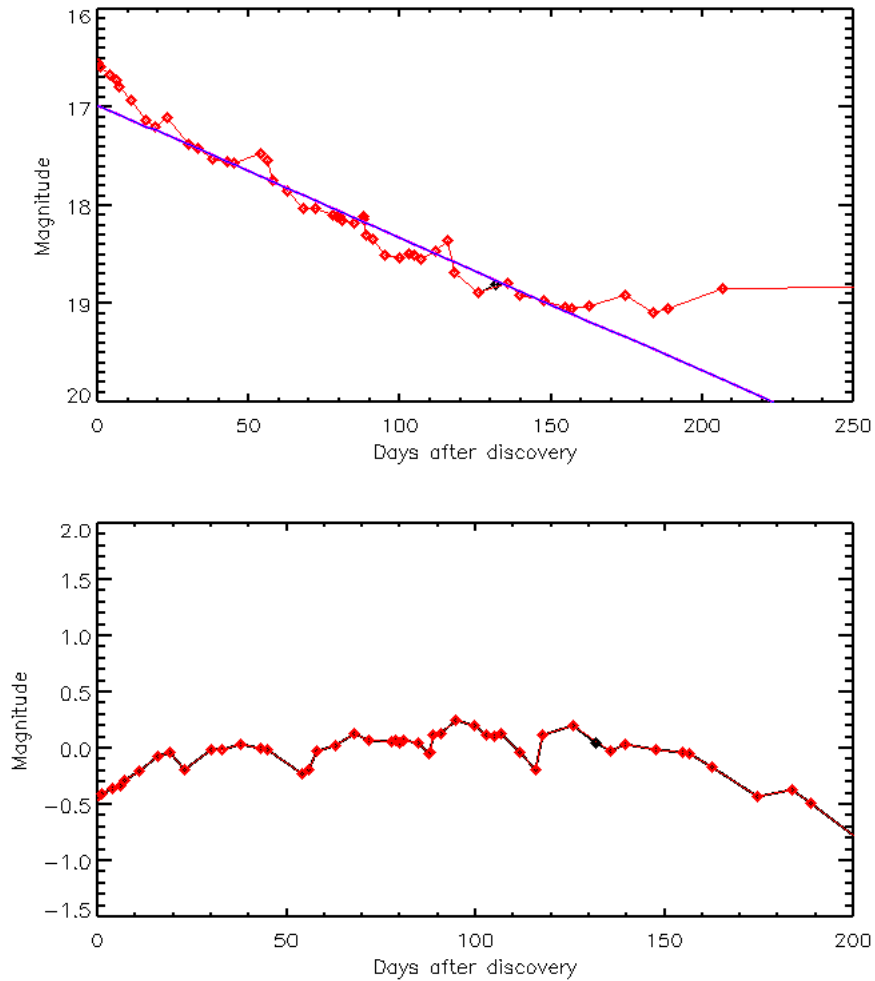


Figure 83: This figure show the r -band light curve with the extra point. The top panel shows the extra point, black point, and with the linear fit, and lower panel shows the extinction over time, with the extra point in black.

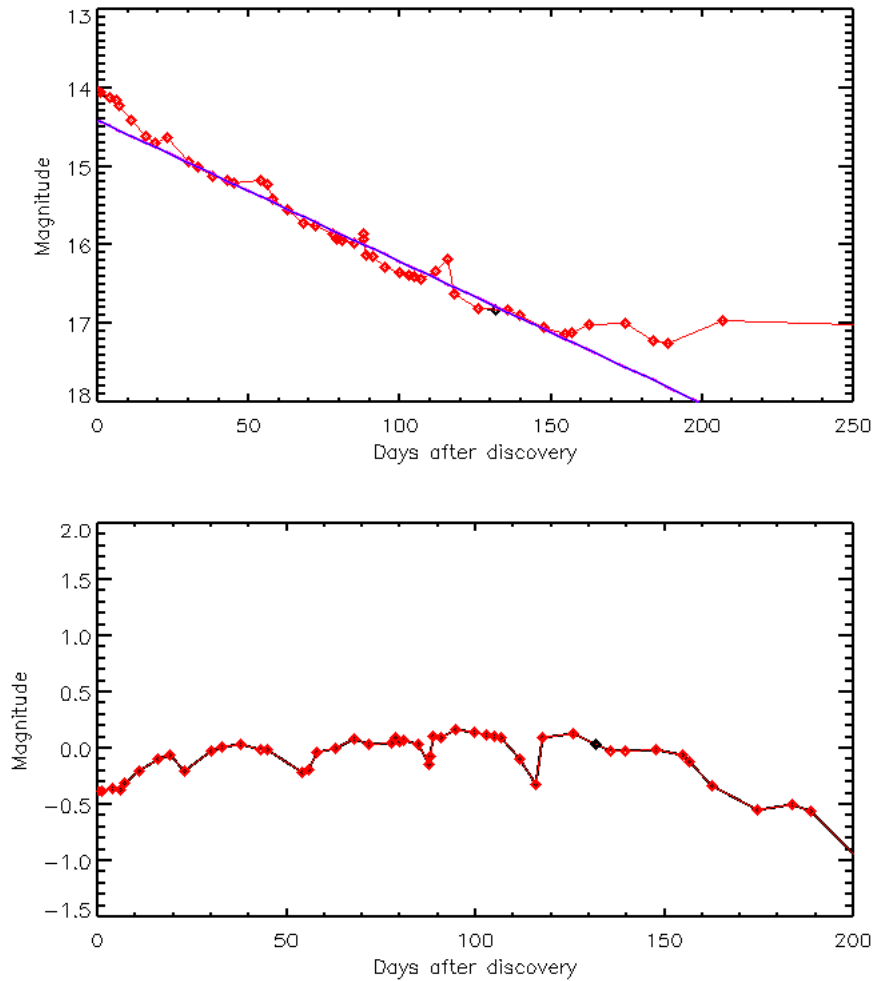


Figure 84: This figure show the *i*-band light curve with the extra point. The top panel shows the extra point, black point, and with the linear fit, and lower panel shows the extinction over time, with the extra point in black.